



NA ALMA Development Cycle 2 (2014)

Design and testing of a Prototype Band 2 Cartridge

Final Report

2017-12-27

| Prepared By: | | |
|---------------------------------|---------------------|-------------|
| Name(s) and Signature(s) | Organization | Date |
| M. Pospieszalski | NRAO | |
| S. Srikanth | NRAO | |
| M. Morgan | NRAO | |
| J. Effland | NRAO | |
| K. Saini | NRAO | |
| K. Crady | NRAO | |


| | | |
|---|--|------------------------------------|
|  | ALMA Project | Date: 2017-12-27 Page: 2 of 117 |
| | Design and testing of a Prototype Band 2 Cartridge Final Report | |

Table of Contents

| | | |
|---------|--|----|
| 1. | PURPOSE AND SCOPE | 8 |
| 2. | ACKNOWLEDGEMENTS | 8 |
| 3. | SCOPE | 8 |
| 4. | REFERENCE DOCUMENTS (RDS) | 9 |
| 5. | CARTRIDGE OVERVIEW | 13 |
| 6. | SPECIFICATIONS | 18 |
| 7. | COMPONENTS | 18 |
| 7.1. | Cascade Design | 18 |
| 7.2. | Optics | 20 |
| 7.2.1. | Requirements and Overview | 20 |
| 7.2.2. | Optics Design Options | 21 |
| 7.2.3. | Feed Horn Design | 21 |
| 7.2.4. | Feed Horn Fabrication | 22 |
| 7.2.5. | Feed Horn Measurement and Characterization | 23 |
| 7.2.6. | Dielectric Lens Design | 25 |
| 7.2.7. | Dielectric Lens Fabrication | 25 |
| 7.2.8. | Optics Measurement and Characterization | 26 |
| 7.2.9. | Fresnel Lens | 28 |
| 7.3. | Orthomode Transducer (OMT) | 29 |
| 7.4. | Cryogenic Low Noise Amplifiers | 31 |
| 7.4.1. | LNA Chip Quantities and Yield | 34 |
| 7.4.2. | LNA Linearity | 34 |
| 7.4.3. | A Note About LNA Biasing | 36 |
| 7.5. | Cartridge RF output | 37 |
| 7.6. | Mechanical Tolerance Analysis, Cartridge Optics Metrology and Alignment | 38 |
| 7.7. | Mechanical Analysis | 42 |
| 7.8. | RF filter (band definition) and Post-amplifier | 47 |
| 7.9. | 2SB Down-converter | 48 |
| 7.9.1. | RF Hybrid Design | 48 |
| 7.9.2. | Warm IF Amplifiers | 56 |
| 7.9.3. | IF Hybrid | 56 |
| 7.10. | LO | 60 |
| 7.10.1. | LO Frequency Range | 60 |
| 7.11. | Thermal Loading | 61 |
| 7.12. | Wiring and cabling | 63 |
| 7.12.1. | Electronic Interface | 64 |
| 7.12.2. | Wiring Diagram | 64 |
| 7.13. | Vacuum Considerations | 64 |
| 8. | PROTOTYPE CARTRIDGE PERFORMANCE | 69 |
| 8.1. | Noise Performance (FEND-40.02.02.00-00180-00/T) | 70 |
| 8.2. | Image Rejection (FEND-40.02.02.00-00190-00/T) | 74 |
| 8.3. | Output Power and Power Density Slope (FEND-40.02.02.00-00200-00/T) (FEND-40.02.02.00-00210-00/T) | 83 |
| 8.4. | Gain Compression (FEND-40.02.02.00-00230-00/T) | 91 |
| 8.5. | Amplitude Stability (FEND-40.02.02.00-00240-00/T) | 91 |
| 8.6. | Signal Path Phase Stability (FEND-40.02.02.00-00250-00/T) | 93 |



| | | |
|---|--|------------------------------------|
|  | ALMA Project | Date: 2017-12-27 Page: 3 of 117 |
| | Design and testing of a Prototype Band 2 Cartridge Final Report | |


Table of Contents

| | | |
|--------|--|-----|
| 8.7. | Beam Efficiency (FEND-40.02.02.00-00260-00/T) | 93 |
| 8.7.1. | Test System | 94 |
| 8.7.2. | Linearity | 94 |
| 8.7.3. | Measurements for Lens 3-2 | 96 |
| 8.7.4. | Measurements with Lens 1-1 | 104 |
| 8.7.5. | Measurements with Fresnel Lens | 108 |
| 8.8. | Spurious Frequencies (FEND-40.00.00.00-00120-00/T) | 113 |
| 8.9. | Leak Rate (FEND-40.02.02.00-00470-00/R) | 114 |
| 8.10. | Measured Mass (FEND-40.02.02.00-00310-00/T) | 115 |
| 9. | DRAWINGS AND PARTS LIST | 115 |
| 9.1. | Mechanical | 115 |

| | | |
|---|--|------------------------------------|
|  | ALMA Project | Date: 2017-12-27 Page: 4 of 117 |
| | Design and testing of a Prototype Band 2 Cartridge Final Report | |


List of Figures

| | |
|---|----|
| Figure 1: 3D rendering showing the layout of Band 2 Cartridge 15 K Components | 14 |
| Figure 2: 3D rendering of the model of the entire Band 2 Cold Cartridge Assembly | 15 |
| Figure 3: WCA Photos | 16 |
| Figure 4: Band 2 Receiver Block Diagram | 17 |
| Figure 5: Cascade noise and gain calculations (Top: Using Cryo-3 device based MIC CLNAs, and Bottom: Using CRAL MMIC based CLNAs) | 19 |
| Figure 6: Calculated output power and headroom to 1 dB compression point for each of the amplifier stages in the receiver | 19 |
| Figure 7: Calculated output power and headroom to 1 dB compression point for each of the amplifier stages in the receiver, for several different source/sky temperatures | 20 |
| Figure 8: Stages of Feed Horn Fabrication | 23 |
| Figure 9: Measured (*-Me) and theoretical (*-Th) patterns in the E- and H-planes of the feed horn | 24 |
| Figure 10: Measured co-polarization (78 GHz) and cross-polarization patterns of the feed horn | 24 |
| Figure 11: Calculated co- and cross-polarization patterns of the feed horn | 24 |
| Figure 12: HDPE lens variants after machining | 26 |
| Figure 13: Far-field feed patterns (horn & lens) were measured in the anechoic chamber in Green Bank | 27 |
| Figure 14: Feed horn & lens # 2 measured co-polar and cross-polar patterns | 27 |
| Figure 15: Feed horn & lens # 3 measured co-polar and cross-polar patterns | 27 |
| Figure 16: Measured return loss of the feed horn without/with lens # 2 | 28 |
| Figure 17: Photo of Fresnel Lens, designed by NAOJ [RD 30] | 29 |
| Figure 18: Noise Temperature of Fresnel Lens compared to Original Lens | 29 |
| Figure 19: Photograph of an assembled 67-90 GHz turnstile junction OMT, fabricated as three separate blocks | 30 |
| Figure 20: Measured input return loss of the 67-90 GHz turnstile junction OMT | 31 |
| Figure 21: Measured cross-polarization performance of the 67-90 GHz turnstile junction OMT | 31 |
| Figure 22: Noise temperature of MIC and Caltech/JPL MMIC LNA | 32 |
| Figure 23: Photo of MMIC LNA Amplifier and enclosed MMIC Chip | 32 |
| Figure 24: Warm S-Parameters for two prototype MMIC amplifier blocks | 33 |
| Figure 25: Measured cryogenic gain and noise temperature performance of the Band 2 MMIC based low noise amplifier | 34 |
| Figure 26: Linearity measurement of amplifier block using 87 GHz test tone with temperature controlled resistive noise source | 35 |
| Figure 27: Gain compression versus frequency with 300K input | 36 |
| Figure 28: Assembly drawing of the WR-12 RF feedthrough | 38 |
| Figure 29: Measured performance of several WR-12 vacuum RF feedthrough assemblies | 38 |
| Figure 30: Photographs of the fully assembled Band 2 prototype cartridge | 39 |
| Figure 31: Cold cartridge compared with FETMS coordinate system | 40 |
| Figure 32: In-house inclinometer measurements of feed horn tilt | 41 |
| Figure 33: Center of the lens measurement | 42 |
| Figure 34: Predicted temperature distribution for Band 2 CCA on cool down | 43 |
| Figure 35: Predicted feed displacement from cooling | 43 |
| Figure 36: Vibration Mode Shapes: 1 st Mode – 82.2 Hz, 2 nd Mode – 111.7 Hz | 45 |
| Figure 37: Proposed location for an additional OMT support frame fasteners (one on each side) | 46 |
| Figure 38: Measured Gain and Return Loss of RF Filters | 47 |
| Figure 39: Photograph of the dual polarization 2SB down-converter assembly | 49 |
| Figure 40: Photograph of the top and bottom portion of the 90° RF hybrid split block assembly (WR-12) | 50 |
| Figure 41: Plot shows the simulated amplitude imbalance between the RF hybrid ports | 51 |
| Figure 42: Plot shows the simulated isolation between the isolated RF hybrid ports | 52 |
| Figure 43: Measured insertion loss of the RF hybrid(s) from the input port to the two output ports | 53 |
| Figure 44: Measured phase imbalance between the two output ports of the quadrature hybrid | 54 |
| Figure 45: Photograph of the top and bottom portion of the Y-splitter split block assembly (WR-12) | 55 |
| Figure 46: MAC Technology C7256D Hybrid Outline Drawing | 57 |

| | | |
|---|---|------------------------------------|
|  | ALMA Project | Date: 2017-12-27 Page: 5 of 117 |
| | Design and testing of a Prototyped Band 2 Cartridge Final Report | |


List of Figures

| | |
|---|-----------|
| Figure 47: Measured Amplitude and Phase Balance for MAC Technology C7256 | 57 |
| Figure 48: Calculation of the amplitude & phase imbalances and estimated image rejection for the 2SB mixer design. | 58 |
| Figure 49: RF, LO, and IF Band Frequency Ranges..... | 61 |
| Figure 50: NASA Outgassing properties for Buna-N | 64 |
| Figure 51: NASA Outgassing properties for Viton..... | 65 |
| Figure 52: Band 2 Cartridge Wiring Diagram, from [RD 20]..... | 66 |
| Figure 53: 15 K Wiring Koller Heat Sink | 67 |
| Figure 54: Band 2 Cartridge Pigtail Wiring, from [RD 21] | 67 |
| Figure 55: Band 2 Cartridge Pigtail LNA Wiring, from [RD 48] | 68 |
| Figure 56: Schematic of the bias protection circuits (Reference only, from [RD 50])..... | 69 |
| Figure 57: Noise Temperature for Polarization-0, using the 80 nm gate length InP HEMT based MIC cryogenic amplifier. | 70 |
| Figure 58: Noise Temperature for Polarization-1, using the 80 nm gate length InP HEMT based MIC cryogenic amplifier. | 71 |
| Figure 59: Measured Retn Loss of OMT+Feed with/without IR filter | 72 |
| Figure 60: Receiver noise temperature of the Band 2 prototype cartridge using a MMIC based LNA | 73 |
| Figure 61: Photo of dual polarization 2SB downconverter | 74 |
| Figure 62: Image Rejection and Conversion Loss for LO = 86 GHz (Pol-0 channel). | 75 |
| Figure 63: Image rejection and Conversion Loss for LO = 84 GHz (Pol-0 channel). | 75 |
| Figure 64: Image rejection and Conversion Loss for LO = 82 GHz (Pol-0 channel). | 76 |
| Figure 65: Image rejection and Conversion Loss for LO = 80 GHz (Pol-0 channel). | 76 |
| Figure 66: Image rejection and Conversion Loss for LO = 78 GHz (Pol-0 channel). | 77 |
| Figure 67: Image rejection and Conversion Loss for LO = 76 GHz (Pol-0 channel). | 77 |
| Figure 68: Image rejection and Conversion Loss for LO = 74 GHz (Pol-0 channel). | 78 |
| Figure 69: Image rejection and Conversion Loss for LO = 72 GHz (Pol-0 channel). | 78 |
| Figure 70: Image rejection and Conversion Loss for LO = 86 GHz (Pol-1 channel). | 79 |
| Figure 71: Image rejection and Conversion Loss for LO = 84 GHz (Pol-1 channel). | 79 |
| Figure 72: Image rejection and Conversion Loss for LO = 82 GHz (Pol-1 channel). | 80 |
| Figure 73: Image rejection and Conversion Loss for LO = 80 GHz (Pol-1 channel). | 80 |
| Figure 74: Image rejection and Conversion Loss for LO = 78 GHz (Pol-1 channel). | 81 |
| Figure 75: Image rejection and Conversion Loss for LO = 76 GHz (Pol-1 channel). | 81 |
| Figure 76: Image rejection and Conversion Loss for LO = 74 GHz (Pol-1 channel). | 82 |
| Figure 77: Image rejection and Conversion Loss for LO = 72 GHz (Pol-1 channel). | 82 |
| Figure 78: Output Power Density, Pol 0 USB..... | 83 |
| Figure 79: Output Power Density, Pol 1 USB..... | 84 |
| Figure 80: Output Power Density, Pol 0 LSB..... | 84 |
| Figure 81: Output Power Density, Pol 1 LSB..... | 85 |
| Figure 82: Power Density Slope, Pol 0 USB | 85 |
| Figure 83: Power Density Slope, Pol 1 USB | 86 |
| Figure 84: Power Density Slope, Pol 0 LSB..... | 86 |
| Figure 85: Power Density Slope, Pol 0 LSB..... | 87 |
| Figure 86: Power variation in 31 MHz window, Pol 0 USB..... | 87 |
| Figure 87: Power variation in 31 MHz window, Pol 1 USB..... | 88 |
| Figure 88: Power variation in 31 MHz window, Pol 0 LSB..... | 88 |
| Figure 89: Power variation in 31 MHz window, Pol 1 LSB..... | 89 |
| Figure 90: Power variation across the entire IF band..... | 89 |
| Figure 91: Total and In-Band Power, Pol 0 (top) and Pol 1 (bottom), USB | 90 |
| Figure 92: Total and In-Band Power, Pol 0 (top) and Pol 1 (bottom), LSB..... | 91 |
| Figure 93: Amplitude Stability, Pol 0 | 92 |
| Figure 94: Amplitude Stability, Pol 1 | 92 |
| Figure 95: Phase Stability | 93 |
| Figure 96: Beam Pattern Phase Lock System Block Diagram | 95 |

| | | |
|---|--|------------------------------------|
|  | ALMA Project | Date: 2017-12-27 Page: 6 of 117 |
| | Design and testing of a Prototype Band 2 Cartridge Final Report | |


List of Figures

| | |
|---|---------------------|
| Figure 97: Final Beam Pointing with Lens 3-2, Cold Az = -0.1798m, El = 0.1876m | 97 |
| Figure 98: Efficiencies for Lens 3-2, Pol 0, cold, nominal secondary position. | 98 |
| Figure 99: Efficiencies for Lens 3-2, Pol 1, cold, pointing: nominal secondary position. | 99 |
| Figure 100: Pol 0 Near- and Far-field Patterns for 78 GHz: Lens 3-2 | 100 |
| Figure 101: Pol 0 Near- and Far-field Patterns for 85 GHz: Lens 3-2, Pol Eff dip, | 101 |
| Figure 102: Final results for Lens 3-2, Pol 0, cold, pointing: actual beam direction. | 102 |
| Figure 103: Efficiencies for Lens 3-2, Pol 1, cold, pointing: actual beam direction. | 103 |
| Figure 104: Measured polarization efficiency of feed horn & lens with and without the 15 K IR filter | 104 |
| Figure 105: Final pointing of Lens 1-1, warm. Lens position was adjusted to match final warm pointing of Lens 3-2. | 105 |
| Figure 106: Lens 1-1, Pol 0, cold, nominal secondary position. Compare to Lens 3-2 in | 106 |
| Figure 107: Lens 1-1, Pol 1, cold, nominal secondary position. Compare to Lens 3-2 in | 107 |
| Figure 108: Pol 0 Near- and Far-field Patterns for 78 GHz: Lens 1-1 | 108 |
| Figure 109: Fresnel lens, Pol 0, cold, actual beam pointing direction. | 110 |
| Figure 110: Fresnel lens, Pol 1, cold, actual beam pointing direction. | 111 |
| Figure 111: Fresnel lens, beam squint, actual beam pointing direction. | 112 |
| Figure 112: Pol 0 Near- and Far-field Patterns for 78 GHz: Fresnel Lens. | 113 |
| Figure 113: Measured Leak Rates of 300K Plates | 114 |
| Figure 114: Assembly Drawing for Band 2 Cartridge | 116 |

| | | |
|---|--|------------------------------------|
|  | ALMA Project | Date: 2017-12-27 Page: 7 of 117 |
| | Design and testing of a Prototype Band 2 Cartridge Final Report | |

List of Tables

| | |
|--|-------------------|
| <u>Table 2: Product Tree for Band 2 Cartridge</u> | <u>8</u> |
| <u>Table 3: Reference Document List</u> | <u>9</u> |
| <u>Table 4 : Simulated values of the beam taper from the corrugated horn in the 20° beam direction.</u> | <u>22</u> |
| <u>Table 5: Lens parameters.</u> | <u>25</u> |
| <u>Table 6: Measured illumination taper at 3.6° for the various feed horn lens combinations.</u> | <u>27</u> |
| <u>Table 7: Feed horn tilt (in degrees)</u> | <u>41</u> |
| <u>Table 8: Displacement of the feed horn aperture center point due to cooling.</u> | <u>43</u> |
| <u>Table 9: Static stresses from thermal loads</u> | <u>44</u> |
| <u>Table 10: Cartridge Mechanical Deflections.</u> | <u>44</u> |
| <u>Table 11: Lowest ten modal (natural) frequencies for the Band 2 cold cartridge assembly.</u> | <u>45</u> |
| <u>Table 12: Lowest Natural Frequencies</u> | <u>47</u> |
| <u>Table 13: Requirements For Band 6 Warm IF Amps.</u> | <u>56</u> |
| <u>Table 14: Specifications for IF Hybrids</u> | <u>56</u> |
| <u>Table 15: Measured Image Rejection Table.</u> | <u>59</u> |
| <u>Table 16: Power Dissipation from Cold LNAs</u> | <u>62</u> |
| <u>Table 17: Thermal Loading from Waveguide</u> | <u>62</u> |
| <u>Table 18: Static and On-State Heat Loads from Waveguides and Wiring</u> | <u>63</u> |
| <u>Table 19: Room Temperature Pointing Compensation Calculations</u> | <u>96</u> |
| <u>Table 20: Mass Budget</u> | <u>115</u> |

| | | |
|---|--|------------------------------------|
|  | ALMA Project | Date: 2017-12-27 Page: 8 of 117 |
| | Design and testing of a Prototype Band 2 Cartridge Final Report | |

1. Purpose and Scope

This document describes the Band 2 cold cartridge design and is written to compare to the specifications in [\[RD 02\]](#). Compliance with specifications is provided in [\[RD 14\]](#).

This document is also intended to serve as the final project report, although at the time of writing, a no-cost extension has been granted to extend the formal project deadline through November 30, 2018. This no-cost extension provides time for the ongoing CRAL wafer fabrication which is intended to produce additional MMIC amplifier devices of the desired type in sufficient quantities to support any future production activity. This was triggered by a request for the no-cost extension of the sub-award for this work under the Band 2 project.

2. Acknowledgements

We wish to thank Alvaro Gonzalez of NAOJ for his detailed design and analysis of optics design for the original Band 2 frequency range of 67 – 90 GHz as well as for designing the Fresnel lens. The patterns using that lens are shown in Section [8.7.5](#).


In addition, we are grateful for Alvaro's design and fabrication of prototype components (HDPE lens, corrugated horn, and waveguide transition) for the extended ALMA Band 2+ (67 – 95 GHz) [\[RD 31\]](#).

3. Scope

The Band 2 Cold cartridge is comprised of the following Level 4 components. Note that the existing ALMA Product Tree only covers the Band 2 cartridge at a high level and does not include specific Level 4 components identified below. Once the cartridge design is adopted, then the ALMA Product Tree will need to be revised appropriately.

The Band 2 Local Oscillator is comprised of the Level 4 components specified in [Table 2](#) under Section 40.10.02. Note that the existing ALMA Product Tree only covers the Band 2 Local Oscillator at a high level and does not include specific Level 4 components identified below. Once the cartridge design is adopted, then the ALMA Product Tree will need to be revised appropriately. The Band 2 local oscillator modules are identical to those in the Band 6 Warm Cartridge Assembly, and are consequently not covered in detail in this report. An overview is provided along with notes on differences, when present.

| Table 1: Product Tree for Band 2 Cartridge | |
|--|--|
| Product Tree No. | Subassembly |
| 40.02.02 | Band 2 Cartridge |
| 40.02.02.00 | General |
| 40.02.02.01 | Band 2 cold optics |
| 40.02.02.02 | Band 2 warm optics/lens |
| 40.02.02.03 | Band 2 ortho mode transducer |
| 40.02.02.04 | Band 2 IQ Downconverter/integrated quadrature hybrid |
| 40.02.02.05 | Band 2 IF Quadrature Hybrid |
| 40.02.02.06 | Band 2 Room temperature RF amplifier |
| 40.02.02.07 | Band 2 support structure |
| 40.02.02.08 | Band 2 protection board |

| | | |
|---|--|------------------------------------|
|  | ALMA Project | Date: 2017-12-27 Page: 9 of 117 |
| | Design and testing of a Prototype Band 2 Cartridge Final Report | |

| Table 1: Product Tree for Band 2 Cartridge | |
|--|--|
| Product Tree No. | Subassembly |
| 40.02.02.09 | Band 2 cartridge wiring |
| 40.02.02.10 | Band 2 cartridge electrical feedthroughs |
| 40.02.02.11 | |
| 40.02.02.12 | Band 2 temperature sensors |
| 40.02.02.13 | Band 2 Warm IF amplifier |
| 40.04.02 | Cartridge Bias Module |
| 40.04.02.00 | General |
| 40.04.02.01 | Cartridge Bias Board Assembly |
| 40.04.02.02 | Wiring Adapter Board Assembly |
| 40.10.02 | Band 2 First Local Oscillator |
| 40.10.02.00 | General |
| 40.10.06 | Band 6 First Local Oscillator |
| 40.10.06.00 | General |
| 40.10.06.01 | YIG Tuned Oscillator |
| 40.10.06.02 | Active Multiplier Chain |
| 40.10.06.03 | PLL Box |
| 40.10.06.04 | LO Controller |
| 40.10.06.05 | Heat Sinks |
| 40.10.06.06 | Waveguides |
| 40.10.06.07 | Cables and Connectors |
| 40.10.06.08 | Power Amplifier |
| 40.11.02 | Band 2 Warm Cartridge assembly |
| 40.11.02.00 | General |
| 40.11.02.01 | Frame |
| 40.11.02.02 | Main Wiring Harness |
| 40.11.02.03 | Cables and Connectors |

4. Reference Documents (RDs)

The documents in [Table 3](#) below are referenced in the text of this document and contain additional information. Documents with ALMA numbers contain hyperlinks to ALMA EDM.

| Table 2: Reference Document List | | |
|----------------------------------|--|--|
| No. | Document Title | Reference |
| [RD 01] | Front-End Sub-System for the 12 m-Antenna Array Technical Specifications | ALMA-40.00.00.00-001-A-SPE |
| [RD 02] | Band 2 Cartridge Specifications | FEND-40.02.06.00-001-A-SPE |
| [RD 03] | ALMA Project Plan | ALMA-10.04.00.00-001-A-PLA |


| | | |
|---|--|-------------------------------------|
|  | ALMA Project | Date: 2017-12-27 Page: 10 of 117 |
| | Design and testing of a Prototype Band 2 Cartridge Final Report | |

Table 2: Reference Document List

| No. | Document Title | Reference |
|---------|--|---|
| [RD 04] | ALMA Documentation Control Plan | ALMA-80.02.00.00-011-F-PLA |
| [RD 05] | ALMA Documentation Standards | ALMA-80.02.00.00-003-G-STD |
| [RD 06] | FE IPT Documentation Approval Plan | FEND-40.00.00.00-100-A-PLA |
| [RD 07] | ALMA Product Tree | ALMA-80.03.00.00-001-R-LIS |
| [RD 08] | Cryostat Technical Specifications | FEND-40.03.00.00-002-C-SPE |
| [RD 09] | Vacuum Requirements for receiver components inside the ALMA Front End Cryostat | FEND-40.03.00.00-015-A-SPE |
| [RD 10] | Band 2+ Receiver Development Plan | FEND-40.02.02.00-0042-A-PLA |
| [RD 11] | Band 2+ Receiver Safety Plan | FEND-40.02.00.00-0039-A-PLA |
| [RD 12] | Band 2+ Receiver Management Plan | FEND-40.02.02.00-0033-A-PLA |
| [RD 13] | Band 2+ Receiver Statement of Work (SOW) | FEND-40.02.02.00-0034-A-SOW |
| [RD 14] | Band 2+ Test Plan and Verification Matrix | FEND-40.02.02.00-0041-A-PLA |
| [RD 15] | Band 2+ Cold Cartridge Assembly Technical Specifications | FEND-40.02.02.00-0037-A-SPE |
| [RD 16] | Band 2+ Test Plan and Verification Matrix | FEND-40.02.02.00-0045-C-VER |
| [RD 17] | Band 2+ Cold Cartridge Assembly Configured Items Data List (CIDL) | FEND-40.02.02.00-0044-A-LIS |
| [RD 18] | Band 2+ Cold Cartridge Assembly Procedures | FEND-40.02.02.00-0032-A-PRO |
| [RD 19] | Band 2+ Cold Cartridge Assembly Test Plan | |
| [RD 20] | Wiring, Band 2 Cartridge, Vacuum Space | FEND-40.02.02.00-0020-A-DWG |
| [RD 21] | Wiring Diagram, Band 2 Cartridge Pigtails | FEND-40.02.02.00-0022-A-DWG |
| [RD 22] | Band 2 Beam Patterns, 2015-06-15, Effland and Meadows | link on cvfiler |
| [RD 23] | Band 2 Beam Patterns, 2015-11-06, Effland, Meadows, and McLeod | link on cvfiler |
| [RD 24] | Calculation of Efficiencies, <i>etc</i> , from Beam-Scanning Data, R. Hills, 2008-06-22 | NRAO Public WIKI |
| [RD 25] | Electromagnetic properties and optical analysis of the ALMA antennas and Front Ends, TICRA | ALMA-80.04.00.00-026-A-REP |
| [RD 26] | Band 5 Cartridge Beam Pattern and Phase Stability Test Procedure | FEND-40.02.05.00-151-B-PRO |
| [RD 27] | ALMA Beam Efficiency Calculator User Manual | FEND-40.09.00.00-014-B-MAN |


| | | |
|---|--|-------------------------------------|
|  | ALMA Project | Date: 2017-12-27 Page: 11 of 117 |
| | Design and testing of a Prototype Band 2 Cartridge Final Report | |

Table 2: Reference Document List

| No. | Document Title | Reference |
|---------|--|--|
| [RD 28] | Band 8 Vacuum WG flange assembly | FEND-40.02.08.09-0004-A-DWG |
| [RD 29] | Band 2 Cartridge Body Mechanical Analysis | FEND-40.02.02.07-0001-A-REP |
| [RD 30] | “Development of ALMA Band 2 Optics at NAOJ” 2015, A. Gonzalez | NAOJ-ALMARX-0202-A |
| [RD 31] | “Development of ALMA Band 2+ Optics at NAOJ” (2017-01-19), A. Gonzalez | NAOJ-ALMA-0017-A |
| [RD 32] | Band 2 Tilted Lens Ring | FEND-40.02.02.00-0028-A-DWG |
| [RD 33] | Band 2 Tilted Lens Cover | FEND-40.02.02.00-0029-A-DWG |
| [RD 34] | Band 2 Lens Zoned Style 50 X 50 Spacing | FEND-40.02.02.00-0027-A-DWG |
| [RD 35] | Band 2 Lens - 87P2D #3 | FEND-40.02.02.00-0026-A-DWG |
| [RD 36] | Band 2 Lens Style 2 50 x 50 Spacing | FEND-40.02.02.00-0025-A-DWG |
| [RD 37] | Band 2 Lens - F865050 | FEND-40.02.02.00-0024-A-DWG |
| [RD 38] | Band 2 Cartridge Assembly Drawing | FEND-40.02.02.00-0021-A-DWG |
| [RD 39] | Band 6 Cartridge 4K Stage Heat Sink Assy | FEND-40.02.06.00-248-A-DWG |
| [RD 40] | Band 6 Cartridge 4K Heatsink (Koller) PCB | FEND-40.02.06.00-156-A-DWG |
| [RD 41] | ICD Between Band 2 Cartridge and WCA | FEND-40.02.02.00-40.11.02.00-A-ICD |
| [RD 42] | Band 6 Cartridge Bias Protection Board Specifications | FEND-40.02.06.07-003-A-SPE |
| [RD 43] | 300K Feed-Thru Connector Housing | FEND-40.00.00.00-076-G-DWG |
| [RD 44] | 300K Feed-Thru Connector Assembly | FEND-40.00.00.00-077-G-DWG |
| [RD 45] | Band 6 Cartridge 15, 110 K Heatsinks | FEND-40.02.06.00-015-C-DWG |
| [RD 46] | Band 6 Cartridge, 4K Prototype Heat Sink | FEND-40.02.06.00-013-D-DWG |
| [RD 47] | Band 6 Cartridge 4K Heat Sink Assembly Procedures | FEND-40.02.06.10-003-A-PRO |
| [RD 48] | Wiring Diagram, Band 2 Cartridge, Vacuum Space | FEND-40.02.02.00-0020-A-DWG |
| [RD 49] | ICD between Band 2 Cartridge and Front End IF Switch | FEND-40.02.02.00-40.08.01.00-A-ICD |
| [RD 50] | Band 6 Cartridge Bias Protection Board Schematic | FEND-40.02.06.07-001-C-DWG |



| | | |
|---|--|-------------------------------------|
|  | ALMA Project | Date: 2017-12-27 Page: 12 of 117 |
| | Design and testing of a Prototype Band 2 Cartridge Final Report | |

Table 2: Reference Document List

| No. | Document Title | Reference |
|---------|--|---|
| [RD 51] | Band 6 LO Waveguide Window Assembly He Leak Test Procedures | FEND-40.02.06.02-009-A-PRO |
| [RD 52] | ICD between Band 2 Cartridge and Bias Circuits | FEND-40.02.02.00-40.04.02.00-A-ICD |
| [RD 53] | Band 2 horn Assembly Drawing | FEND-40.02.02.00-0030-A-DWG |
| [RD 54] | ICD Between Band 2 Cartridge and Dewar | FEND-40.02.02.00-40.03.01.00-A-ICD |
| [RD 55] | A. R. Kerr and R. Groves, "Measurements of Copper Heat Straps Near 4 K With and Without Apiezon-N Grease," NRAO Electronics Division Technical Note No. 204 | http://www.gb.nrao.edu/electronics/edtn/edtn_204.pdf |
| [RD 56] | CRE To Increase Static Thermal Loading of 110K stage | FEND-40.00.00.00-001-A-CRE |
| [RD 57] | Front End Local Oscillator Design Report | FEND-40.10.00.00-064-F-REP |
| [RD 58] | Band 2 Lens - F865050 (lens 3-1) | FEND-40.02.02.00-0024-A-DWG |
| [RD 59] | Band 2 Lens Style 2 50 x 50 Spacing (Lens 3-2) | FEND-40.02.02.00-0025-A-DWG |
| [RD 60] | Band 2 Lens - 87P2D (Lens 3-3) | FEND-40.02.02.00-0026-A-DWG |
| [RD 61] | Band 2 Lens Zoned Style 50 X 50 Spacing | FEND-40.02.02.00-0027-A-DWG |
| [RD 62] | Band 2 Lens Zoned Style 50 X 50 Spacing | FEND-40.02.02.00-0027-A-DWG |
| [RD 63] | E. Bryerton, X. Mei, Y. Kim, W. Deal, W. Yoshida, M. Lange, J. Uyeda, M. Morgan, and R. Lai, "A W-Band Low-Noise Amplifier with 22K Noise Temperature," IEEE MTT-S Intl. Microwave Symposium, Boston, MA, June 2009. | http://ieeexplore.ieee.org/document/5165788/ |
| [RD 64] | Slides from "Vacuum Sealing Technology", Kurt Sonderegger, Product Group Manager, All Metal Valve Group | https://cas.web.cern.ch/cas/Spain-2006/PDFs/Sonderegger.pdf |
| [RD 65] | NASA Outgassing Properties | https://outgassing.nasa.gov/ |
| [RD 66] | Front End Optics Design Report | FEND-40.02.00.00-035-B-REP |
| [RD 67] | Appendix 2 to the Front End Optics Design Report | FEND-40.02.00.00-035-B-REP-Appendix2 |
| [RD 68] | E.D. Marquardt, J.P. Le, and Ray Radebaugh, "Cryogenic Material Properties Database," 11th International Cryocooler Conf., Keystone, Co, June 2000 | http://cryogenics.nist.gov/Papers/Cryo_Materials.pdf |
| [RD 69] | Band 6 LO Specifications | FEND-40.10.06.00-001-A-SPE |

| | | |
|---|--|-------------------------------------|
|  | ALMA Project | Date: 2017-12-27 Page: 13 of 117 |
| | Design and testing of a Prototype Band 2 Cartridge Final Report | |

5. Cartridge Overview

The ALMA Band 2 cartridge converts dual-linearly polarized millimeter wave signals in the band from 67 GHz to 90 GHz to an intermediate frequency band from 4 GHz to 12 GHz (with reduced performance over the extended Band 2+ RF band, 90-95 GHz). The two orthogonal polarization inputs are converted to four outputs corresponding to upper and lower sidebands for each polarization. Low-noise millimeter wave performance is obtained using cryogenic low noise amplifiers operating at a physical temperature of 15 K. The Band 2 local oscillator modules are identical to those in the Band 6 Warm Cartridge Assembly, and are consequently not covered in detail in this report. The existing ALMA local oscillator design report already contains the necessary design details for the Band 2 local oscillator system. Consequently, only an overview of the local oscillator is provided in this report along with notes on differences, if and when present.

[Figure 1](#) shows the layout of the cold cartridge components and [Figure 2](#) shows the entire Band 2 cold cartridge – *i.e.*, the cartridge without the Warm Cartridge Assembly which contains the downconverter, local oscillator components and monitor and control circuits.

The cartridge consists of two cooled stages with operating temperatures 15 K, and 110 K, and a room-temperature base-plate which acts as the vacuum seal. The stages are supported by G10 shells which have low thermal conductance. On the 110 K stage are the heat sinks for the RF waveguide, coax cables, and wiring. The 15 K stage has the, horn, OMT, cryogenic low noise amplifiers, necessary heat sinks, and output RF waveguides.

A block diagram of the Band 2 receiver (comprising of the cold cartridge assembly and the warm cartridge assembly) is shown in [Figure 4](#). After passing through the room temperature lens (which also functions as the vacuum window) and infrared filters, which are considered part of the outer vacuum vessel, the RF signal enters the feed horn (Section [7.2.3](#)). The two polarizations are then split in an OMT (Section [7.2.2](#)) and delivered to the two cryogenic low noise amplifiers which are biased as per the ICD [\[RD 52\]](#) using the standard ALMA preamp bias supply from the cartridge bias module.

A temperature sensor is installed on each cryogenic low noise amplifier body for troubleshooting and to monitor block temperatures. Additional temperature sensors are installed on the 110 K and 15 K cartridge stages to facilitate trouble-shooting of the cartridge.

Each polarization channel has a sideband-separating downconverter as described in Section [7.9](#). These are physically located outside of the vacuum/cold space on the warm cartridge assembly alongside the local oscillator components. Each sideband-separating mixer contains two component mixers (*i.e.*, double-sideband mixers), and receive the RF signal from the RF quadrature hybrids described in Section [7.9](#). The two I & Q IF outputs operating from 4-12 GHz from each mixer pair are connected via phase matched cables to an IF quadrature hybrid which separates the IF signals originating in the two sidebands. Both sidebands from each polarization channel are brought out of the cartridge on coaxial cables.

Each receiver contains four warm IF amplifiers, one for each sideband in each polarization, following the IF hybrids again on the room temperature area at the back of the cartridge to increase IF output power level prior to routing to the IF selector switch. [Figure 3](#) shows the photo of the Warm Cartridge Assembly and the arrangement of the IF downconverter and LO components on it.

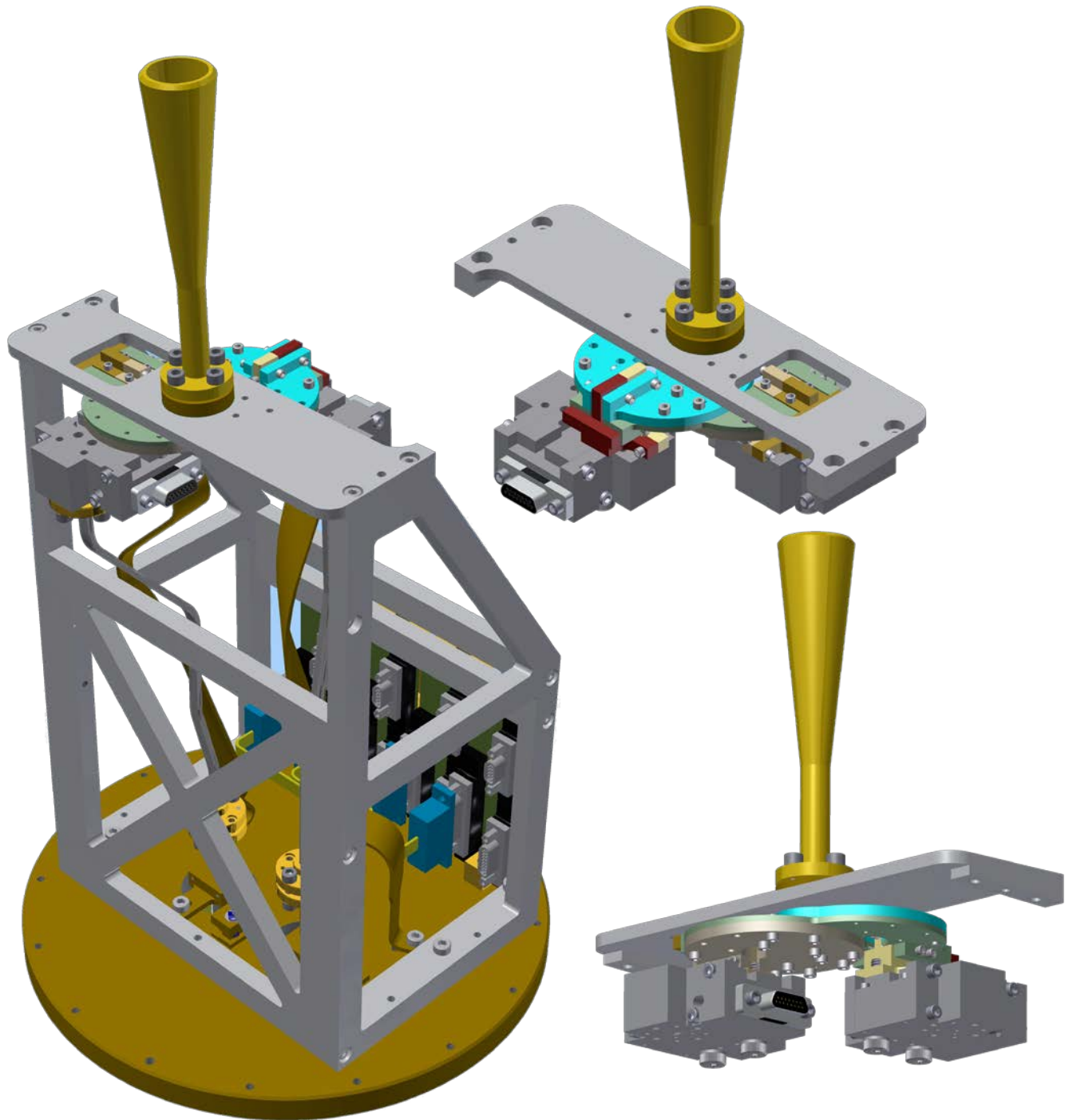


Figure 1: 3D rendering showing the layout of Band 2 Cartridge 15 K Components.

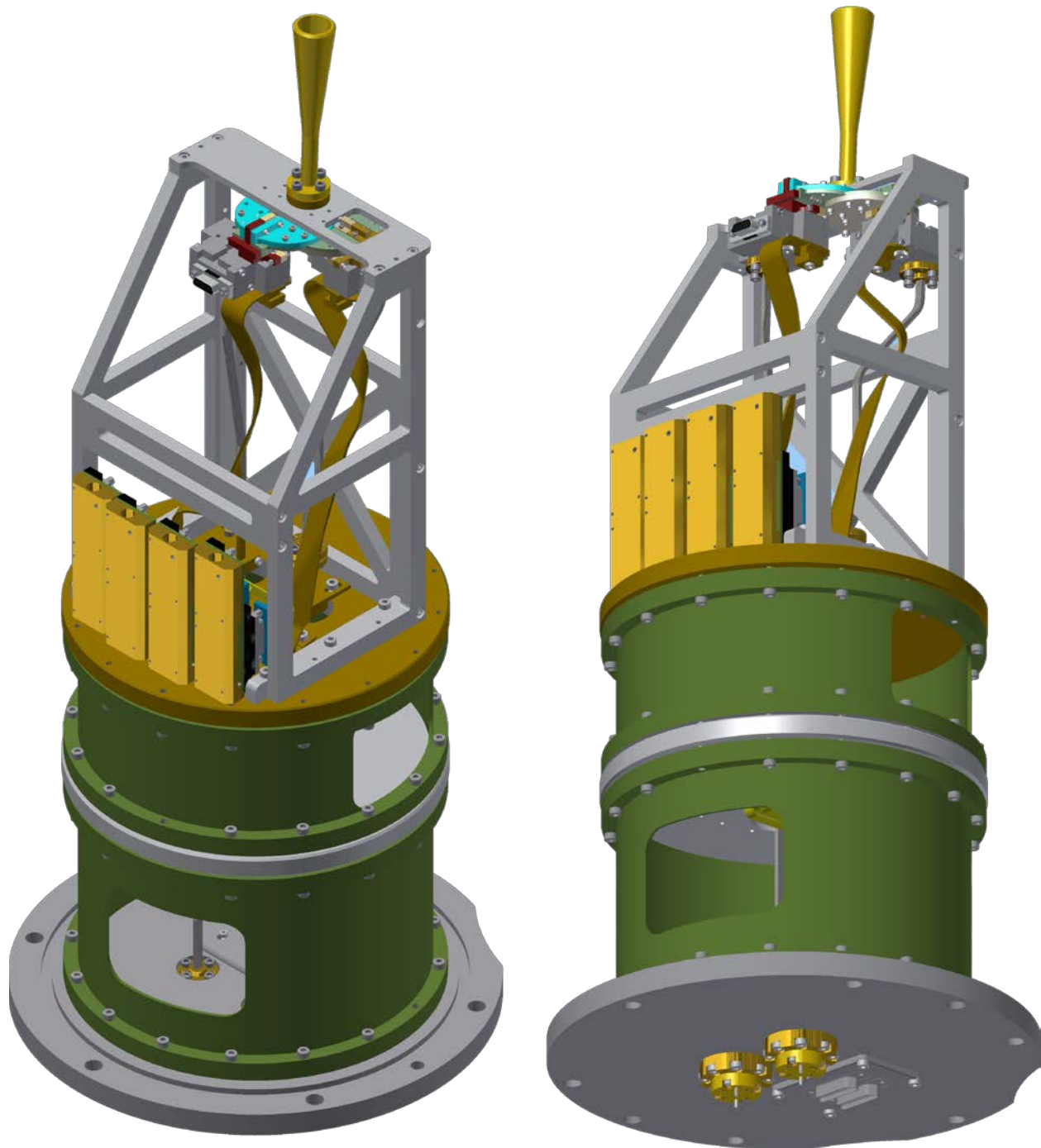



Figure 2: 3D rendering of the model of the entire Band 2 Cold Cartridge Assembly.

| | | |
|---|--|-------------------------------------|
|  | ALMA Project | Date: 2017-12-27 Page: 16 of 117 |
| | Design and testing of a Prototype Band 2 Cartridge Final Report | |

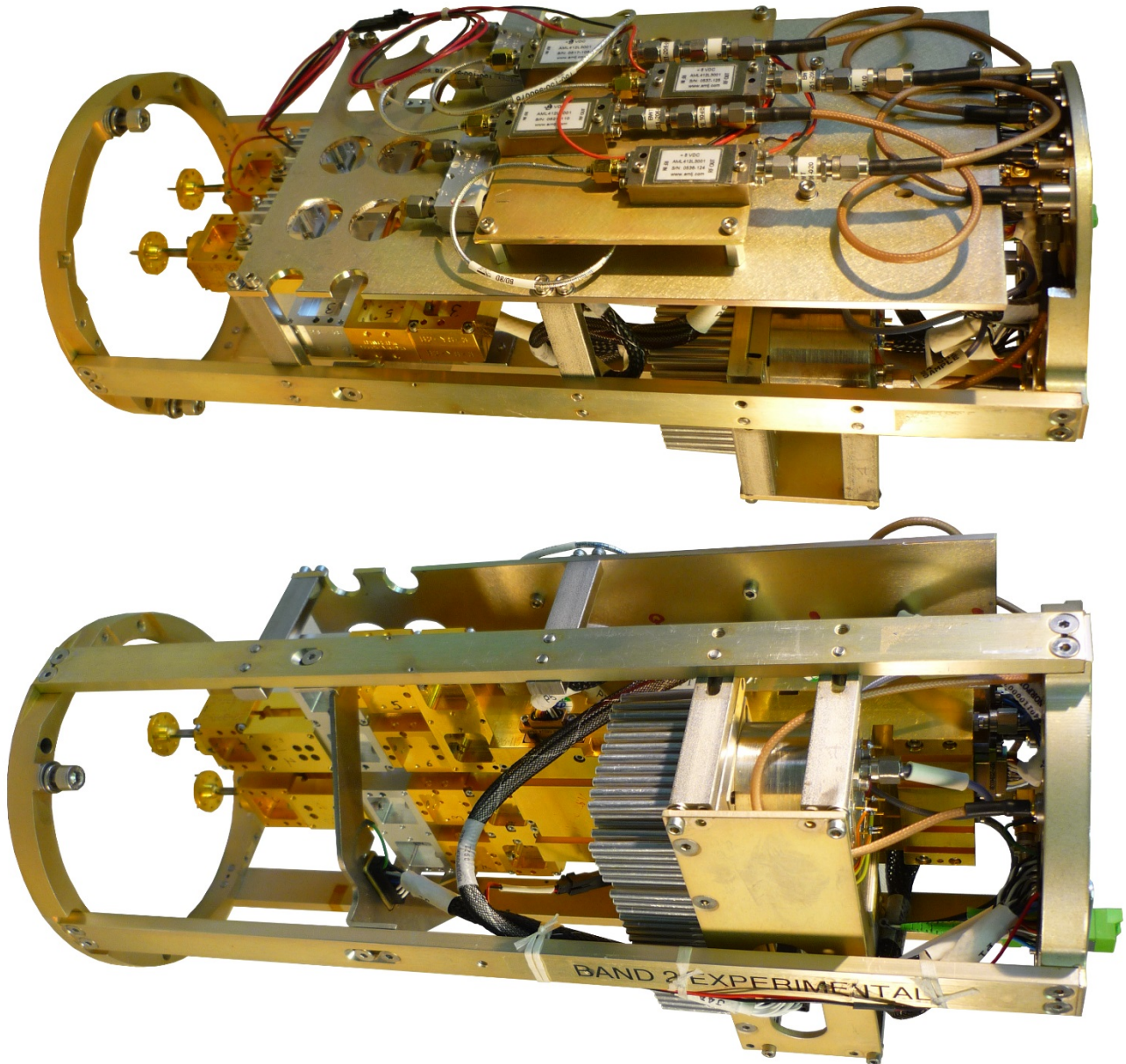


Figure 3: WCA Photos

Photographs of the Warm Cartridge Assembly showing the layout of the LO and downconverter components (lower photo), and the placement of IF amplifiers (upper photo).



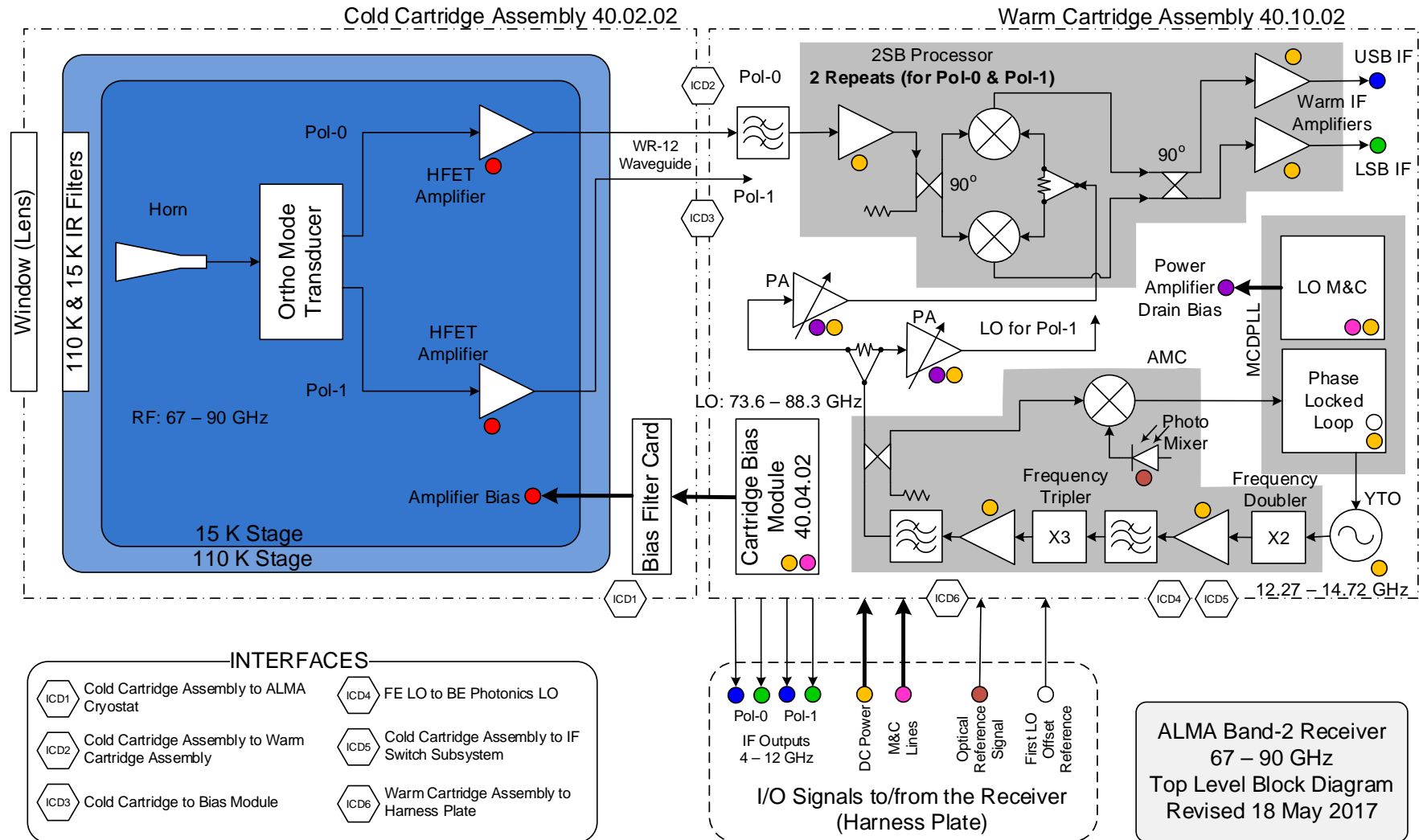
Design and testing of a Prototype Band 2 Cartridge: Final Report

Doc #: Final **Report**

Date: 2017-12-27

Status: **Error! Reference source not found.**

Page: 17 of 117





| | | |
|--|--|--|
|  | <p>Design and testing of a Prototype Band 2 Cartridge: Final Report</p> | <p>Doc #: Final <u>Report</u> Date: 2017-12-27 Status: Error! Reference source not found. Page: 18 of 117</p> |
|--|--|--|

Figure 4: Band 2 Receiver Block Diagram

| | | |
|---|--|-------------------------------------|
|  | ALMA Project | Date: 2017-12-27 Page: 19 of 117 |
| | Design and testing of a Prototype Band 2 Cartridge Final Report | |

6. Specifications

Cartridge specifications are given in [\[RD 15\]](#). For convenience, they are repeated in Section 8, “[Prototype Cartridge performance](#)”.

7. Components

7.1. Cascade Design


The block diagram of the cartridge is shown in [Figure 4](#) and a cascade analysis is given in [Figure 5](#). Notes regarding the tabulated values:

1. The horn and OMT losses were not measured at cryogenic temperatures. So the insertion loss numbers provided in the table are best guess estimates.
2. The IR filter losses are based on their 1.5% loss specification values (Band 2 IR filters were not evaluated prior to integration into the test cryostat.)
3. Lens loss is an estimate based on the lens thickness and best available tan delta values.
4. E-band amplifier gain and noise figure are frequency averages of measured values.
5. For the rest of the components (which are not significant contributors to system noise) the gain/loss and noise figures are a combination of measured/specification values.

The goal of the exercise to tabulate these values, was to provide a way to confirm that we were not seeing unexplained excess noise in the measurements (measurement data presented later in this report), and to provide a way to understand the most significant contributors to the overall performance.

| Band 2 Receiver stage | Gain | Cumulative Gain to preceding stage | Noise Figure | Noise Temperature | Tequivalent |
|-------------------------------------|----------------|------------------------------------|--------------|-------------------|---------------|
| Lens/Window (room temperature) | -0.1 dB | 0.0 dB | 0.1 dB | 8.9 K | 8.9 K |
| IR Filters | -0.1 dB | -0.1 dB | 0.1 dB | 1.4 K | 1.5 K |
| Feedhorn (15 K) | -0.1 dB | -0.3 dB | 0.1 dB | 0.3 K | 0.4 K |
| OMT | -0.1 dB | -0.4 dB | 0.1 dB | 0.3 K | 0.4 K |
| E-Band MIC Amplifier (15 K) | 35.0 dB | -0.5 dB | | 36.5 K | 40.6 K |
| Waveguides, feed-thru and BPF | -4.0 dB | 34.5 dB | 4.0 dB | 453.6 K | 0.2 K |
| W-Band Amplifier (room temperature) | 14.0 dB | 30.5 dB | 3.5 dB | 371.6 K | 0.3 K |
| 2 SB Downconverter | -12.0 dB | 44.5 dB | 12.0 dB | 4454.7 K | 0.2 K |
| Warm IF Amplifier | 30.0 dB | 32.5 dB | 2.0 dB | 175.5 K | 0.1 K |
| | | | | | |
| Total | 62.5 dB | | | | 52.4 K |

[https://sharepoint.nrao.edu/cdl/Shared Documents/ALMA/Band 2/Block Diagrams/\[Band-2 Teq calculator COLD.xlsx\]MIC](https://sharepoint.nrao.edu/cdl/Shared Documents/ALMA/Band 2/Block Diagrams/[Band-2 Teq calculator COLD.xlsx]MIC)

| | | |
|---|--|-------------------------------------|
|  | ALMA Project | Date: 2017-12-27 Page: 20 of 117 |
| | Design and testing of a Prototype Band 2 Cartridge Final Report | |

| Band 2 Receiver stage | Gain | Cumulative Gain to preceding stage | Noise Figure | Noise Temperature | Tequivalent |
|-------------------------------------|----------------|------------------------------------|--------------|-------------------|---------------|
| Lens/Window (room temperature) | -0.1 dB | 0.0 dB | 0.1 dB | 8.9 K | 8.9 K |
| IR Filters | -0.1 dB | -0.1 dB | 0.1 dB | 1.4 K | 1.5 K |
| Feedhorn (15 K) | -0.1 dB | -0.3 dB | 0.1 dB | 0.3 K | 0.4 K |
| OMT | -0.1 dB | -0.4 dB | 0.1 dB | 0.3 K | 0.4 K |
| E-Band MMIC Amplifier (15 K) | 35.0 dB | -0.5 dB | | 26.3 K | 29.2 K |
| Waveguides, feed-thru and BPF | -4.0 dB | 34.5 dB | 4.0 dB | 453.6 K | 0.2 K |
| W-Band Amplifier (room temperature) | 14.0 dB | 30.5 dB | 3.5 dB | 371.6 K | 0.3 K |
| 2 SB Downconverter | -12.0 dB | 44.5 dB | 12.0 dB | 4454.7 K | 0.2 K |
| Warm IF Amplifier | 30.0 dB | 32.5 dB | 2.0 dB | 175.5 K | 0.1 K |
| | | | | | |
| Total | 62.5 dB | | | | 41.1 K |

[https://sharepoint.nrao.edu/cdl/Shared Documents/ALMA/Band 2/Block Diagrams/\[Band-2 Teq calculator COLD.xlsx\]CRAL MMIC](https://sharepoint.nrao.edu/cdl/Shared Documents/ALMA/Band 2/Block Diagrams/[Band-2 Teq calculator COLD.xlsx]CRAL MMIC)

Figure 5: Cascade noise and gain calculations (Top: Using Cryo-3 device based MIC CLNAs, and Bottom: Using CRAL MMIC based CLNAs)

The following tables and discussion provide the power budget and the calculated headroom to 1 dB compression point for each amplifier.

| Amplifier stage in CCA/WCA | Cumulative Gain | Eff. Bandwidth | Output Power | Headroom |
|---------------------------------|-----------------|----------------|--------------|----------|
| Cryogenic Amplifier (15 K) | 34.5 dB | 28 GHz | -31.7 dBm | 33.7 dB |
| RF Amplifier (room temperature) | 44.5 dB | 28 GHz | -21.7 dBm | 23.7 dB |
| IF Amplifier | 62.5 dB | 8 GHz | -9.1 dBm | 19.1 dB |

273 K source case

Figure 6: Calculated output power and headroom to 1 dB compression point for each of the amplifier stages in the receiver.

The above tabulation indicates the power level/budget situation for the prototype cartridge as built. While the headroom is sufficient, the output power exceed the recommended values for the FE IF switch interface. For purpose of continued receiver evaluation, a ~ 10 dB attenuator was utilized at the output to make the power levels compliant with the FE requirements. The “excess gain” is due to the use of commercial 30 dB IF amplifiers which were readily available. For the final receiver construction, a 15 dB gain IF amplifier will be specified and procured commercially. The following tables summarize the resulting situation for varying source/sky temperatures and confirm that there is sufficient dynamic range in the signal path and the FE power level requirements are met for all cases.

| Amplifier stage in CCA/WCA | Cumulative Gain | Eff. Bandwidth | Output Power | Headroom |
|---------------------------------|-----------------|----------------|--------------|----------|
| Cryogenic Amplifier (15 K) | 34.5 dB | 28 GHz | -34.3 dBm | 36.3 dB |
| RF Amplifier (room temperature) | 44.5 dB | 28 GHz | -24.3 dBm | 26.3 dB |
| IF Amplifier | 47.5 dB | 8 GHz | -26.7 dBm | 36.7 dB |

Cold sky case

| Amplifier stage in CCA/WCA | Cumulative Gain | Eff. Bandwidth | Output Power | Headroom |
|---------------------------------|-----------------|----------------|--------------|----------|
| Cryogenic Amplifier (15 K) | 34.5 dB | 28 GHz | -31.1 dBm | 33.1 dB |
| RF Amplifier (room temperature) | 44.5 dB | 28 GHz | -21.1 dBm | 23.1 dB |
| IF Amplifier | 47.5 dB | 8 GHz | -23.5 dBm | 33.5 dB |

100C source case

| Amplifier stage in CCA/WCA | Cumulative Gain | Eff. Bandwidth | Output Power | Headroom |
|---------------------------------|-----------------|----------------|--------------|----------|
| Cryogenic Amplifier (15 K) | 34.5 dB | 28 GHz | -29.0 dBm | 31.0 dB |
| RF Amplifier (room temperature) | 44.5 dB | 28 GHz | -19.0 dBm | 21.0 dB |
| IF Amplifier | 47.5 dB | 8 GHz | -21.5 dBm | 31.5 dB |

800 K source case

Figure 7: Calculated output power and headroom to 1 dB compression point for each of the amplifier stages in the receiver, for several different source/sky temperatures.


7.2. Optics

7.2.1. Requirements and Overview

The specifications [\[RD 15\]](#) require a tertiary optics aperture efficiency exceeding 80% and a polarization efficiency greater than 99.5%.

The Band 2 Dewar window located on the top plate of the cryostat is located at a radial distance of 255 mm from the center of the cryostat. To point at the center of the sub reflector, which is located above the center of the cryostat, the Band 2 beam needs to be tilted at an angle of 2.48° towards the cryostat axis.

The sub reflector subtends a half-angle of 3.6° from the secondary focus of the telescope. In order to achieve 80% aperture efficiency, the Band 2 beam, as incident on the sub reflector, should have a nominal illumination taper of about -12 dB at the beam edge. In the ALMA cryostat, the 15 K Gortex filter (1.5 mm thick) has a lower clamp (10 mm thick aluminum) with an aperture of ~ 60 mm, and an upper clamp (1 mm thick aluminum), with an aperture of ~ 25 mm. The 110 K filter has an aperture of ~ 60 mm. The window aperture is ~ 92 mm in diameter.

| | | |
|---|--|-------------------------------------|
|  | ALMA Project | Date: 2017-12-27 Page: 22 of 117 |
| | Design and testing of a Prototype Band 2 Cartridge Final Report | |

7.2.2. Optics Design Options

The baseline ALMA optics design [RD 66], [RD 67] served as the foundation for the Band 2 design presented below. In fact, calculated performance of our design exhibits nearly constant edge taper with frequency, which is similar to the performance of the design given in [RD 66].

Obtaining a frequency independent illumination taper of -12 dB for the desired beam size over the entire frequency range requires feed horns with a diameter of 106 mm and length of 785 mm. The beam waist at 68 GHz was calculated to be 23.71 mm. With the feed aperture placed 5 mm below the 15 K filter, the maximum power that is transmitted through the 92 mm window aperture is 94.53% *i.e.* the beam is truncated. In order to minimize its loss (or noise temperature contribution), the feed horn needs to be cooled to 15 K. Therefore, in addition to a beam truncation of nearly 6%, such a large feed horn will result in excessive thermal loading. In order to circumvent these problems, it was decided to attempt an optics design with a moderate beam waist from the feed horn and transform the beam to the required size by use of reflective or refractive optics.


Reflective optics incorporating a pair of mirrors, one curved and one flat to refocus the beam from the feed horn presented the best option as the losses could be kept low compared to the refractive (lens) optics option. Because of the space constraints inside the cartridge assembly and the cryostat, the mirrors needed to be located on top of the cryostat outside the vacuum space. With the curved mirror located on the top of the window, the flat mirror needed to be located outside the 255 mm radius circle to clear other windows and widgets. The angles of the mirrors were chosen so that the reflected beam was directed towards the sub reflector with an angle larger than 2.48° . The additional offset of the beam from the center of the cryostat and the increased angle of incidence on the sub reflector contributed to a lower overall aperture efficiency and poorer cross polarization performance. Further, the location of the curved mirror above the Band 2 window would also hinder the movement of the robotic arm of the Amplitude Calibration Device. For these reasons, the reflective optics approach was abandoned after some initial analysis.

The beam waist at the Cassegrain focus of the telescope varies between 21.7 and 23.1 mm for edge taper values between -10.8 dB and -12.2 dB at 78 GHz. A properly designed dielectric lens located at an appropriate distance from the feed horn can synthesize the required beam waist size at the Cassegrain focus. Three lenses were designed with varied focal lengths and distances from a moderate-size feed horn. In order to maximize the aperture efficiency, the lens needs to be large – for 84% efficiency, the lens size was calculated to be 20.5λ in diameter at the lowest frequency. Since the 110 K filter aperture is only 60 mm diameter, the lens needs to be located at or outside the 300 K window and since the feed horn is cooled to 15 K, it has to be located on the 15 K stage of the Band 2 receiver cold cartridge. The change of dielectric constant versus temperature was another factor that ruled out cooling the lens to 15 K or 110 K.

7.2.3. Feed Horn Design

Corrugated horns are considered ideal for illuminating reflector antennas since they have desirable characteristics such as wide bandwidth, low loss, circularly symmetric patterns, low cross polarization and a good input impedance match. A linearly tapered corrugated horn with input diameter of 2.06 mm, an aperture diameter of 15.02 mm and length of 86.75 mm was designed for operation with lenses of three different focal lengths.

The spherical phase error at the aperture of the horn is less than 0.1λ , which still causes some changes to the patterns as a function of frequency. Calculated edge taper values (in the 20° beam direction) at three different frequencies are tabulated in Table 4 in the E- and H-planes. This beam when refocused by a dielectric lens results in a nearly constant beam size, independent of frequency. The beam waist radius of the horn is also indicated in the table. For the final horn design, 76 corrugations with a pitch of 0.86 mm were specified and they render about 4 corrugations per wavelength at

| | | |
|---|--|-------------------------------------|
|  | ALMA Project | Date: 2017-12-27 Page: 23 of 117 |
| | Design and testing of a Prototype Band 2 Cartridge Final Report | |

the highest frequency. The depth of the corrugations varies continuously from 0.46λ at the throat to 0.23λ at the aperture (as calculated at the center of the frequency band).

Table 3 : Simulated values of the beam taper from the corrugated horn in the 20° beam direction.

| Frequency (GHz) | Taper in dB at 20° | | Beam waist (mm) | Phase center (mm) |
|--------------------|--------------------|---------|--------------------|----------------------|
| | E-plane | H-plane | | |
| 67 | -9.07 | -10.52 | 4.73 | 2.7 |
| 78 | -14.40 | -15.72 | 4.71 | 3.8 |
| 90 | -23.44 | -22.18 | 4.67 | 5.0 |

7.2.4.Feed Horn Fabrication

At the horn input, a circular to square transition is required, as the feed horn needs to be mated with the ortho-mode transducer (OMT) which has a square input. A stepped circular to square transition was designed for this application. In order to avoid compromising alignment by having to mate another component between the feed horn and the OMT, it was decided to build the transition either into the OMT input or the feed horn flange. Considering the fact that the OMT has to be fabricated in its entirety by milling and that the transition cannot be milled, it was difficult to incorporate the transition into the OMT. The feed horn is fabricated using an electroforming process, so the transition could be integrated as an extension on the flange end of the feed horn. An aluminum mandrel shaped identical to the inside of the feed with a built-in transition was machined using a lathe. Copper was electroformed on the mandrel, cut to size and the aluminum was dissolved in sodium hydroxide. A UG-387 flange was subsequently soldered and the feed horn assembly was flashed with a thin layer of gold. The mechanical drawing of the complete feed horn is given in [\[RD 53\]](#). (As an alternative, a major portion of the feed was machined out of aluminum; the section with the first few corrugations and the transition were fabricated by electroforming and the two pieces mated together with screws. This process is faster as it takes fewer days to electroform the smaller section of the feed, and could be promising for the production phase.)


| | | |
|---|--|-------------------------------------|
|  | ALMA Project | Date: 2017-12-27 Page: 24 of 117 |
| | Design and testing of a Prototype Band 2 Cartridge Final Report | |



Figure 8: Stages of Feed Horn Fabrication

- (Top left) Finished aluminum mandrel after flashing with gold, prior to electro-deposition.
- (Top middle) Mandrel after electro-deposition.
- (Top right) Test mandrel, cut open to reveal the electro-deposition details.
- (Bottom left) Feed horn after dissolving out the aluminum mandrel, but prior to final machining to introduce a taper on the lip.
- (Bottom right) Finished feed horn assembly.

7.2.5. Feed Horn Measurement and Characterization

Far-field patterns of the feed horn were measured in an anechoic chamber. Measurement was done between $\pm 120^\circ$ at 0.5° intervals and from 65 to 92 GHz in 0.5 GHz steps. Co-polarization measurements were made in E-, H- and 45° -planes. In addition, cross-polarization was measured in the 45° -plane. [Figure 9](#) shows the measured (*-Me) and theoretical (*-Th) patterns in the E- and H-planes. The theoretical patterns were calculated using mode-matching software. There is excellent agreement between measurement and theory to the -35 dB level. Additionally, the E- and H-plane patterns match very well demonstrating circular symmetry of the beam. The patterns were measured with the feed horn located such that its phase center was at the center of rotation. The phase center location with respect to the aperture is shown in [Table 4](#).

Cross-polarization was measured with respect to co-polarization in the 45° -plane, which should contain the peak of the cross-polar pattern. Measured co- and cross-polarization patterns in the range of $\pm 60^\circ$ are shown in [Figure 10](#) and for reference, co-polarized beam at 78 GHz is also shown in the figure. The poorest cross-polar peak is noted to be approximately -26 dB at 90 GHz. Predicted co- and cross-pol patterns for 67, 78, 90, and 95 GHz, [Figure 11](#), show peak cross-pol levels ranging from -32 dB to -38 dB with a null on axis. The discrepancies with measured data result from imperfect 45-degree twists that were used on the AUT and source feed during the cross-polarization measurement.

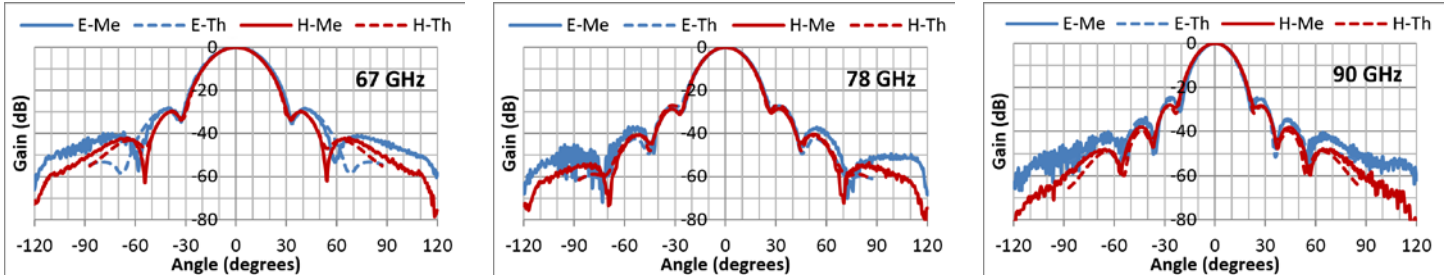


Figure 9: Measured (*-Me) and theoretical (*-Th) patterns in the E- and H-planes of the feed horn.

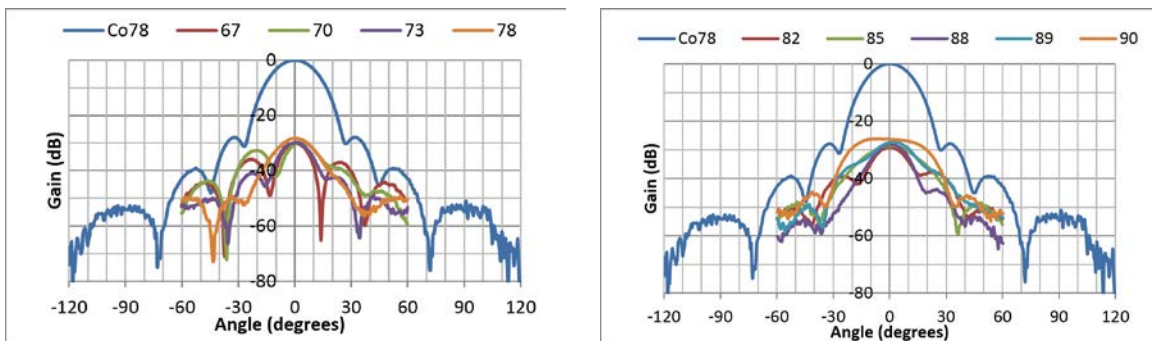


Figure 10: Measured co-polarization (78 GHz) and cross-polarization patterns of the feed horn.

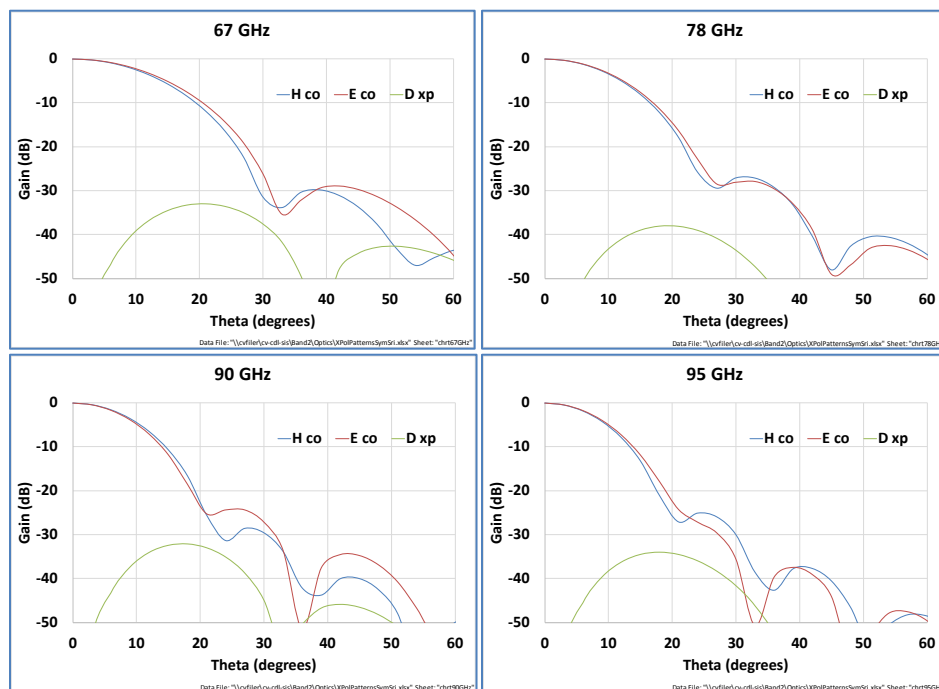



Figure 11: Calculated co- and cross-polarization patterns of the feed horn.

| | | |
|---|--|-------------------------------------|
|  | ALMA Project | Date: 2017-12-27 Page: 26 of 117 |
| | Design and testing of a Prototype Band 2 Cartridge Final Report | |

7.2.6. Dielectric Lens Design

As described earlier, a bi-hyperbolic dielectric lens was found to effectively match the beam waist of the feed horn to the telescope beam waist at the Cassegrain focus for all frequencies. The distance of the lens from the feed horn and the focal length of the lens were the free parameters used to determine the output waist, for a given input waist at a given frequency. The lens has to be located at the 300 K window for reasons explained in Section [7.2.2](#). Since the feed horn is positioned below the 15 K IR filter, the minimum distance of the lens from the feed horn aperture is 83 mm. Operating with this constraint, three lenses were designed and the resulting parameters are listed in [Table 5](#). The thickness of the lens decreases with increasing focal length, for a fixed dielectric constant, while absorptive losses are proportional to the thickness. In an attempt to further reduce the thickness, a Fresnel lens with a single zone at a radius of 42.5 mm was also designed [\[RD 32\]](#). This lens is listed as #4 in [Table 5](#).


Table 4: Lens parameters.

| Lens # | Focal length (mm) | Distance from feed (mm) | Thickness (mm) |
|--------|----------------------|----------------------------|-------------------|
| 1 | 86 | 86.76 | 26.60 |
| 2 | 87.2 | 89 | 26.34 |
| 3 | 92 | 93 | 25.36 |
| 4 | 86.5 | 87.1 | 23.28 |

Different materials like high-density polyethylene (HDPE), quartz, fused silica, poly-tetrafluoroethylene (PTFE) etc. are suitable for lens fabrication. HDPE was selected because of its low dielectric constant, low loss tangent, mechanical properties and ease of machining. ALMA Band 1 uses a HDPE lens and the dielectric constant of the material as measured at the University of Chile is 2.347. NRAO obtained blocks of HDPE from the same supplier. The thickness of lenses listed in [Table 5](#) were calculated using this value of dielectric constant. Since the lens also serves as the vacuum barrier (cryostat window), a thickness of 5 mm was chosen for the flange. The thickness at the center of the lens includes the 5 mm flange. Anti-reflection (AR) structure was required to compensate for the difference in relative permittivity between HDPE and air. This would minimize reflection loss and standing waves between the lens and adjacent surfaces. The AR structure consists of circular corrugations on both sides of the lens. The pitch and width of the corrugations were determined to be 2 mm and 1 mm, respectively. The depth of the corrugations takes into account the angle of incidence on the lens surface and the average depth was determined to be 0.77 mm.

7.2.7. Dielectric Lens Fabrication

The dielectric lenses were machined on a numerically controlled mill using the drawing in [\[RD 58\]](#), [\[RD 59\]](#), [\[RD 60\]](#), and the Fresnel lens in [\[RD 61\]](#). The both surfaces of the lens are hyperbolic. If the corrugation depths follow the hyperbolic curve, the bottom surface of the corrugations will have a continuously changing slope requiring a number of cutting tools with tips ground to the right slope. Instead, the bottom of the corrugations in all of the lenses were horizontal and hence the cutting tools used had flat or rounded tip.

| | | |
|---|--|-------------------------------------|
|  | ALMA Project | Date: 2017-12-27 Page: 27 of 117 |
| | Design and testing of a Prototype Band 2 Cartridge Final Report | |

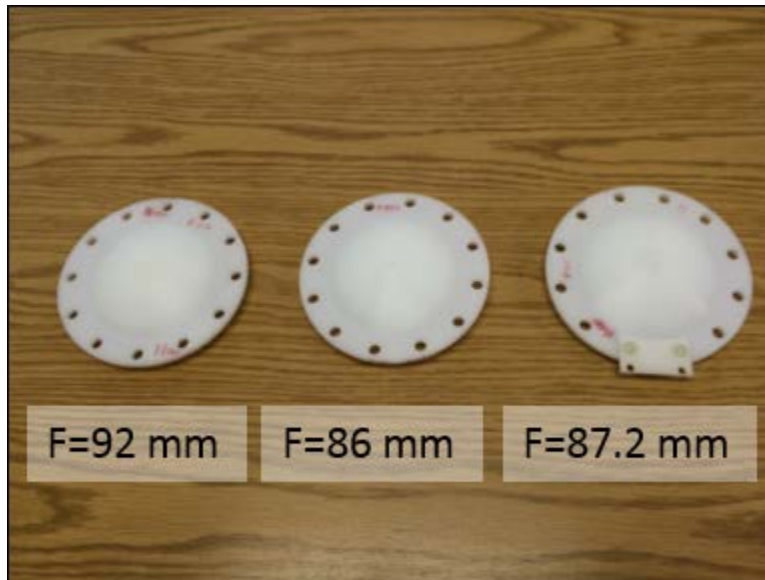


Figure 12: HDPE lens variants after machining.

7.2.8. Optics Measurement and Characterization

Prior to installation in the ALMA test cryostat, the far-field patterns of the feed horn/lens combination were measured in an anechoic chamber. In the initial measurements, the IR filters were not included. Each of the four lenses was measured by placing the lens at the appropriate distance from the feed horn aperture. Co-polar patterns were measured in the E-, H-, and D-planes (45° cut) while cross-polar patterns were measured only in the D-planes. [Figure 14](#) and [Figure 15](#) show measured co-polar patterns in E-, H- and D-planes and cross-polar pattern at 78 GHz in the D-plane for lens #2 and #3, respectively. The illumination taper at the edge of the sub reflector (3.6°) for lenses 2, 3 and 4 are shown in [Table 6](#). The worst case cross-polarization was measured to be -22 dB below the peak of the co-polarized beam at 90 GHz. The lens contributed about 3 dB to the peak of the cross-polarization pattern for all of the lens designs. [Figure 16](#) shows measured return loss of the feed horn and feed horn with lens #2 at the appropriate distance from the feed aperture. This demonstrates that the lens does not have any effect on the overall return loss. Measurements with other lenses indicated very similar results.

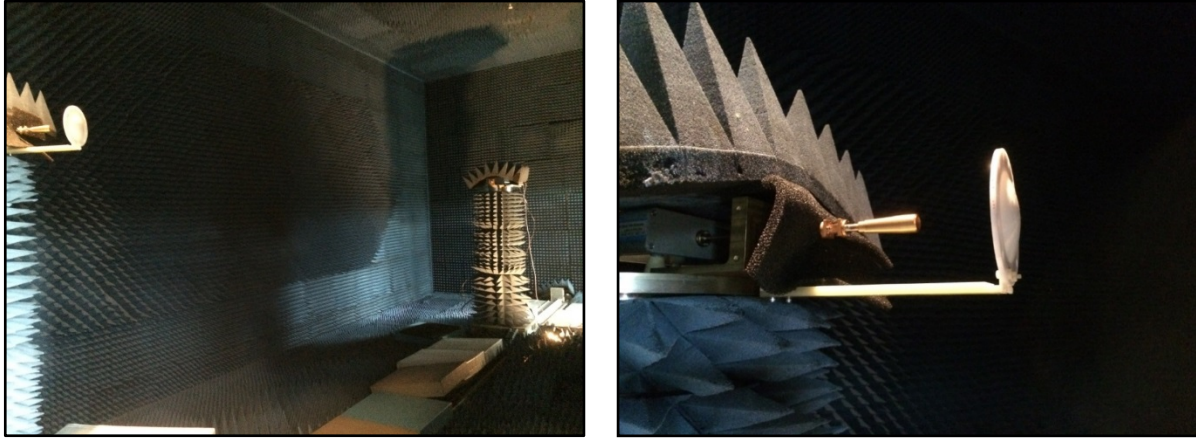


Figure 13: Far-field feed patterns (horn & lens) were measured in the anechoic chamber in Green Bank.

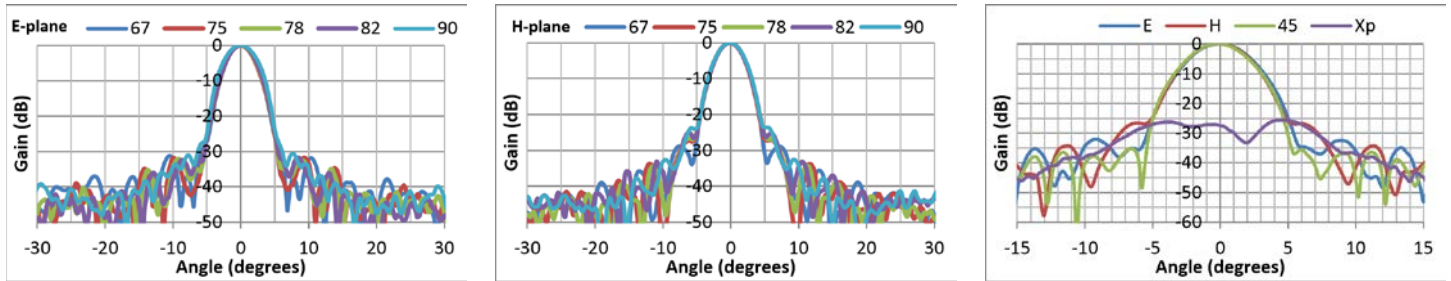


Figure 14: Feed horn & lens # 2 measured co-polar and cross-polar patterns

Measured co-polar patterns in E-, H- and D-planes for 67, 75, 78, 82 & 90 GHz (two left panels), and cross-polar pattern at 78 GHz (right panel) in the D-plane for the combination of feed horn with lens #2.

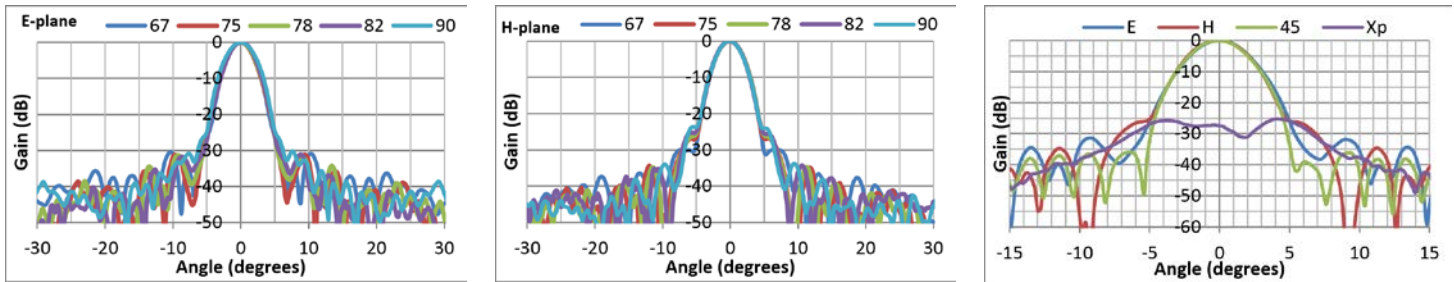



Figure 15: Feed horn & lens # 3 measured co-polar and cross-polar patterns

Measured co-polar patterns in E-, H- and D-planes for 67, 75, 78, 82 & 90 GHz (two left panels), and cross-polar pattern at 78 GHz (right panel) in the D-plane for the combination of feed horn with lens #3.

Table 5: Measured illumination taper at 3.6° for the various feed horn lens combinations.

| Lens # | Illumination taper at subreflector edge, 3.6° (dB) | | |
|--------|---|--------|--------|
| | 67 GHz | 78 GHz | 90 GHz |
| 2 | -13.44 | -12.80 | -11.33 |
| 3 | -14.37 | -14.03 | -12.60 |

| | | |
|---|--|-------------------------------------|
|  | ALMA Project | Date: 2017-12-27 Page: 29 of 117 |
| | Design and testing of a Prototype Band 2 Cartridge Final Report | |

| | | | |
|---------------------|--------|--------|--------|
| 4 (Fresnel, 1-zone) | -10.88 | -11.56 | -11.36 |
|---------------------|--------|--------|--------|

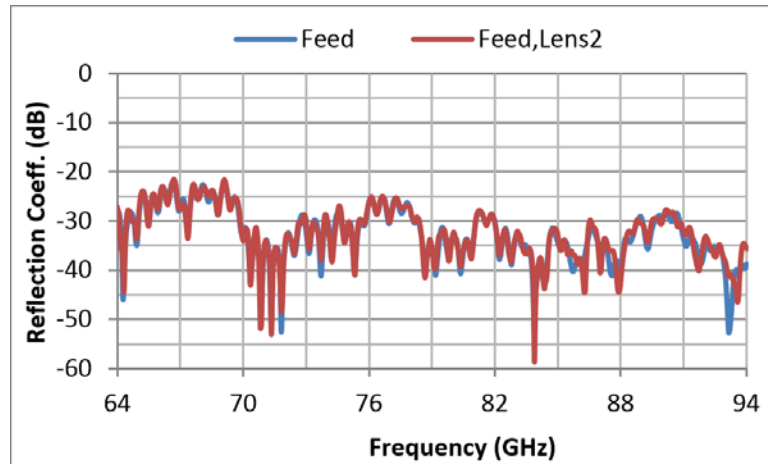


Figure 16: Measured return loss of the feed horn without/with lens # 2

Measured return loss of the feed horn and feed horn with lens #2 at the appropriate distance from the feed aperture. This demonstrates that the lens does not have any effect on the overall return loss.

7.2.9. Fresnel Lens

Alvaro Gonzales of NAOJ designed a Fresnel lens (with one zone) for Band 2 ([IRD 301](#)), which was subsequently modified by Sri Srikanth and the final design is shown in [Figure 17](#).

The Fresnel lens is 15% thinner than lenses 3-2 and lens 1-1, which should exhibit proportionately less loss and thereby improve the receiver noise temperature. However, as shown in [Figure 16](#), noise temperature measured with the Fresnel lens averaged 3 K higher than with the conventional lens. Additional wide-angle spillover might cause the higher noise temperature, and since pattern measurements and efficiency calculations for this lens (Section [8.7.5](#)) show good performance, additional work is planned to understand the noise temperature degradation. Also, alignment of the lens can't be optimized due to the mechanical design of the current lens holder and the lens. Alvaro Gonzalez of NAOJ offers that the percentage of beam terminated at room temperature is slightly higher than for the case the lens can be aligned properly. The physical temperature is 290K, and therefore 2% difference in the truncated beam would account for the extra 6K in the measurement result.

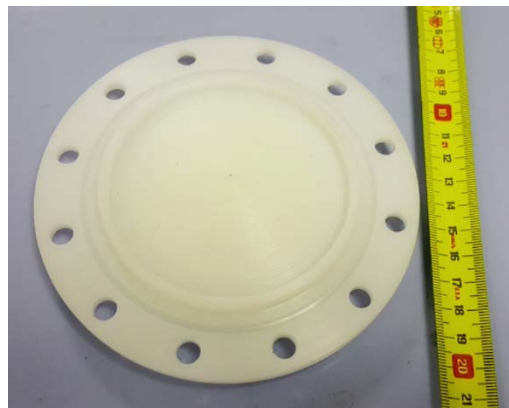


Figure 17: Photo of Fresnel Lens, designed by NAOJ [\[RD 30\]](#)

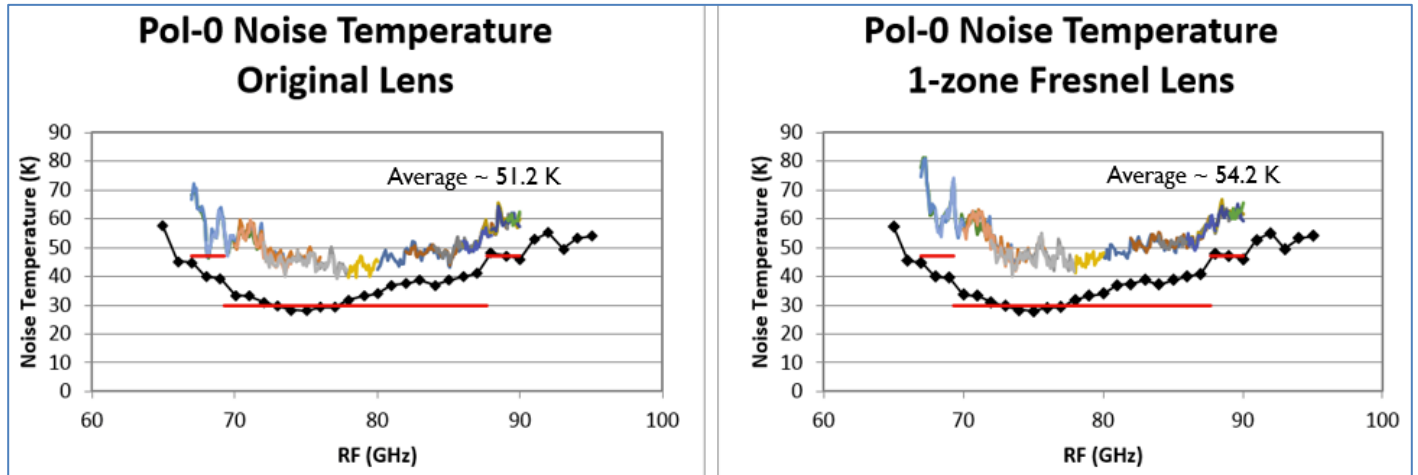



Figure 18: Noise Temperature of Fresnel Lens compared to Original Lens

7.3. Orthomode Transducer (OMT)

The orthomode transducer separates the two orthogonal polarizations present in the received signal. At the outset, it was desirable for the OMT to have the following features: ease of manufacturing and assembly, no need for tuning, repeatable performance, and low in cost. The Boifot junction OMT, which has a split-block construction, is routinely employed in many receivers on the JVL. ALMA Bands 3 and 6 also incorporate the Boifot junction OMT in their receiver design. These OMTs have pins at the entry into the ports of the side arms and a septum in the main-arm port. Experience with the production of such OMTs indicates that the number of rejections arising from such a configuration is fairly high and the assembly is not trivial.

Consequently, an OMT based on turnstile junction that possesses two-plane symmetry, was developed. This OMT does not employ any pins or the septum as is the case for the Boifot junction OMT. The turnstile junction has a square input and four WR-12 output ports. A square prism at the base of the square waveguide acts as a tuning element providing good input match. Each output port of the junction goes through two 90° H-plane bends before a pair of opposing arms are joined in an E-plane Y-junction. To allow two of the arms to cross without interference, stepped transformers are located before the cross-over to reduce the height of the waveguides. Design of the various sub-components of the turnstile junction OMT was optimized individually using an EM simulator.

[Figure 19](#) shows the assembled turnstile junction OMT. The main body of the OMT is composed of three major blocks. The center block has the side arms associated with one set of ports with H-plane bends and stepped transformer, on one side; while the other side has the side arms associated with the other set of ports. The two Y-junctions are of split-block construction and this assembly fits snugly in the openings of the main body assembly. Guides and stops on the Y-junction assembly ensure precise alignment of the waveguides in both assemblies. This mechanical design ensures easy assembly and requires no tuning. All the component parts of the OMT are milled out of aluminum AL6064. The parts are gold plated with Pur-a-gold 125 with a thickness of 50μ", to ensure low insertion loss. The specified manufacturing tolerance was ±0.0005" and three OMTs were machined in the CDL machine shop.

| | | |
|---|--|-------------------------------------|
|  | ALMA Project | Date: 2017-12-27 Page: 31 of 117 |
| | Design and testing of a Prototype Band 2 Cartridge Final Report | |

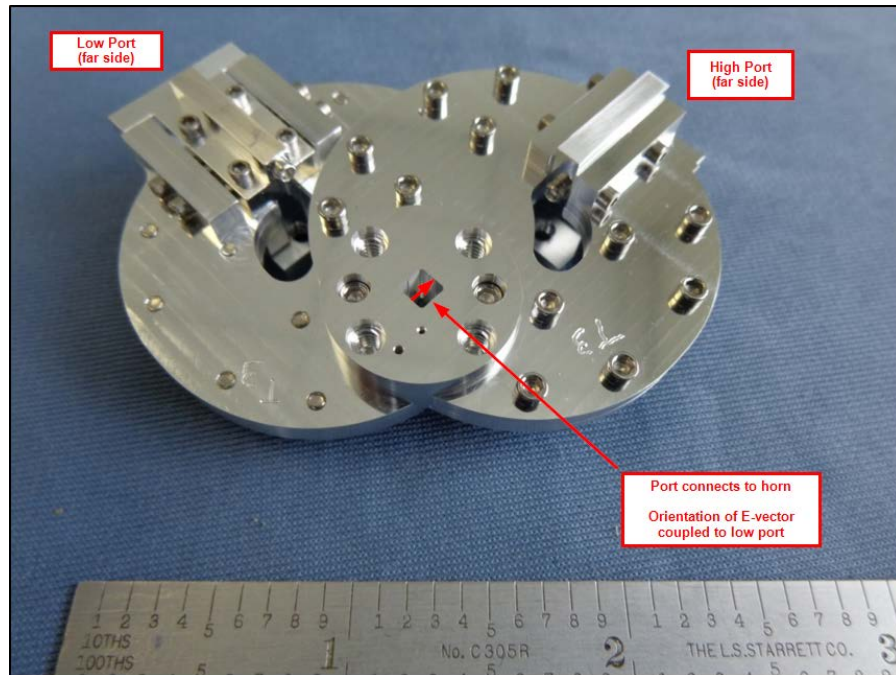


Figure 19: Photograph of an assembled 67-90 GHz turnstile junction OMT, fabricated as three separate blocks.

Measurements of s-parameters carried out on three assembled OMT blocks showed good performance. Measurements are made one polarization at a time: While the high port is measured, both S11 and S21 are measured with high port connected thru and the low port is terminated in a load and *vice-versa*.

Measurements of return loss and cross-polarization performance of OMT #3 are shown in [Figure 20](#) and [Figure 21](#), respectively. Input return loss was measured to be better than 20 dB and the cross-polarization levels were below -35 dB. Measured insertion loss was 0.3 dB. Enquiries made to commercial machine shops indicate that the OMTs can be easily manufactured in bulk at a reasonable cost.

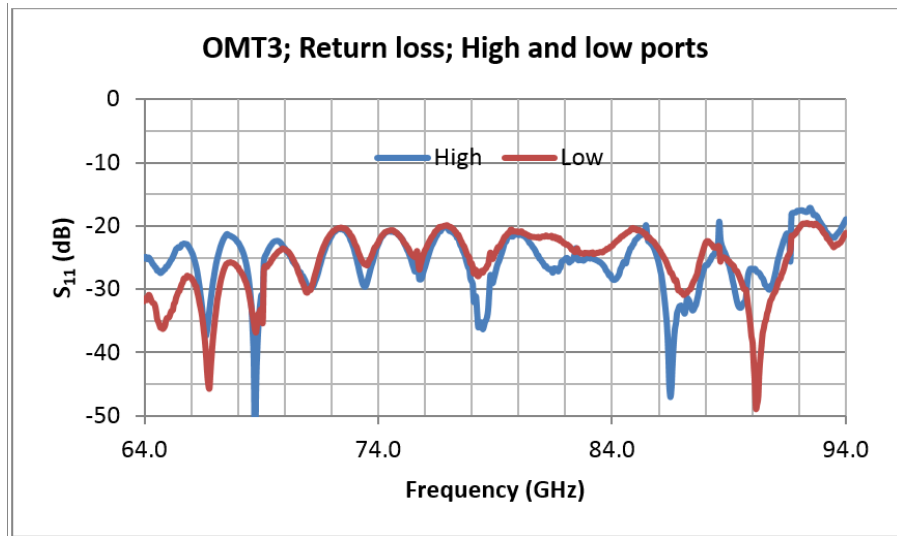


Figure 20: Measured input return loss of the 67-90 GHz turnstile junction OMT.

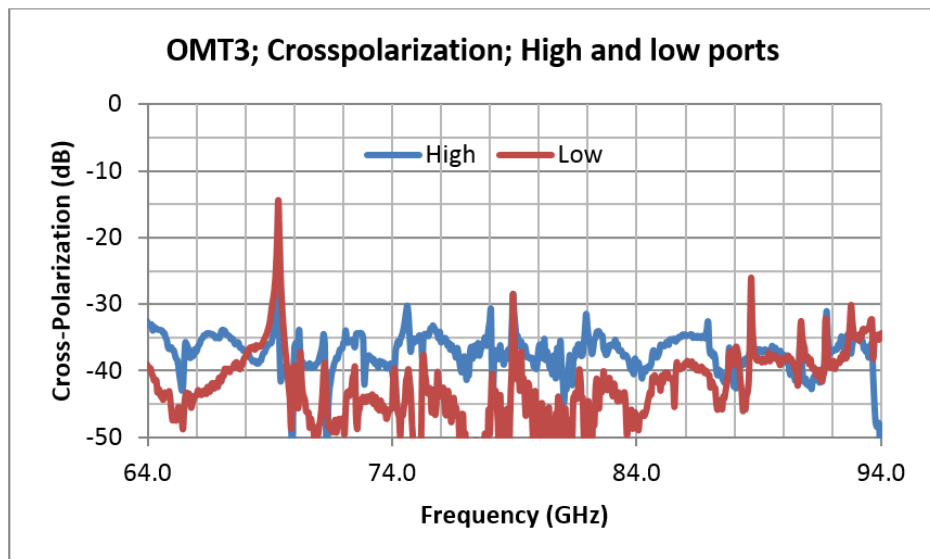



Figure 21: Measured cross-polarization performance of the 67-90 GHz turnstile junction OMT.

The large spikes in the measurements are attributed to reflections at the waveguide flanges during the VNA calibration process. No cross-polar degradation is noticeable around these frequencies in the overall receiver measurements to characterize the optic performance.

7.4. Cryogenic Low Noise Amplifiers

Along with the receiver optics, the cryogenic LNA (CLNA) is the most significant contributor to the overall receiver noise. Although decent receiver performance was obtained using “chip and wire” LNAs using the best 80 nm gate length InP HEMTs, significantly improved performance was demonstrated using the state-of-the-art NGC 35 nm gate length MMICs produced under the Band 2 cartridge prototype project sub-contract with Cahill Radio Astronomy Laboratory (CRAL) at the California Institute of Technology.

| | | |
|---|--|-------------------------------------|
|  | ALMA Project | Date: 2017-12-27 Page: 33 of 117 |
| | Design and testing of a Prototype Band 2 Cartridge Final Report | |

[Figure 22](#) compares the noise temperature of an MIC based LNA (produced using the best 80 nm gate length InP HEMTs) with that of an MMIC based LNA. The MMIC based LNA was produced using the state-of-the-art NGC 35 nm gate length MMICs produced by the Cahill Radio Astronomy Laboratory (CRAL) at the California Institute of Technology and by JPL, under a Band 2 cartridge prototype project sub-contract. Block measurements at CRAL are performed at 18 K and have been verified at NRAO at a nominal temperature of 21 K. (Cryo-probe measurements for initial chip selections typically performed at 25 K).

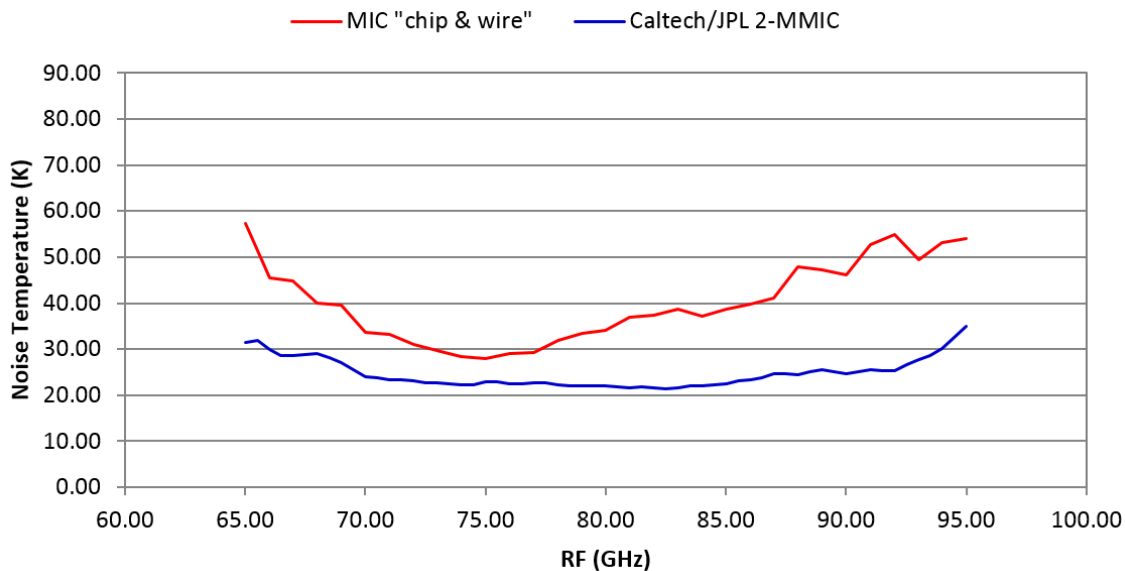


Figure 22: Noise temperature of MIC and Caltech/JPL MMIC LNA

The above compares the amplifier (only) noise temperature of an MIC based LNA (hybrid “chip and wire” amplifier) produced using the best 80 nm gate length InP HEMTs (red) with that of a waveguide-packaged MMIC-based LNA (blue) using the state-of-the-art NGC 35 nm gate length MMICs produced by Caltech/JPL under a Band 2 cartridge prototype project sub-contract. Also shown is the gain of the MMIC-based amplifier (blue).

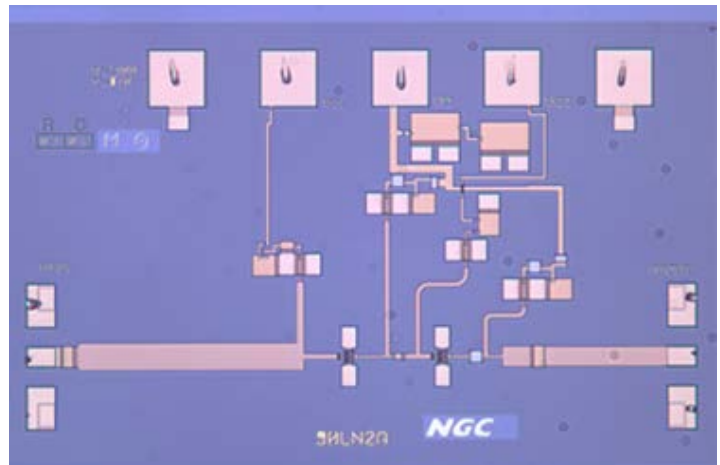



Figure 23: Photo of MMIC LNA Amplifier and enclosed MMIC Chip

| | | |
|---|--|-------------------------------------|
|  | ALMA Project | Date: 2017-12-27 Page: 34 of 117 |
| | Design and testing of a Prototype Band 2 Cartridge Final Report | |

The packaged 2-chip Band 2 prototype MMIC LNA using devices produced by the Cahill Radio Astronomy Laboratory (CRAL) at the California Institute of Technology and by JPL, under a Band 2 cartridge prototype project sub-contract. (Right) Photograph of a 90LN2A MMIC amplifier chip used in the first stage of the MMIC LNA package.

The MMIC LNA amplifier package and the first stage MMIC device are shown in [Figure 23](#). Warm s-parameters for two such prototype blocks are in shown in [Figure 24](#). Cryogenic performance is given in [Figure 25](#).

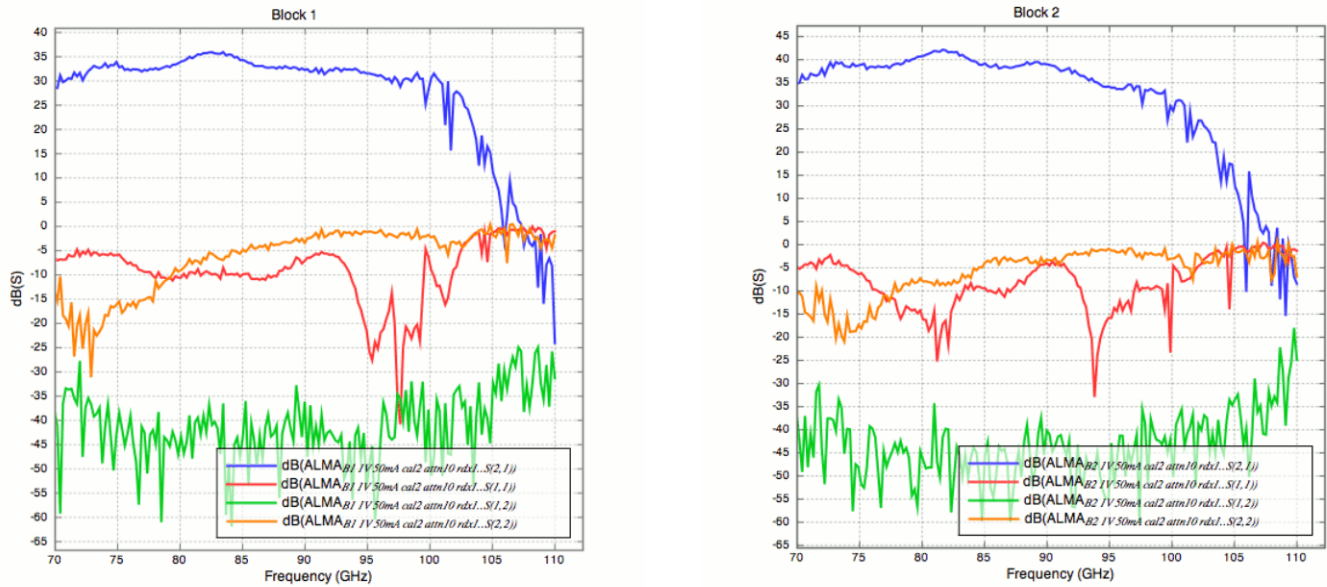


Figure 24: Warm S-Parameters for two prototype MMIC amplifier blocks.

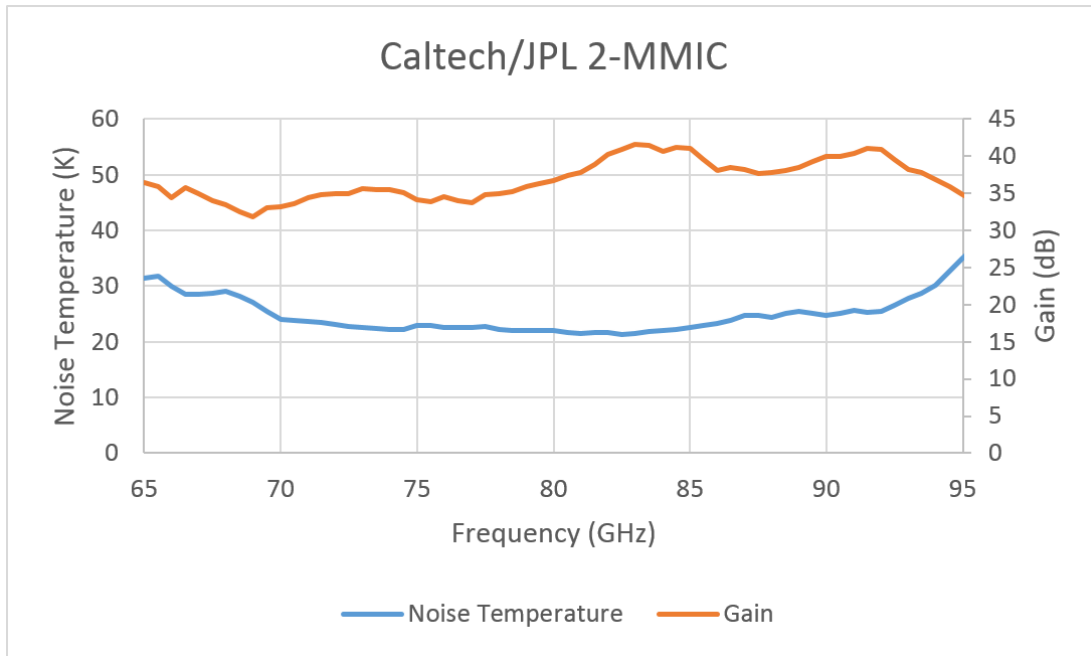


Figure 25: Measured cryogenic gain and noise temperature performance of the Band 2 MMIC based low noise amplifier.

7.4.1. LNA Chip Quantities and Yield

The first wafers producing Band 2 MMICs were tested by cryogenic probe station at CRAL. Functional yield for these wafers varied between 73% and 90%, depending on the particular chip design and the nominal Indium content of the channel. Typical standard deviations of the "passing" chips were 1-3 K in noise temperature and 1 dB in gain. To mitigate the risk of yield variations from lot to lot, the first wafer run carried a sufficient quantity of chips (of the best known design at the time) to complete production. We therefore have on-hand a quantity of 300 MMICs of the EBLNA81 design reported in [\[RD 63\]](#) having 75% Indium content in the channel, and another 251 of the same design with 100% Indium content.

These 300 plus 251 chips (first and second-stage, respectively) are currently our fall-back option. The first wafer run also produced a new design (90LN2A) with the superior performance shown here. Of this new design, we currently have 54 on hand, but the follow-up wafer run (already included in the CRAL subcontract) will carry a production quantity of these chips. The first 300 EBLNA81 chips already in our possession could then be used as a second-stage amplifiers.

7.4.2. LNA Linearity

Linearity of the amplifier blocks was verified by CRAL by measuring the IF output power on a CW test tone with a noise background provided by a heated absorbing vane. The temperature of the vane was monitored and stepped from 30K to 300K in 10K increments. The result at a typical frequency is shown in [Figure 26](#). Gain compression versus frequency is shown in [Figure 27](#). Although inherently a noisy measurement at these low compression levels, the compression with 300K input is relatively independent of frequency and averages about 0.8%.

Linearity; ALMA_B2, Block4_Linearity, North

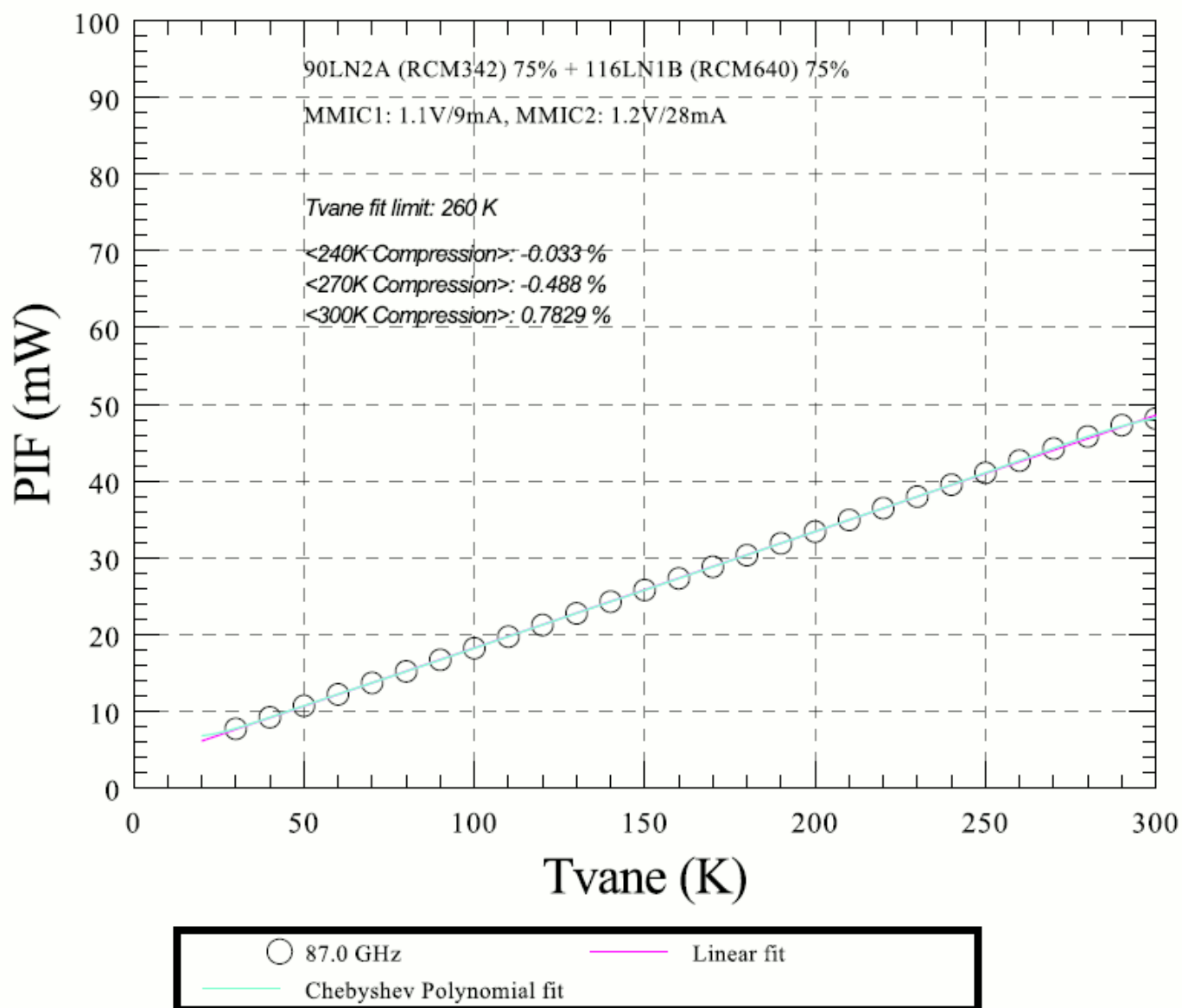


Figure 26. Linearity measurement of amplifier block using 87 GHz test tone with temperature controlled resistive noise source.

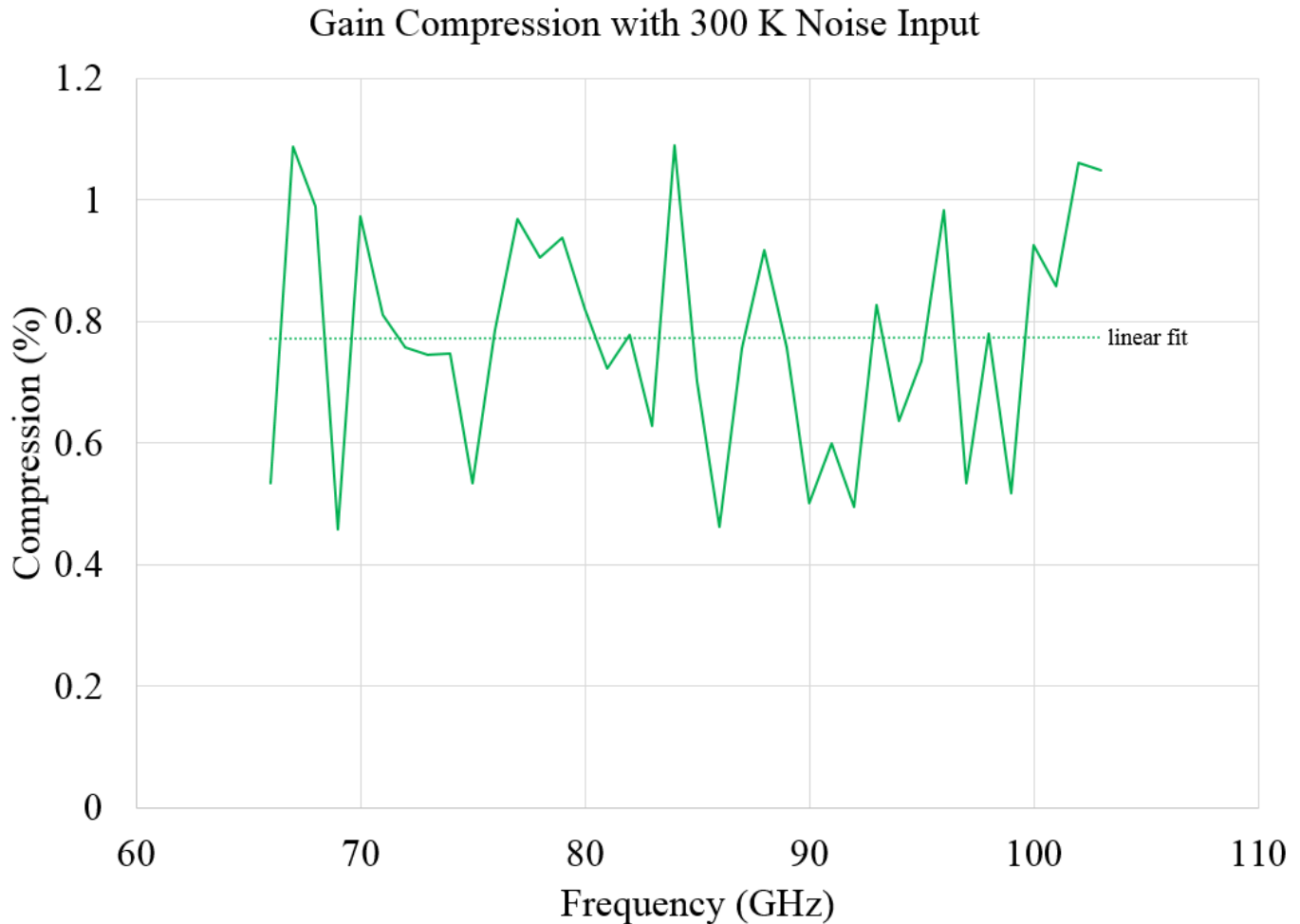



Figure 27. Gain compression versus frequency with 300K input.

7.4.3.A Note About LNA Biasing

There is a trade-off to be made regarding the flexibility afforded by multi-wire (and potentially servo-controlled) biasing of the amplifiers versus cryogenic loading from the wires.

The HFET devices used require dual-polarity supplies (positive for drain, negative for gate), especially to achieve optimum noise performance which is critical here. That alone means each amplifier will need at least two wires. In contrast, SiGe HBTs (not yet competitive in noise performance at this frequency) can often be biased with one wire from a single-polarity supply.

Regarding servo-control, there was a time that it was considered essential to achieving optimum gain stability with the best-performing cryogenic transistors. Some recent work, however, suggests it is no longer needed (in some cases and with some technologies) for that purpose. There are other reasons to do it, however, most importantly that the pinchoff, and therefore optimum gate voltage is not precisely repeatable

| | | |
|---|--|-------------------------------------|
|  | ALMA Project | Date: 2017-12-27 Page: 38 of 117 |
| | Design and testing of a Prototype Band 2 Cartridge Final Report | |

with this type of device. One must therefore "hardwire" a specific, experimentally-determined voltage for each and every amplifier, and then be prepared to change it again when the chip is replaced, or else implement a servo-control loop in which case the configuration of every cartridge is the same and never changes. The latter is of course desirable in a production environment.

In any case, whether one servos or not has no direct impact on the number of wires, unless one wishes to bias different stages at different currents, or one expects the optimum gate voltage to vary from transistor to transistor within the amplifier. With the classic MIC LNAs produced at the CDL, devices in the same amplifier were taken from different parts of the wafer, different wafers, or even from different foundries, so the gate voltage from transistor to transistor varied greatly. Thus each stage had to be biased separately (and would have anyway regardless of servoing) leading to a great number of wires.


With MMICs, it is far more common to tie the stages within a chip together. This is usually acceptable since the optimum gate voltage of several devices a few hundred microns apart on the same piece of semiconductor can be expected to be quite similar.

There is a compromise to be made, however, with regard to optimized performance versus wiring complexity. The Band 2+ cryogenic LNA packages comprise two MMIC stages each (to have enough gain with slope equalization included). The first- and second-stage MMICs will likely not be the same design or come from the same wafer, so independent biasing of the stages is required. However, each MMIC stage itself, comprising (typically) two to three transistor stages, is collectively biased with a single pair of wires, drain and gate. And they are, incidentally, servo-controlled.

We believe this is the best compromise between performance, chip yield, cryogenic loading, and configuration management.

7.5. Cartridge RF output

The RF corresponding to the two linear polarizations is routed to the cartridge 300 K base plate via WR-12 waveguides and brought out of the vacuum/cold space using two WR-12 waveguide feedthrough assemblies. The design of these feedthrough assemblies is amenable to blind mating and was adopted from the NAOJ Band 8 cartridge LO waveguide feedthrough design [\[RD 28\]](#), and is depicted in [Figure 28](#). In this assembly, the vacuum barrier is provided by a 15 mm diameter, 18 μm thick mica disk. Since there is sufficient RF gain in the cold cartridge, loss was not a significant concern. The performance of four of these assemblies is shown in [Figure 29](#). Only two of these feedthroughs were required for building the prototype cartridge.

| | | |
|---|--|-------------------------------------|
|  | ALMA Project | Date: 2017-12-27 Page: 39 of 117 |
| | Design and testing of a Prototype Band 2 Cartridge Final Report | |

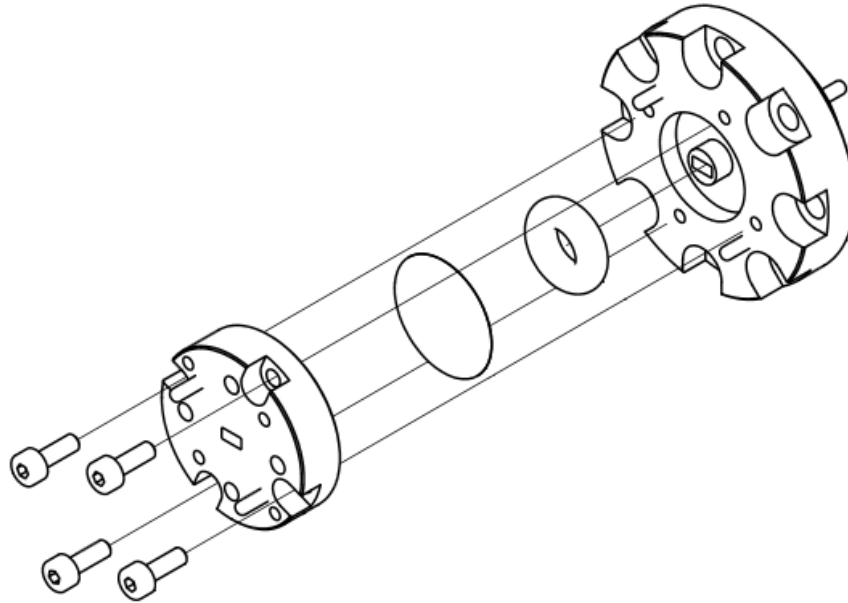


Figure 28: Assembly drawing of the WR-12 RF feedthrough

Assembly drawing of the WR-12 RF feedthrough assembly used to bring the amplified signal out of the cold cartridge assembly (this design is adopted from the NAOJ Band 8 LO waveguide feedthrough design [\[RD 28\]](#)). The vacuum barrier is a thin mica disk. One such assembly is used for each of the two polarization channels.

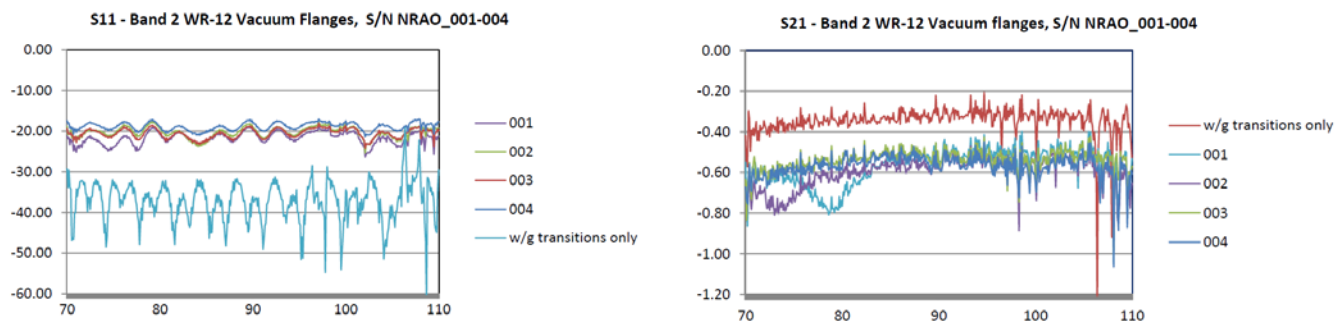



Figure 29: Measured performance of several WR-12 vacuum RF feedthrough assemblies.

7.6. Mechanical Tolerance Analysis, Cartridge Optics Metrology and Alignment

Prior to the assembly of the cartridge, a preliminary optical tolerance analysis was carried out using the “as specified” machine tolerances of the cartridge body, the 15 K optical support structure including the OMT/horn mounting arrangement, as well as the lens mount. After some iteration of the specified tolerances, the analysis indicated that a beam pointing of within ~ 4 mrad of the nominal direction (in the root sum square sense) was achievable, by simply relying on the tolerance of parts. The screw holes in the lens mount assembly could be used to adjust the pointing of the beam. It was estimated that a beam pointing adjustment of about ± 15 mrad could be made by adjusting the x-y positioning

| | | |
|---|--|-------------------------------------|
|  | ALMA Project | Date: 2017-12-27 Page: 40 of 117 |
| | Design and testing of a Prototype Band 2 Cartridge Final Report | |

of the lens mount assembly (± 3 mm adjustment available). [Figure 30](#) shows the fully assembled Band 2 prototype cartridge.

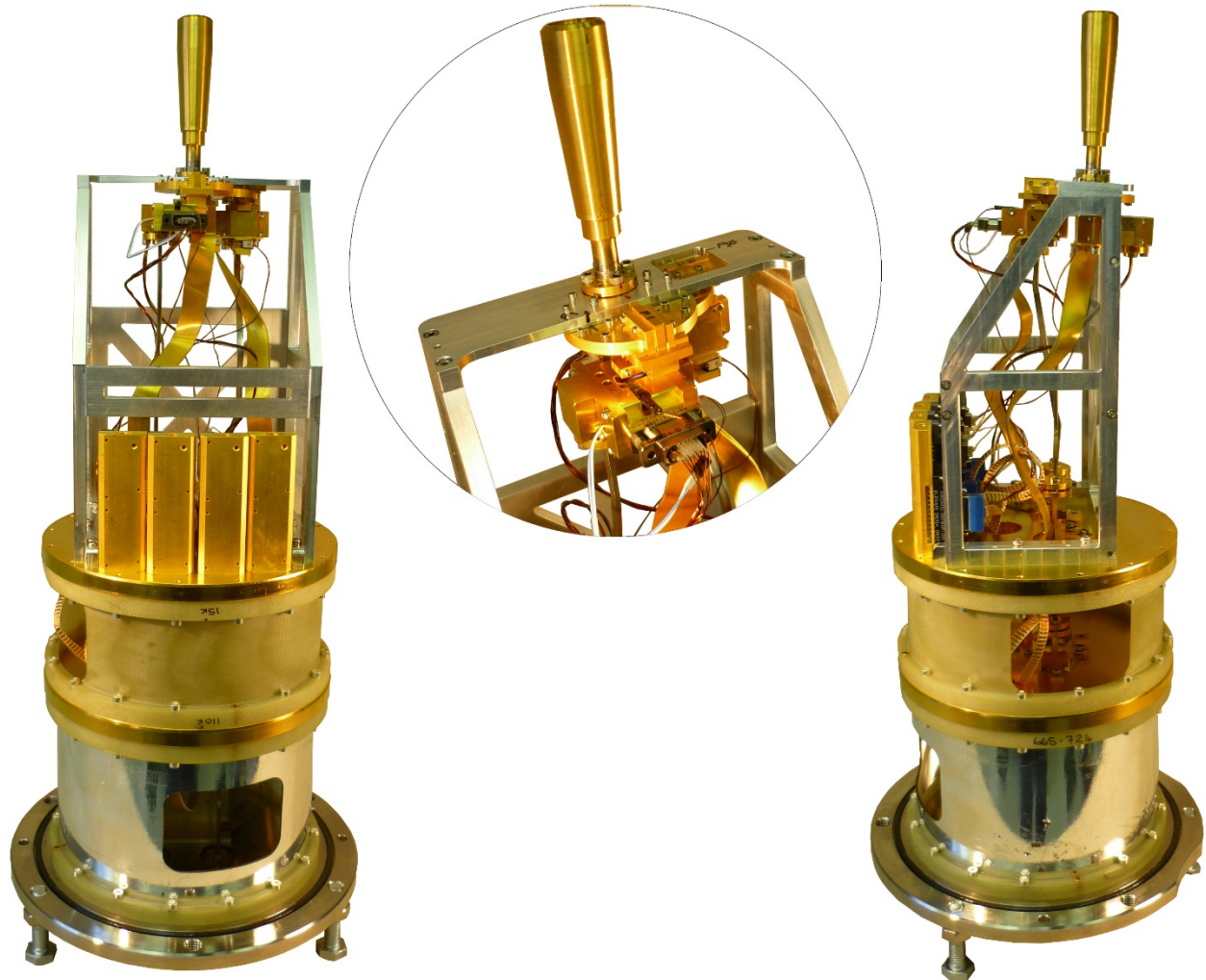


Figure 30: Photographs of the fully assembled Band 2 prototype cartridge
Details of the horn-OMT arrangement are shown in inset.

The tilt of the feed horn as well as the location of the center of the aperture of the feed horn (and a few other critical points on the cartridge assembly) were measured at a metrology lab and compared against the nominally desired location indicated by the cartridge 3D model. Results are tabulated in [Table 7](#). The center of the aperture was offset by about $0.038''$ ($965.2 \mu\text{m}$) in the y-direction, and about $0.011''$ ($279.4 \mu\text{m}$) in the x-direction (in the cold cartridge coordinate system, described in [Figure 31](#)). The tilt angle differed from the desired nominal direction by about 0.4° (7 mrad). All of these values were well within the adjustment range available in the lens mount (as described earlier). Nevertheless, to exercise caution and maximize the adjustment range available, the OMT mount was shimmed to correct the 0.4° (7 mrad) tilt. This adjustment also removed $0.0254''$ ($645 \mu\text{m}$) of the $0.038''$ ($965.2 \mu\text{m}$) linear offset in the y-direction (due to the


| | | |
|---|--|-------------------------------------|
|  | ALMA Project | Date: 2017-12-27 Page: 42 of 117 |
| | Design and testing of a Prototype Band 2 Cartridge Final Report | |

Table 6: Feed horn tilt (in degrees)


Tabulation of the measurements of the tilt of the feed horn (in degrees) as well as its location of the center of the aperture of the feed horn (and a few other critical points on the assembly, in inches).

| Winchester Machine and Tool Metrology Results, Band 2 CCA | | | | | | |
|--|---------|---------|----------|---------|----------|-----------------------|
| 6/29/2015 | | | | | | |
| * Note: measurements include 4mm spacer (Lens 3 configuration) | | | | | | |
| | Model | Run 1 | vs Model | Run 2 | vs Model | Repeatability of Runs |
| feedhorn aperture center, x | 0.0000 | 0.0114 | 0.0114 | 0.0115 | 0.0115 | 0.0001 |
| feedhorn aperture center, y | 1.4322 | 1.4699 | 0.0377 | 1.4713 | 0.0391 | 0.0014 |
| feedhorn aperture center, z | 19.2517 | 19.2654 | 0.0137 | 19.2136 | -0.0381 | -0.0518 |
| feedhorn aperture angle to base | 2.4800 | 2.8671 | 0.3871 | 2.8864 | 0.4064 | 0.0193 |
| omt bracket angle to base | 2.4800 | 2.6009 | 0.1209 | 2.5680 | 0.0880 | -0.0329 |
| omt waveguide center, x | 0.0000 | 0.0090 | 0.0090 | | | |
| omt waveguide center, y | | 1.2900 | | | | |
| omt waveguide center, z | | 15.7250 | | | | |



Figure 32: In-house inclinometer measurements of feed horn tilt

In-house inclinometer measurements of the feed horn tilt (with respect to the 300 K base plate plane) after shimming of the OMT mount indicating near ideal 2.44° tilt angled towards the center of the cryostat. By rotating the inclinometer by 45°, the tilt could be resolved into the FETMS “X” and “Y” direction components (-1.73° and 1.73° respectively).

| | | |
|---|--|-------------------------------------|
|  | ALMA Project | Date: 2017-12-27 Page: 43 of 117 |
| | Design and testing of a Prototype Band 2 Cartridge Final Report | |

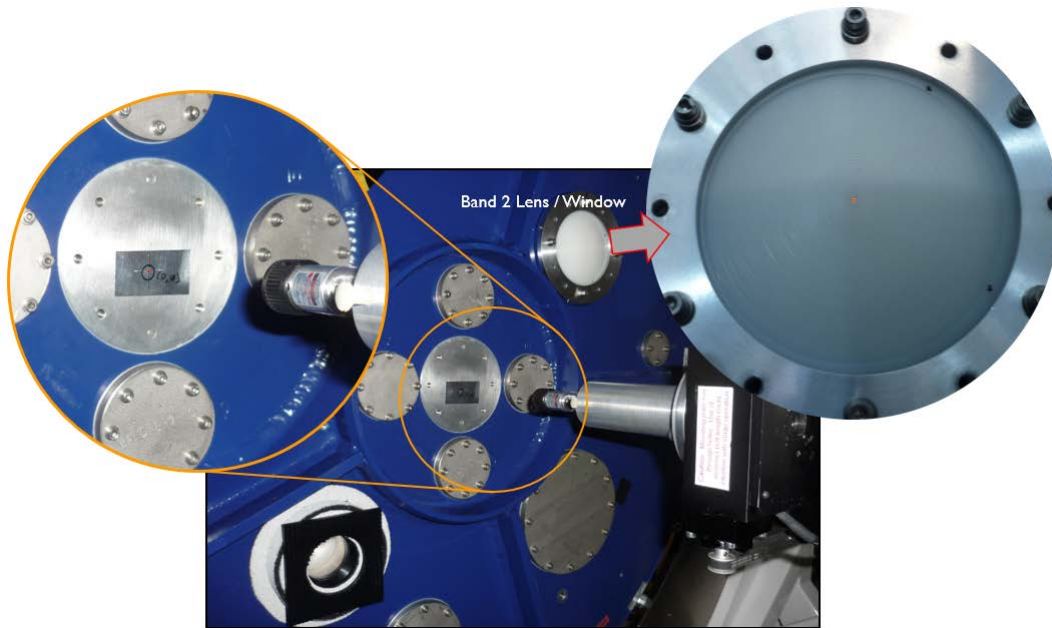


Figure 33: Center of the lens measurement

Location of center of the lens can be measured from an arbitrary (fixed) fiduciary mark on the cryostat using a beam-scanner mounted red laser. This provides a mechanism to adjust lens position by a given (delta) amount from existing position, to get desired beam pointing.

7.7. Mechanical Analysis

A mechanical design analysis was performed by employing the Finite Element Analysis (FEA) technique using the NX NASTRAN (with FEmap) version provided by Siemens. This FEA study analysis for the Band 2 CCA considered the following design conditions (as derived from the Band 2 technical specifications) in order to determine the mechanical adequacy of the proposed CCA configuration:

1. The deflections and stresses derived from thermal contractions following a 300K-to-15K cool-down evolution.
2. The deflections and stresses resulting from 1-G loading in the 3 orthogonal directions (“x,” “y,” and “z”) with the cartridge vacuum interface plate (300 K plate) held fixed.
3. The lowest fundamental eigen-frequencies with the cartridge baseplate held fixed (to be compared with the 70 Hz requirement)

Comprehensive details of the modeling as well as analysis are contained in [\[RD 29\]](#). Only significant results are summarized in this section.

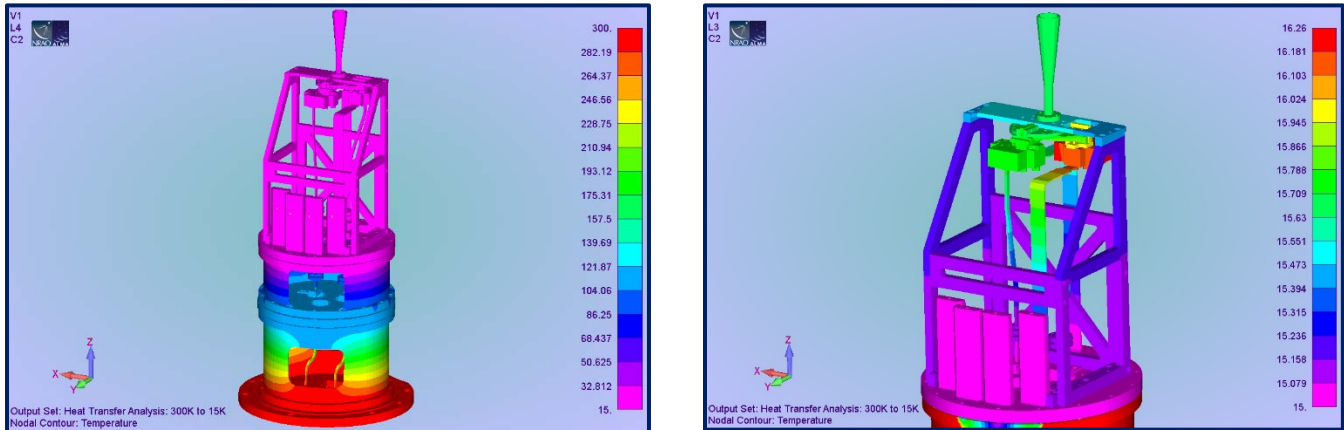


Figure 34: Predicted temperature distribution for Band 2 CCA on cool down
Indicated temperatures are in kelvins.

Table 7: Displacement of the feed horn aperture center point due to cooling.

| Deformation Component | Deformation (mm) |
|-----------------------|------------------|
| X-Direction | -0.00036 |
| Y-Direction | -0.081 |
| Z-Direction | -1.857 |

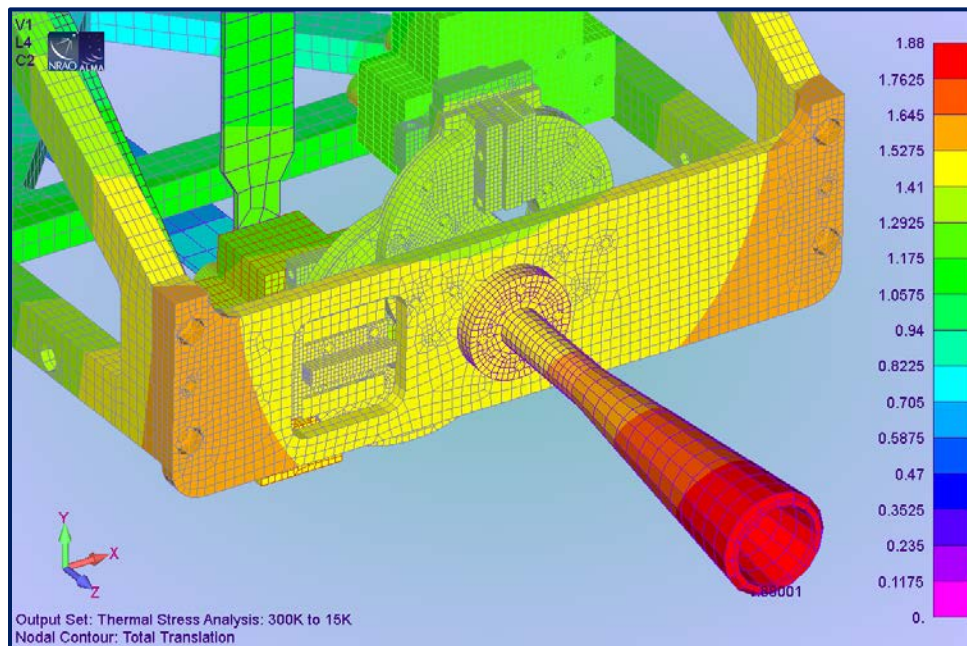


Figure 35: Predicted feed displacement from cooling
Total displacement due to x-, y- , and z- direction components


| | | |
|---|--|-------------------------------------|
|  | ALMA Project | Date: 2017-12-27 Page: 45 of 117 |
| | Design and testing of a Prototype Band 2 Cartridge Final Report | |

Table 8: Static stresses from thermal loads

The equivalent static stresses associated with the thermal loading boundary conditions are summarized in this table. In general, all stress conditions during cool-down are provided with sufficient material factors of safety.

| Band 2 Structural Component | Material | Peak Stress (MPa) | Factor of Safety (on Yield Stress) |
|-----------------------------|--|-------------------|------------------------------------|
| 300K Base Plate | 6061 AL | 48.2 | 5.73 |
| 300K-110K Spacer Tube | G10 | 100.9 | 2.39 |
| 110K Plate | Aluminum Alloy conforming to BS1470 6081/6082 (T6) | 127.2 | 2.17 |
| 110K-15K Spacer Tube | G10 | 154.7 | 1.56 |
| 15K Plate | OFHC Copper conforming to BS2870 – C103/C110 | 169.9 | 1.62 |
| OMT Support Structure | 6061 AL | 48.4 | 5.70 |

Table 9: Cartridge Mechanical Deflections

The mechanical analysis of the Band 2 cold cartridge assembly included assessment of gravity loading in each of the three orthogonal directions. The results of these three gravity load cases are summarized in this table. A comparison with the thermal stress results summarized in [Table 9](#) indicates that gravity loading stresses are significantly lower than the equivalent thermal stresses; as a result we should expect that the Band 2 cold cartridge assembly should adequately handle shipping loads.

| Gravity Alignment | | X Deflection (mm) | Rotation about X (arcsecs) | Y Deflection (mm) | Rotation about Y (arcsecs) | Z Deflection (mm) |
|-------------------|-----------|-------------------|----------------------------|-------------------|----------------------------|-------------------|
| X- Direction | HORN BASE | 0.0491 | --- | -0.0002 | --- | -0.0002 |
| | HORN TIP | 0.0496 | --- | 0.0006 | --- | -0.0002 |
| | | | 1.89 | | 1.29 | |
| Y- Direction | HORN BASE | 0.0007 | --- | -0.0278 | --- | -0.0012 |
| | HORN TIP | 0.0006 | --- | -0.0334 | --- | -0.0015 |
| | | | 14.12 | | 0.28 | |
| Z- Direction | HORN BASE | -0.0004 | --- | -0.0001 | --- | -0.0048 |
| | HORN TIP | -0.0045 | --- | -0.0037 | --- | -0.0050 |
| | | | 9.07 | | 10.44 | |


| | | |
|---|--|-------------------------------------|
|  | ALMA Project | Date: 2017-12-27 Page: 46 of 117 |
| | Design and testing of a Prototype Band 2 Cartridge Final Report | |

Table 10: Lowest ten modal (natural) frequencies for the Band 2 cold cartridge assembly.

| Vibration Mode | Frequency (Hz) | Predominant Mode Shape |
|----------------|----------------|---|
| Mode 1 | 82.2 Hz | Flexing of the OMT Frame in the X-direction |
| Mode 2 | 111.7 Hz | Bending of the Cooling Straps about the X-Axis with Flexing of the OMT Frame in the Y-direction |
| Mode 3 | 139.2 Hz | Bending of the Cooling Straps about the X-Axis (No OMT Frame Movement) |
| Mode 4 | 143.0 Hz | Bending of the Cooling Straps about the X-Axis (No OMT Frame Movement) |
| Mode 5 | 174.6 Hz | Flexing (Bending) of the OMT Frame Top-Plate about the X-Axis |
| Mode 6 | 190.0 Hz | Flexing (Bending) of the OMT Frame Plus Bending of Top-Plate about the Y-Axis |
| Mode 7 | 219.0 Hz | Flexing (Bending) of the OMT Frame Top-Plate Only about the Y-Axis |
| Mode 8 | 269.2 Hz | Flexing (Bending) of the OMT Frame Plus Bending of Top-Plate about the X-Axis |
| Mode 9 | 294.0 Hz | Twisting of the OMT Frame about the Z-Axis |
| Mode 10 | 326.2 Hz | Local Bending of Horn Plus Flexing of the OMT Frame Top-Plate about the Y-Axis |

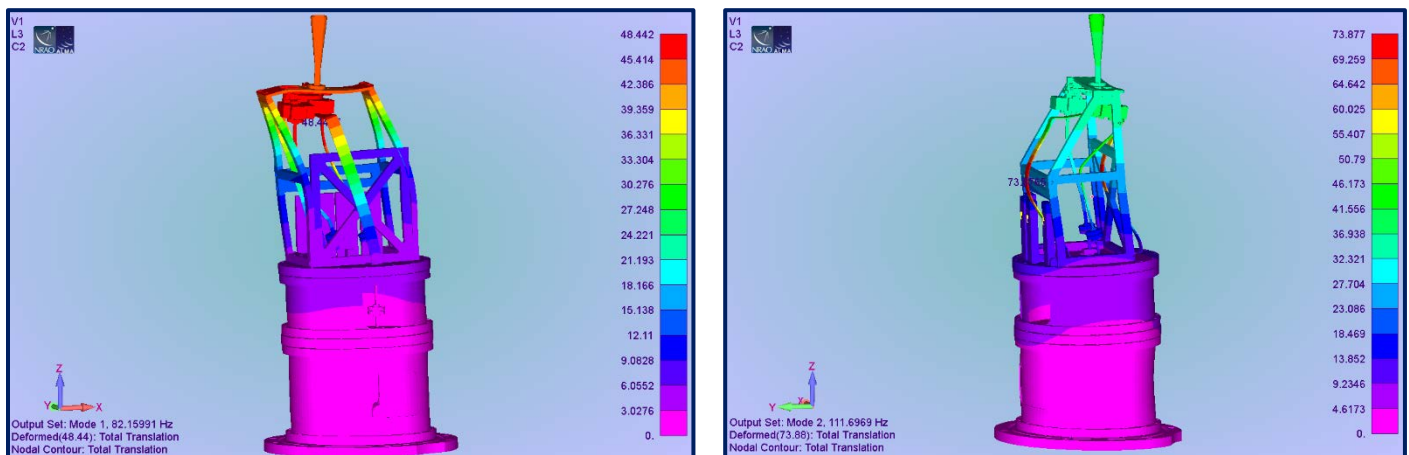



Figure 36: Vibration Mode Shapes: 1st Mode – 82.2 Hz, 2nd Mode – 111.7 Hz.

Based on the findings and results presented above, the proposed structural configuration for the Band 2 cold cartridge assembly was determined to be structurally adequate. The governing load condition is the thermal loading associated with cool-down of the cold cartridge assembly to 15K operating temperature. Gravity loading (i.e., 1 g loading in each orthogonal direction) yields very low deflections and stresses and indicates that the cold cartridge assembly could sustain quasi-static shock loadings in excess of 30 g without causing damage.

Finally, having a fundamental modal frequency of 82.1 Hz, the predicted modal frequencies of Band 2 cold cartridge assembly exceeds the specified frequency requirement of 70 Hz (minimum). However, during the course of this analysis, a minor structural alteration to the OMT Support Frame was identified which would result in a somewhat stiffer frame

| | | |
|---|--|-------------------------------------|
|  | ALMA Project | Date: 2017-12-27 Page: 47 of 117 |
| | Design and testing of a Prototype Band 2 Cartridge Final Report | |

thus yielding slightly higher modal frequencies (without adding a significant amount of mass to the assembly). This proposed structural alteration to the OMT Frame is depicted in [Figure 37](#).

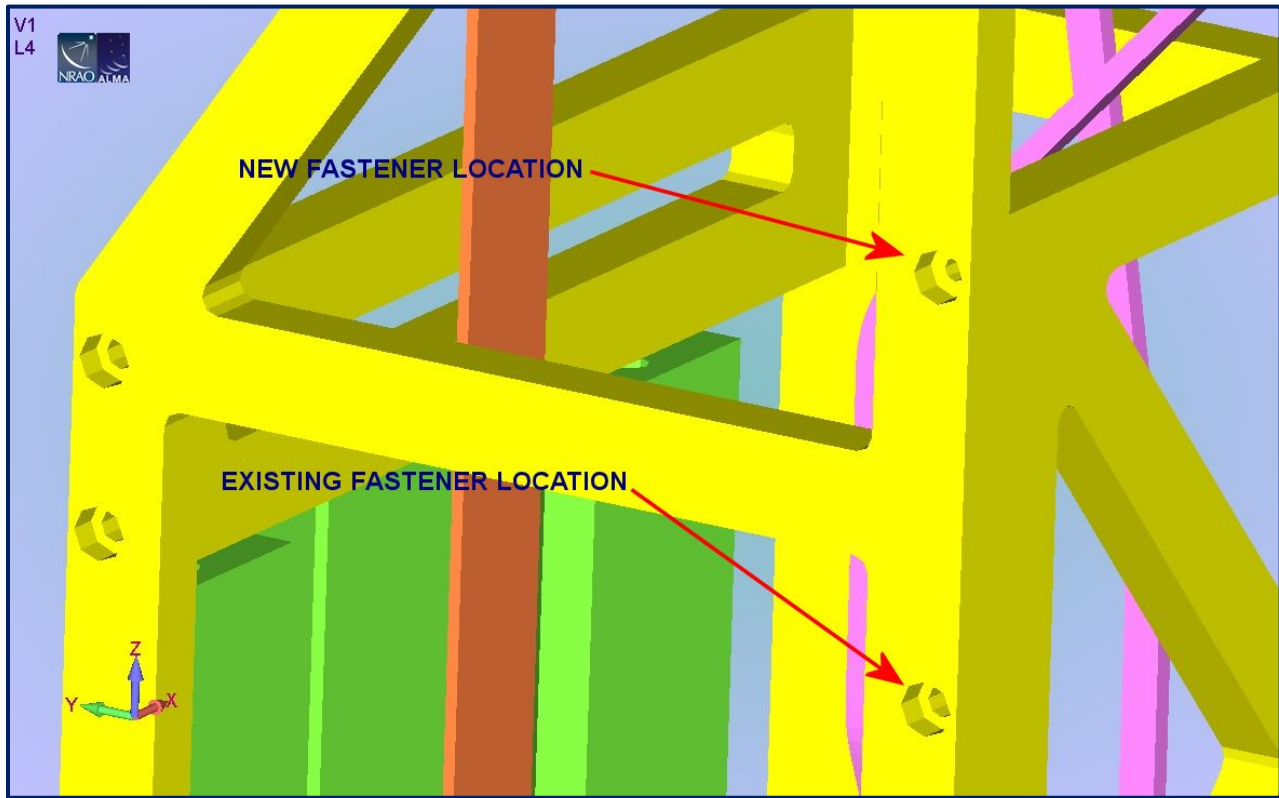


Figure 37: Proposed location for an additional OMT support frame fasteners (one on each side).

The lowest ten modal frequencies for the revised CCA configuration are shown in [Table 12](#). As expected, the proposed revision to the cold cartridge assembly configuration only affects the first mode fundamental frequency that is dominated by movement in the X-direction. These modal results indicate that proposed cold cartridge assembly revision would increase the margin between the frequency limit (70 Hz) and the calculated fundamental frequency to roughly 40 percent.

The effect of the proposed modification on thermal and gravitational stresses as well as deformations and deflections is also analyzed in [\[RD 29\]](#), and the cartridge found to be satisfactory. This change can easily be implemented in the pre-production/production versions of the Band 2 cold cartridge assembly.

Table 11: Lowest Natural Frequencies

Lowest ten modal (natural) frequencies for the Band 2 cold cartridge assembly incorporating additional fasteners in the OMTR support structure.

| Vibration Mode | Frequency (Hz) | Predominant Mode Shape |
|----------------|----------------|---|
| Mode 1 | 99.0 Hz | Flexing of the OMT Frame in the X-direction |
| Mode 2 | 111.2 Hz | Bending of the Cooling Straps about the X-Axis with Flexing of the OMT Frame in the Y-direction |
| Mode 3 | 139.2 Hz | Bending of the Cooling Straps about the X-Axis (No OMT Frame Movement) |
| Mode 4 | 143.0 Hz | Bending of the Cooling Straps about the X-Axis (No OMT Frame Movement) |
| Mode 5 | 175.6 Hz | Flexing (Bending) of the OMT Frame Top-Plate about the X-Axis |
| Mode 6 | 198.5 Hz | Flexing (Bending) of the OMT Frame Plus Bending of Top-Plate about the Y-Axis |
| Mode 7 | 223.2 Hz | Flexing (Bending) of the OMT Frame Top-Plate Only about the Y-Axis |
| Mode 8 | 269.7 Hz | Flexing (Bending) of the OMT Frame Plus Bending of Top-Plate about the X-Axis |
| Mode 9 | 295.0 Hz | Twisting of the OMT Frame about the Z-Axis |
| Mode 10 | 323.9 Hz | Local Bending of Horn Plus Flexing of the OMT Frame Top-Plate about the Y-Axis |

7.8. RF filter (band definition) and Post-amplifier

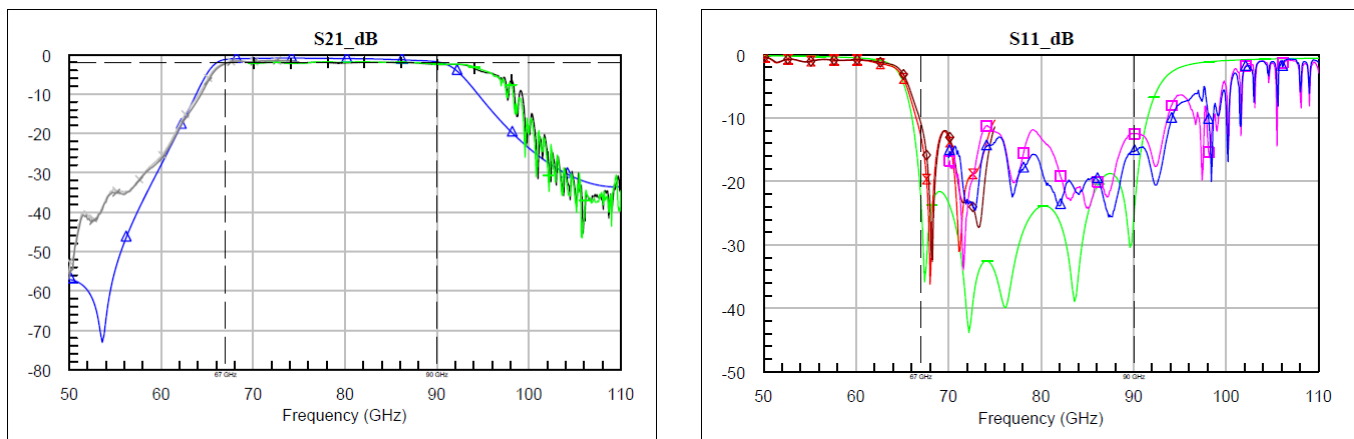



Figure 38: Measured Gain and Return Loss of RF Filters

Plot on the left shows the insertion loss for the two (one per polarization) coupled line filters, with simulation results (coupled line only, not including input and output probe loss) indicated by the blue trace. Plot on the right shows return loss for the same filters, with simulation results indicated by the green trace.

| | | |
|---|--|-------------------------------------|
|  | ALMA Project | Date: 2017-12-27 Page: 49 of 117 |
| | Design and testing of a Prototype Band 2 Cartridge Final Report | |

7.9. 2SB Down-converter

As indicated in the block diagram of [Figure 4](#), the side-band separating down-converters are outside of the cold cartridge in room temperature space and situated on the warm cartridge assembly as shown in [Figure 39](#). Each of the two 2SB down-converters (one per polarization channel) is comprised of a 90° RF hybrid followed by two component mixers. The I and Q IF outputs are combined in a 90° IF hybrid. Subsequently, the sideband separated IF signals are amplified by warm IF amplifiers, and forwarded to the WCA harness plate, from where they are routed to the FE IF switches in the FE assembly. The local oscillator signal is provided via a LO Y-splitter to the two component mixers ([Figure 45](#)).

7.9.1. RF Hybrid Design

The 90° RF hybrid shown in [Figure 40](#) uses a conventional split block design with WR-12 waveguide channels in the block. Simulated amplitude imbalance is 1.2 dB as shown in [Figure 41](#) while port-to-port isolation is predicted to be better than 25 dB as shown in [Figure 42](#). Measured amplitude ([Figure 43](#)) and phase ([Figure 44](#)) responses closely match predictions.

The frequencies where the amplitude match is perfect, simulated in [Figure 41](#) and measured in [Figure 43](#), are at the edges of Band 2. While most designs place these frequencies inside the band edges and minimize the amplitude match over the design band, experience has shown that amplitude match near the band edges is sensitive to fabrication errors and often is significantly worse than simulations. The additional benefit is that this RF hybrid design maintains a reasonable amplitude match up to the Band 2+ frequency of 95 GHz.



| | | |
|---|--|-------------------------------------|
|  | ALMA Project | Date: 2017-12-27 Page: 50 of 117 |
| | Design and testing of a Prototype Band 2 Cartridge Final Report | |



Figure 39: Photograph of the dual polarization 2SB down-converter assembly.

This test bench photo taken prior to the integration into the WCA shows (L to R) the RF post-amplifier (one per polarization, SN 49 & 50), 90° RF hybrid (one per polarization), component mixers (SN 5, 6 & 3, 7 – one pair per polarization), LO Y-splitter (one per polarization). The LO power amplifier (and part of the AMC) is visible to the right side of the photograph. The coaxial output connectors (I & Q IF outputs, one pair per polarization) are visible on the mixer modules. The IF cables and the IF hybrids are not shown in this photograph.

| | | |
|---|--|-------------------------------------|
|  | ALMA Project | Date: 2017-12-27 Page: 51 of 117 |
| | Design and testing of a Prototype Band 2 Cartridge Final Report | |

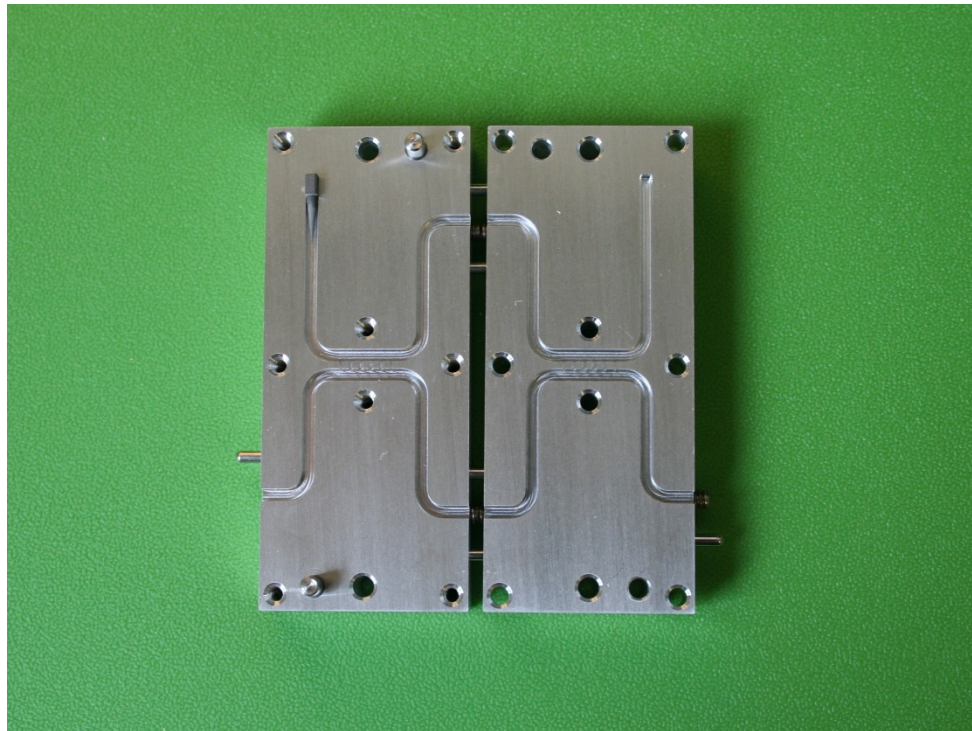


Figure 40: Photograph of the top and bottom portion of the 90° RF hybrid split block assembly (WR-12).

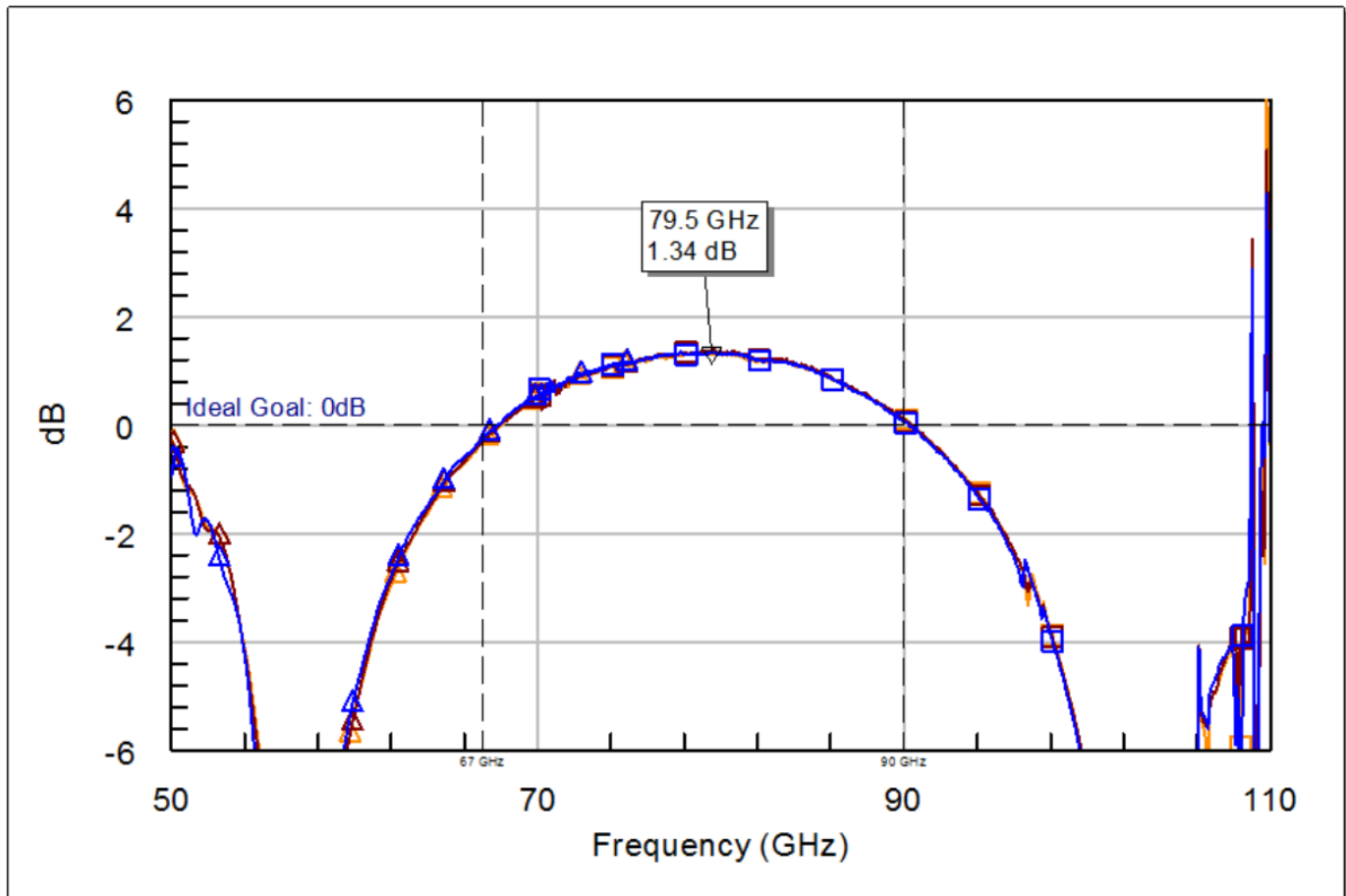


Figure 41: Plot shows the simulated amplitude imbalance between the RF hybrid ports.

See Section [7.9.1](#) for the rationale behind the selection of frequencies with perfect match.

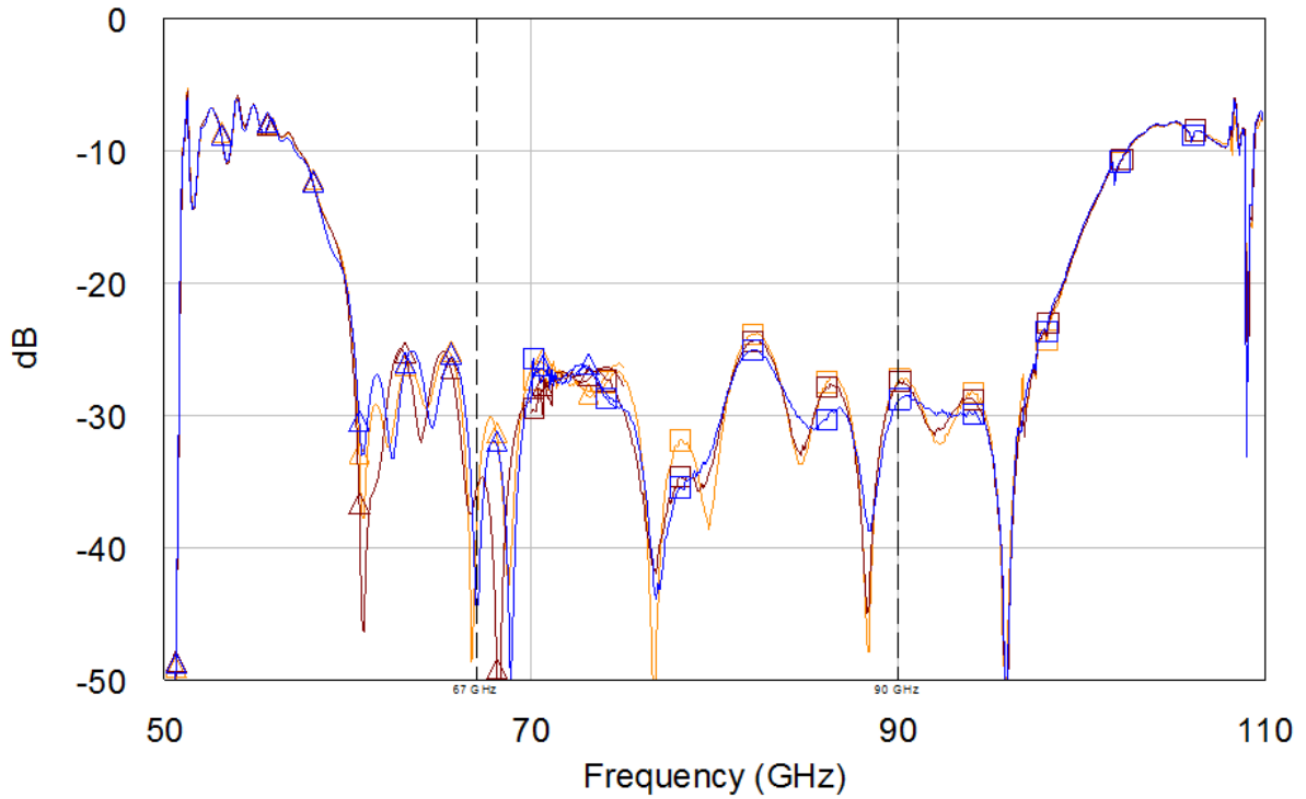


Figure 42: Plot shows the simulated isolation between the isolated RF hybrid ports.

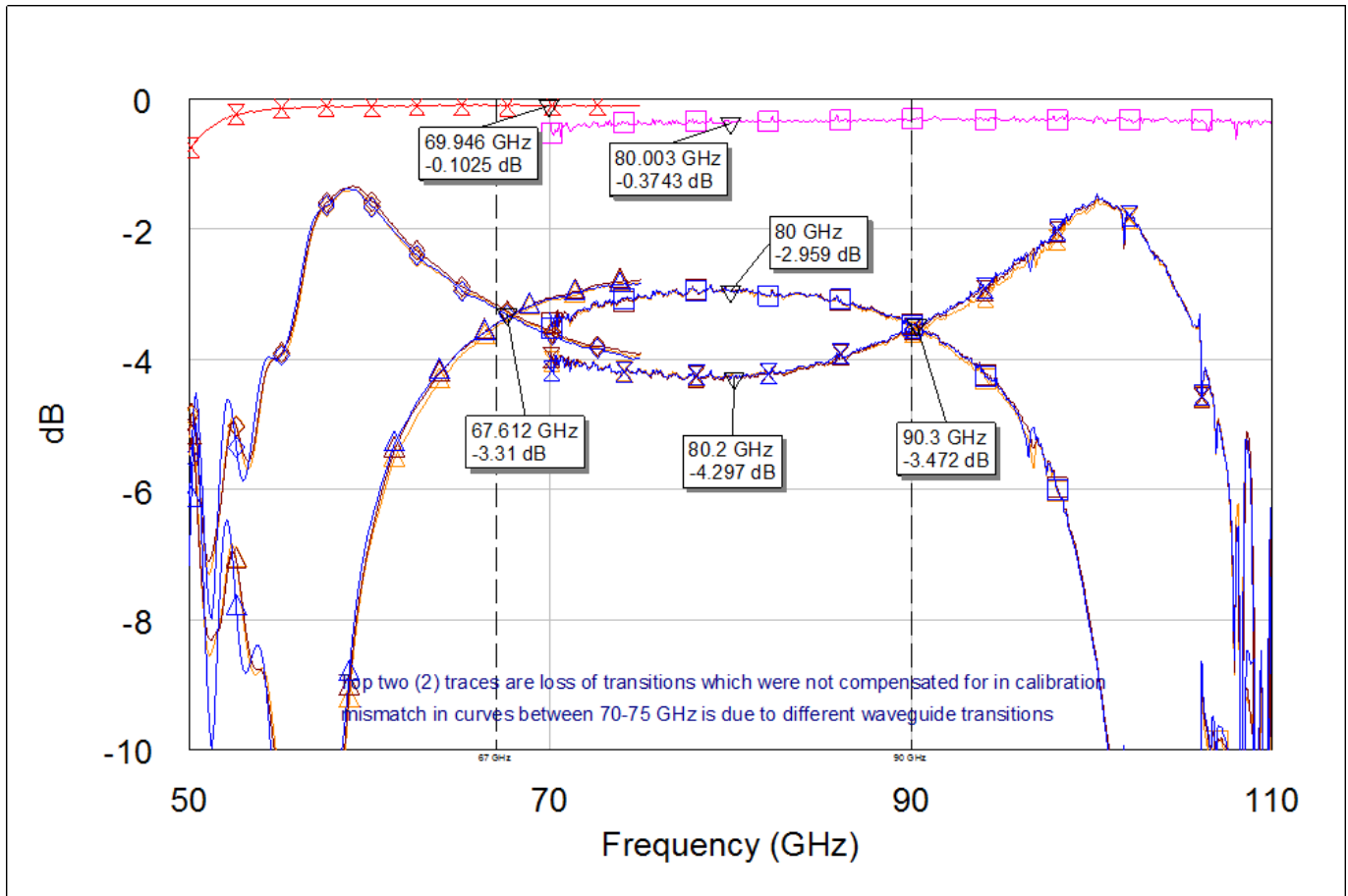


Figure 43: Measured insertion loss of the RF hybrid(s) from the input port to the two output ports.

The blue and the orange traces correspond to two separate blocks. See Section [7.9.1](#) for the rationale behind the selection of frequencies with perfect match.

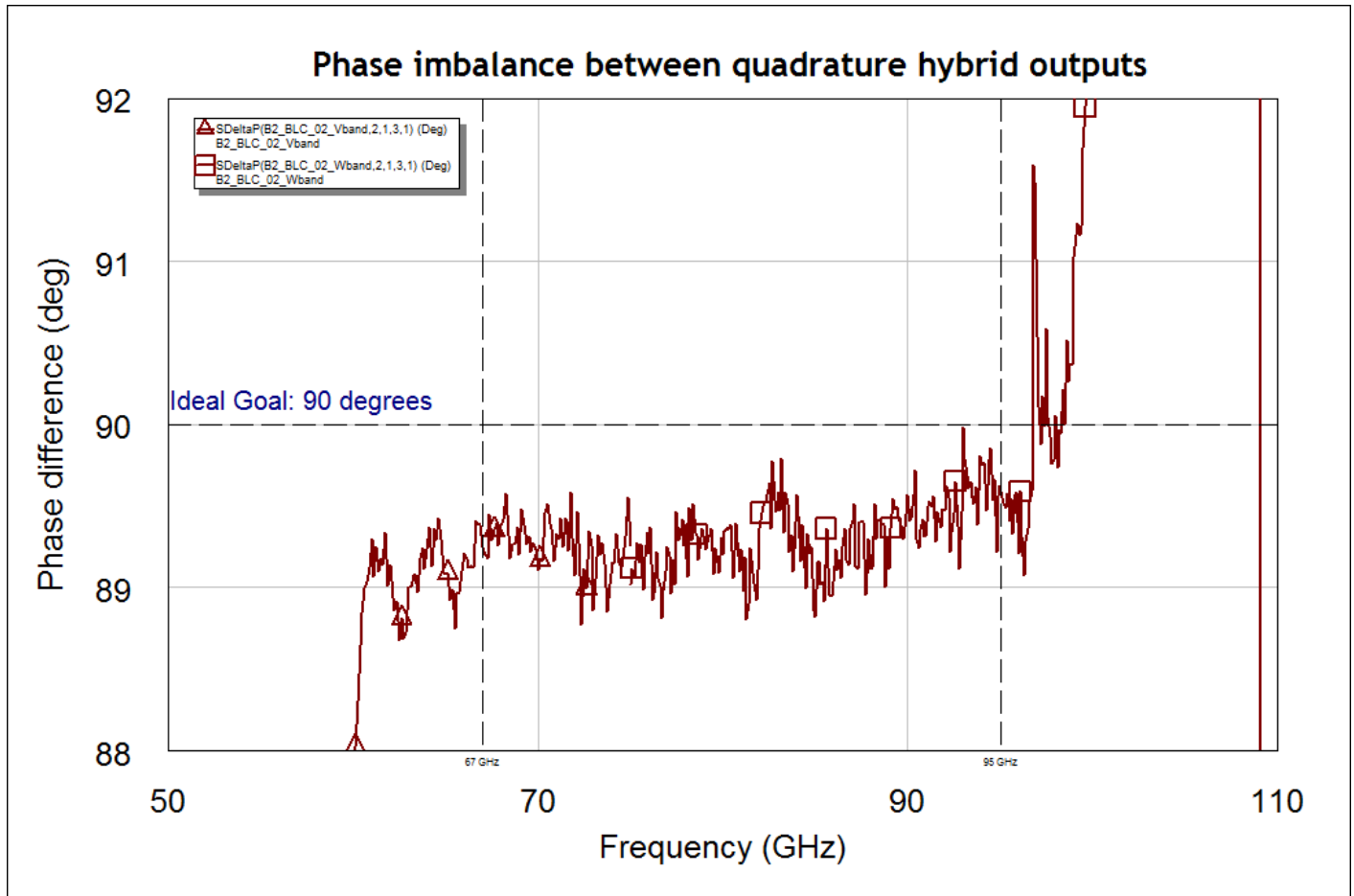



Figure 44: Measured phase imbalance between the two output ports of the quadrature hybrid.

| | | |
|---|--|-------------------------------------|
|  | ALMA Project | Date: 2017-12-27 Page: 56 of 117 |
| | Design and testing of a Prototype Band 2 Cartridge Final Report | |

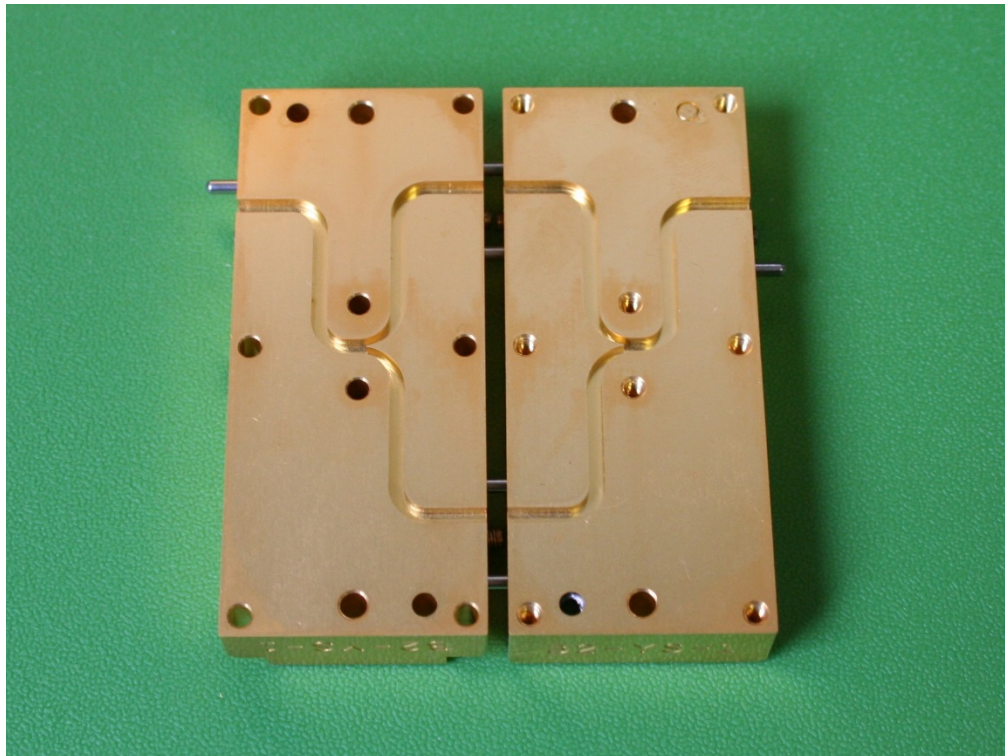



Figure 45: Photograph of the top and bottom portion of the Y-splitter split block assembly (WR-12).

| | | |
|---|--|-------------------------------------|
|  | ALMA Project | Date: 2017-12-27 Page: 57 of 117 |
| | Design and testing of a Prototype Band 2 Cartridge Final Report | |

7.9.2. Warm IF Amplifiers

The IF amplifiers located at the output of the down converter meet specifications given in [Table 13](#):

| Table 12: Requirements For Band 6 Warm IF Amps | |
|--|-------------------------------|
| Frequency Range | 4 - 12 GHz |
| Gain ¹ | 27 dB min |
| Gain slope (4-12 GHz) | ± 1.5 dB peak-to-peak max |
| Gain slope (any 2-GHz section) | ± 0.7 dB peak-to-peak max |
| Noise figure | 1.5 dB max |
| Power @ 1-dB Compression Point | +10 dBm |
| Input VSWR | 1.8:1 max. |
| Output VSWR ² | 1.33:1 max |
| DC Supply Voltage | 8 volts |
| Operating Temperature Range | +10°C to +40°C |
| Storage Temperature Range | -30°C to +65°C |
| Altitude | 16,400 feet |
| RF connectors | SMA female |

7.9.3. IF Hybrid

The IF hybrids used in the downconverter are MAC Technology Model C7256D as described in [Table 14](#). The same hybrids were used in Band 6 sideband separating mixers, but for Band 2, the hybrids operate at room temperature and hence either designs sufficient; the original design or the cryogenic design (with the D suffice) used in Band 6. An outline drawing is given in [Figure 46](#) and measured amplitude and phase balance is shown in [Figure 47](#).

| Table 13: Specifications for IF Hybrids | |
|---|------------------|
| Manufacturer | MAC Technologies |
| Model | C7256D |
| Frequency Range | 4 – 12.4 GHz |
| Coupling | 3.3 ± 0.8 dB |
| Frequency Sensitivity | ± 0.40 dB |
| Minimum Isolation | 15 dB |
| VSWR | 1.5:1 |
| Power @ 1-dB Compression Point | +10 dBm |
| Input VSWR | 1.8:1 max. |
| Output VSWR ³ | 1.33:1 max |

¹ Gain assumes integral attenuator on output to improve output VSWR to 1.33:1

² Output VSWR specified with integral attenuator.

³ Output VSWR specified with integral attenuator.

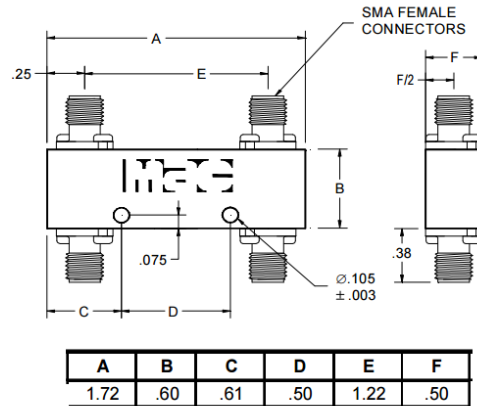


Figure 46: MAC Technology C7256D Hybrid Outline Drawing

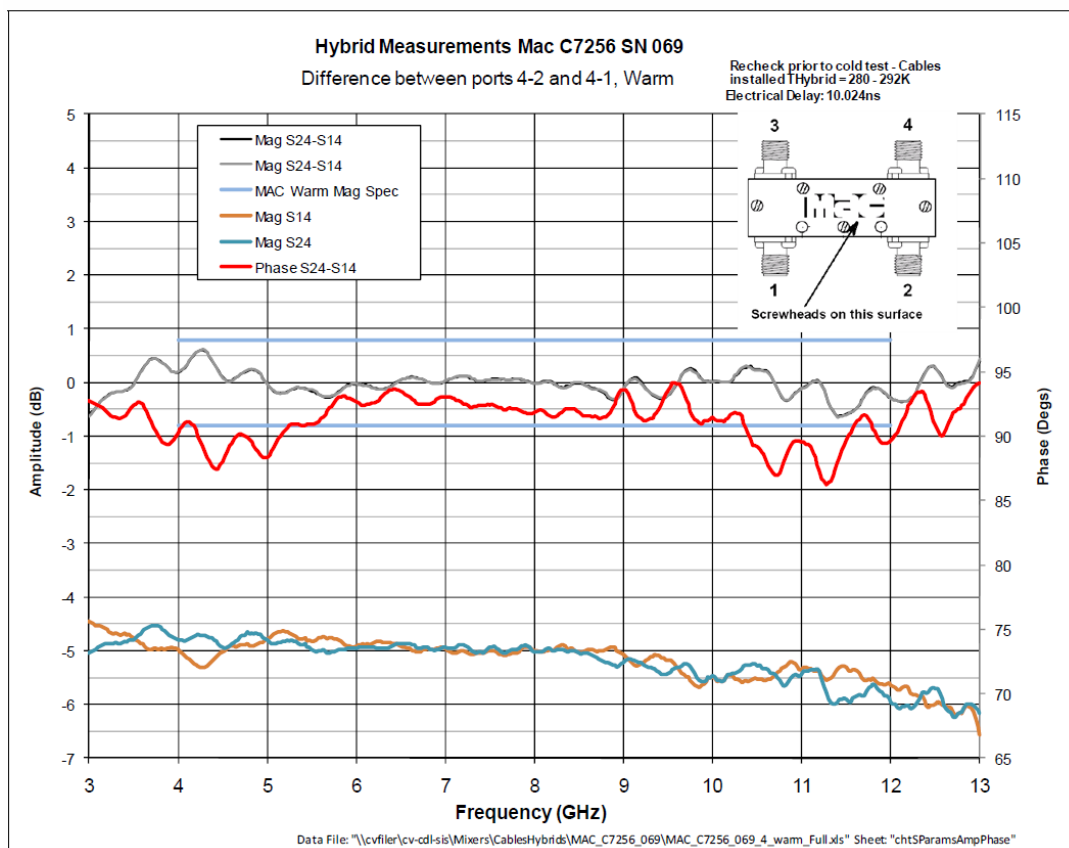


Figure 47: Measured Amplitude and Phase Balance for MAC Technology C7256

Table 15 provides a summary of the image rejection measurements for 2SB downconverters for the two polarization channels, measured in 1 GHz RF step size. Detailed (in RF step size of 200 MHz) measurement plots are provided in Section-8.2.

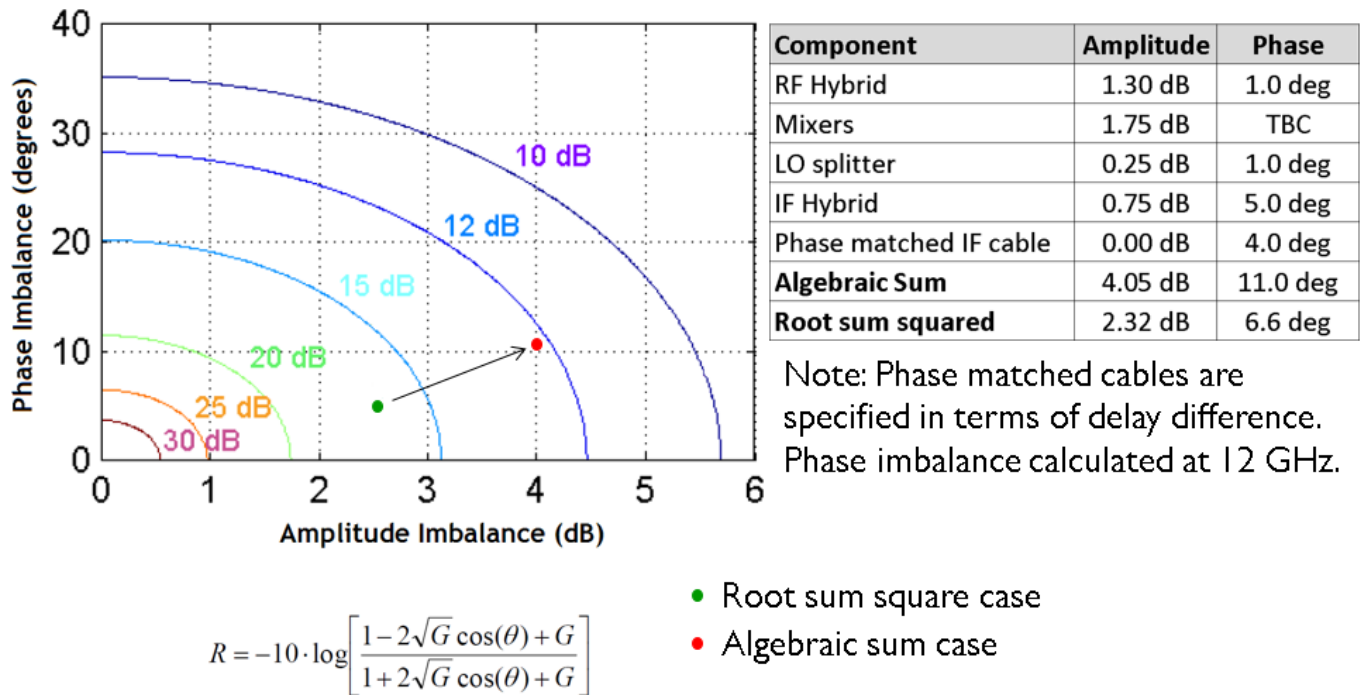


Figure 48: Calculation of the amplitude & phase imbalances and estimated image rejection for the 2SB mixer design.

Table 14: Measured Image Rejection Table


Summary of the image rejection measurements for 2SB downconverters for the two polarization channels.
Detailed measurements plots are provided in Section 8.2.

| LO | Polarization-0 Image Rejection Data | | | | | | | | | | | | | | | | | | (USB) | | | | | | | | |
|---|-------------------------------------|----------|----------|----------|----------|----------|----------|----------|----------|-------------------|-------------------|-------------------|-------------------|-------------------|-------------------|-------------------|-------------------|-------------------|----------|--------|--------|--------|--------|--------|--------|--------|--------|
| | (LSB) | RF IR | RF IR | RF IR | RF IR | RF IR | RF IR | RF IR | RF IR | RF IR | IR RF | IR RF | IR RF | IR RF | IR RF | IR RF | IR RF | IR RF | | | | | | | | | |
| 72 GHz | | | | | | | | | | 67 GHz No meas | 68 GHz 28.1 dB | 76 GHz 14.5 dB | 77 GHz No meas | 78 GHz | 79 GHz | 80 GHz | 81 GHz | 82 GHz | 83 GHz | 84 GHz | | | | | | | |
| 74 GHz | | | | | | | | | | 67 GHz No meas | 68 GHz 36.3 dB | 69 GHz 16.6 dB | 70 GHz 27.8 dB | 78 GHz | 79 GHz | 80 GHz | 81 GHz | 82 GHz | 83 GHz | 84 GHz | 85 GHz | 86 GHz | | | | | |
| 76 GHz | | | | | | | | | | 67 GHz No meas | 68 GHz 19.8 dB | 69 GHz 19.0 dB | 70 GHz 22.1 dB | 71 GHz 16.5 dB | 72 GHz 29.0 dB | 80 GHz | 81 GHz | 82 GHz | 83 GHz | 84 GHz | 85 GHz | 86 GHz | 87 GHz | 88 GHz | | | |
| 78 GHz | | | | | | | | | | 67 GHz No meas | 68 GHz 20.0 dB | 69 GHz 20.8 dB | 70 GHz 14.8 dB | 71 GHz 19.6 dB | 72 GHz 16.0 dB | 73 GHz 14.2 dB | 74 GHz 19.6 dB | 82 GHz | 83 GHz | 84 GHz | 85 GHz | 86 GHz | 87 GHz | 88 GHz | 89 GHz | 90 GHz | |
| 80 GHz | | | | | | | | | | 68 GHz 23.1 dB | 69 GHz 26.2 dB | 70 GHz 28.4 dB | 71 GHz 33.6 dB | 72 GHz 23.2 dB | 73 GHz 35.5 dB | 74 GHz 24.0 dB | 75 GHz 26.2 dB | 76 GHz 34.0 dB | 84 GHz | 85 GHz | 86 GHz | 87 GHz | 88 GHz | 89 GHz | 90 GHz | 91 GHz | 92 GHz |
| 82 GHz | | | | | | | | | | 70 GHz | 71 GHz No meas | 72 GHz 27.2 dB | 73 GHz 36.0 dB | 74 GHz 24.6 dB | 75 GHz 33.7 dB | 76 GHz 24.1 dB | 77 GHz 18.8 dB | 78 GHz 30.1 dB | 86 GHz | 87 GHz | 88 GHz | 89 GHz | 90 GHz | 91 GHz | 92 GHz | 93 GHz | 94 GHz |
| 84 GHz | | | | | | | | | | 72 GHz | 73 GHz | 74 GHz | 75 GHz No meas | 76 GHz 23.6 dB | 77 GHz 28.9 dB | 78 GHz 23.9 dB | 79 GHz 18.1 dB | 80 GHz 35.9 dB | 88 GHz | 89 GHz | 90 GHz | 91 GHz | 92 GHz | 93 GHz | 94 GHz | | |
| 86 GHz | | | | | | | | | | 74 GHz | 75 GHz | 76 GHz | 77 GHz | 78 GHz | 79 GHz No meas | 80 GHz 25.9 dB | 81 GHz 20.5 dB | 82 GHz 24.4 dB | 90 GHz | 91 GHz | 92 GHz | 93 GHz | 94 GHz | | | | |
| | | | | | | | | | | 12 GHz | 11 GHz | 10 GHz | 9 GHz | 8 GHz | 7 GHz | 6 GHz | 5 GHz | 4 GHz | 4 GHz | 5 GHz | 6 GHz | 7 GHz | 8 GHz | 9 GHz | 10 GHz | 11 GHz | 12 GHz |
| | | | | | | | | | | IF (LSB) | | | | | | | | | IF (USB) | | | | | | | | |
| Number in green and blue font represent image rejection values corresponding to lower and upper sidebands respectively. Specification is better than 10 dB IR over 80% of the IF range, and better than 7 dB IR over the full range. Intermediate frequencies outside of the contiguous diamond shaped area correspond to RFs that are "in-band" but have out-of-band image falling on it. "Out-of-band" RFs that are of interest are shown grayed out. | | | | | | | | | | | | | | | | | | | | | | | | | | | |

Number in green and blue font represent image rejection values corresponding to lower and upper sidebands respectively. Specification is better than 10 dB IR over 80% of the IF range, and better than 7 dB IR over the full range. Intermediate frequencies outside of the contiguous diamond shaped area correspond to RFs that are "in-band" but have out-of-band image falling on it. "Out-of-band" RFs that are of interest are shown grayed out.

| LO | Polarization-1 Image Rejection Data | | | | | | | | | | | | | | | | | | (USB) | | | | | | | | | | | | | | | | |
|--|-------------------------------------|----------|----------|----------|----------|----------|----------|----------|-------------------|-------------------|-------------------|-------------------|-------------------|-------------------|-------------------|-------------------|-------------------|----------|--------|--------|--------|--------|--------|--------|--------|--------|--|--|--|--|--|--|--|--|--|
| | (LSB) | RF IR | RF IR | RF IR | RF IR | RF IR | RF IR | RF IR | RF IR | IR RF | IR RF | IR RF | IR RF | IR RF | IR RF | IR RF | IR RF | IR RF | | | | | | | | | | | | | | | | | |
| 72 GHz | | | | | | | | | 67 GHz No meas | 68 GHz 17.6 dB | 76 GHz 17.4 dB | No meas | 77 GHz | 78 GHz | 79 GHz | 80 GHz | 81 GHz | 82 GHz | 83 GHz | 84 GHz | | | | | | | | | | | | | | | |
| 74 GHz | | | | | | | | | 67 GHz No meas | 68 GHz 23.8 dB | 69 GHz 19.1 dB | 70 GHz 16.5 dB | 78 GHz | 79 GHz | 80 GHz | 81 GHz | 82 GHz | 83 GHz | 84 GHz | 85 GHz | 86 GHz | | | | | | | | | | | | | | |
| 76 GHz | | | | | | | | | 67 GHz No meas | 68 GHz 20.4 dB | 69 GHz 22.4 dB | 70 GHz 19.3 dB | 71 GHz 17.4 dB | 72 GHz 16.2 dB | 80 GHz | 81 GHz | 82 GHz | 83 GHz | 84 GHz | 85 GHz | 86 GHz | 87 GHz | 88 GHz | | | | | | | | | | | | |
| 78 GHz | | | | | | | | | 67 GHz No meas | 68 GHz 25.7 dB | 69 GHz 24.6 dB | 70 GHz 22.9 dB | 71 GHz 29.5 dB | 72 GHz 31.7 dB | 73 GHz 29.8 dB | 74 GHz 15.0 dB | 82 GHz | 83 GHz | 84 GHz | 85 GHz | 86 GHz | 87 GHz | 88 GHz | 89 GHz | 90 GHz | | | | | | | | | | |
| 80 GHz | | | | | | | | | 68 GHz 23.6 dB | 69 GHz 28.2 dB | 70 GHz 21.4 dB | 71 GHz 27.1 dB | 72 GHz 22.7 dB | 73 GHz 25.5 dB | 74 GHz 22.8 dB | 75 GHz 17.9 dB | 76 GHz 19.0 dB | 84 GHz | 85 GHz | 86 GHz | 87 GHz | 88 GHz | 89 GHz | 90 GHz | 91 GHz | 92 GHz | | | | | | | | | |
| 82 GHz | | | | | | | | | 70 GHz | 71 GHz No meas | 72 GHz 20.9 dB | 73 GHz 25.1 dB | 74 GHz 21.6 dB | 75 GHz 22.2 dB | 76 GHz 25.9 dB | 77 GHz 26.2 dB | 78 GHz 14.7 dB | 86 GHz | 87 GHz | 88 GHz | 89 GHz | 90 GHz | 91 GHz | 92 GHz | 93 GHz | 94 GHz | | | | | | | | | |
| 84 GHz | | | | | | | | | 72 GHz | 73 GHz | 74 GHz | 75 GHz No meas | 76 GHz 21.0 dB | 77 GHz 25.8 dB | 78 GHz 19.8 dB | 79 GHz 18.1 dB | 80 GHz 16.2 dB | 88 GHz | 89 GHz | 90 GHz | 91 GHz | 92 GHz | 93 GHz | 94 GHz | | | | | | | | | | | |
| 86 GHz | | | | | | | | | 74 GHz | 75 GHz | 76 GHz | 77 GHz | 78 GHz | 79 GHz No meas | 80 GHz 32.9 dB | 81 GHz 20.4 dB | 82 GHz 19.2 dB | 90 GHz | 91 GHz | 92 GHz | 93 GHz | 94 GHz | | | | | | | | | | | | | |
| | | | | | | | | | 12 GHz | 11 GHz | 10 GHz | 9 GHz | 8 GHz | 7 GHz | 6 GHz | 5 GHz | 4 GHz | 4 GHz | 5 GHz | 6 GHz | 7 GHz | 8 GHz | 9 GHz | 10 GHz | 11 GHz | 12 GHz | | | | | | | | | |
| | | | | | | | | | IF (LSB) | | | | | | | | | IF (USB) | | | | | | | | | | | | | | | | | |
| <p>Number in green and blue font represent image rejection values corresponding to lower and upper sidebands respectively. Specification is better than 10 dB IR over 80% of the IF range, and better than 7 dB IR over the full range. Intermediate frequencies outside of the contiguous diamond shaped area correspond to REs that are "in-band" but have out-of-band image falloff on it. "Out-of-band" REs that are of interest are shown around out.</p> | | | | | | | | | | | | | | | | | | | | | | | | | | | | | | | | | | | |

Number in green and blue font represent image rejection values corresponding to lower and upper sidebands respectively. Specification is better than 10 dB IR over 80% of the IF range, and better than 7 dB IR over the full range. Intermediate frequencies outside of the contiguous diamond shaped area correspond to RFs that are "in-band" but have out-of-band image falling on it. "Out-of-band" RFs that are of interest are shown grayed out.

| | | |
|---|--|-------------------------------------|
|  | ALMA Project | Date: 2017-12-27 Page: 61 of 117 |
| | Design and testing of a Prototype Band 2 Cartridge Final Report | |

7.10. LO

Each polarization channel is driven by its own LO chain. The LO consists of three basic modules. The fundamental oscillator, starting from 12.3-14.7 GHz, is a YIG tuned oscillator (YTO). The YTO is a commercially available unit and is the only choice for broadband electronically tunable VCOs with the low phase noise required for ALMA. Following the YTO are two custom modules, the AMC (Active Multiplier Chain) and the PA (power amplifier). The function of the AMC is to frequency multiply, filter, and amplify the YTO output up to the final warm LO frequency. The AMC also performs the function of mixing the generated LO with the millimeter-wave phase reference from the photo-mixer, which bolts directly to the AMC. The AMC has an IF output from this mixer that is routed to a PLL module to phase lock the YTO. The PA module divides the LO signal into two channels and independently amplifies the output of the AMC. The final power level at each PA output is computer controllable for optimization of the LO power, if necessary.

Originally, the Band 2 down conversion was envisaged as SSB, requiring an LO coverage of 79 – 94 GHz to cover the full RF band (67 – 90 GHz) using the lower sideband. Since the baseline scheme used in the Band 2 cartridge prototype is 2SB with 4 – 12 GHz IF, the entire RF can be covered with a smaller LO range of 79 – 87 GHz for Band 2+. The RF/LO/IF frequency mapping scheme is shown in [Figure 49](#). This is a subset of the ALMA Band 6 WCA LO range (which is 73.667 – 88.333 GHz), so the Band 6 LO design was adopted for the Band 2 LO scheme. Since Band 2 does not have cryogenic multipliers and the LO signal does not need to be routed to the inside of the cold cartridge assembly, the mechanical arrangement of the LO modules was adjusted to accommodate the downconverter components alongside the LO components on the WCA as depicted in [Figure 3](#). The wider than required frequency range of the Band 6 LO should allow for some added frequency flexibility for the Band 2 receiver. Since amplitude noise from the LO is not of significant concern for Band 2, there was no need to limit the frequency range to improve amplitude noise performance.

The Band 6 LO and the relevant modules as well as their performance(s) are described in detail in the ALMA LO Design Report [\[RD 57\]](#). Those details apply verbatim to Band 2 and are consequently not repeated here in this design document.

7.10.1. LO Frequency Range

RF, LO, and IF frequency mappings are shown in [Figure 49](#). The band 2 LO reuses the Band 6 LO design, and the Band 6 LO is specified ([\[RD 69\]](#)) to operate from 73.7 to 88.3 GHz. The diagram specifically shows how the selection of just 79 and 87 GHz allows the Band 2 cartridge to cover the entire Band 2+ frequency range with just these two LO frequencies. Although the theoretical tuning limit for using the Band 6 LO is $88.2 + 12 = 100.2$ GHz, the upper end of the Band 2+ range is limited to 95 GHz by components other than the LO.

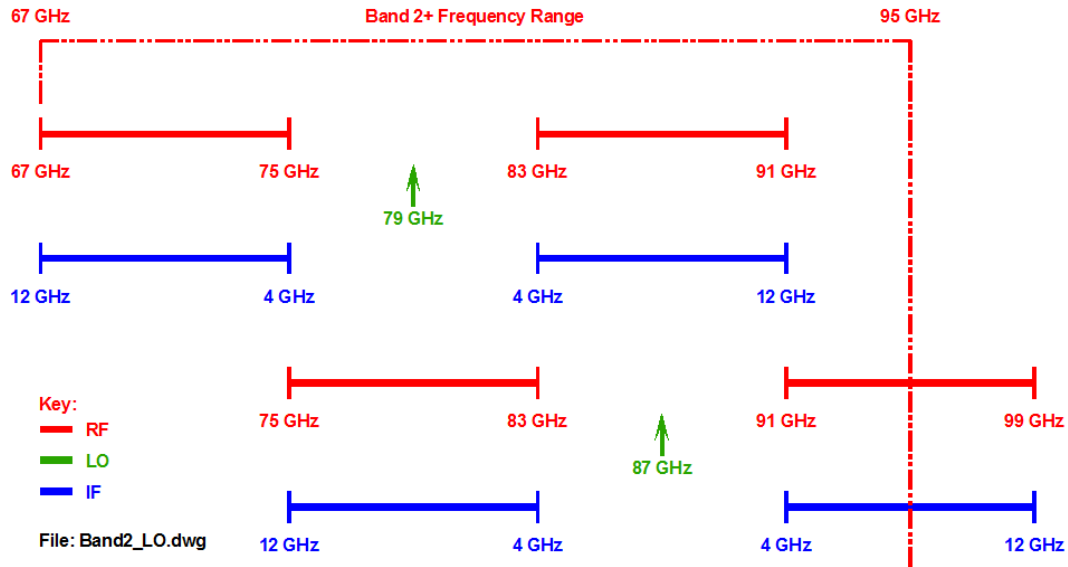


Figure 49: RF, LO, and IF Band Frequency Ranges

7.11. Thermal Loading


In order to meet thermal loading requirements ([\[RD 54\]](#), [\[RD 56\]](#)) and to minimize thermal conduction to the cryogenic amplifiers, all wires, cables, and waveguides are thermally connected to the 110 K and 15 K plates before reaching the cryogenic preamplifiers. Materials with low thermal conductance are used (*i.e.* stainless steel waveguide and phosphor bronze DC wiring) except where this leads to excessive electrical loss

Gold plated, annealed copper heat straps are used, as described in the drawings in Section [7.12](#). Thermally conducting grease is not used at the ends of heat straps. [\[RD 55\]](#) gives measurements of the thermal resistance of the heat straps used in the cartridge and shows that Apiezon-N grease is advantageous only for bolted joints whose contact area is 10 cm² or larger, but Apiezon-N actually increases thermal resistances for smaller contact areas. In Band 2 cartridges, Apiezon-N grease is used only in the cable heat sinks where it is an essential part of the thermal path.

Power dissipation for the MIC and MMIC versions of the cold LNAs is shown in [Table 16](#). In the MMIC LNAs, each “stage” is an independent MMIC chip. Each Band 2 cartridge contains two such cold LNAs thermally attached to the 15-K stage.

Static heat loading on each of the stages from the 96 phosphor-bronze wires and 2 stainless steel waveguides is given in [Table 18](#). Additional heat loads due to dissipation in the cryogenic amplifiers on the 15 K stage are also shown in [Table 18](#) from the values presented in [Table 16](#).

[Table 17](#) provides details of thermal loading calculations for the stainless steel WR-12 waveguide. Thermal conductivities are a function of temperature at cryogenic temperatures, so the 8-term NIST conductivity equation [\[RD 68\]](#) was integrated between the relevant temperatures to find thermal conductivity in units of Wm⁻¹. Power conduction is then found by multiplying by the cross-sectional area and dividing by the length of the waveguide. A more realistic 80K was assumed as the temperature for the 110K stage. Ideal thermal conductivity was also assumed for the 25 mm gold-plated sections on the exterior of the waveguides [\[RD 18\]](#) between the 300K and 110K stages and the 110K and

| | | |
|---|--|-------------------------------------|
|  | ALMA Project | Date: 2017-12-27 Page: 63 of 117 |
| | Design and testing of a Prototype Band 2 Cartridge Final Report | |

15K stages. Since that assumption reduces the length of the intervening stainless steel waveguides sections, it results in the worst-case thermal loads.

Table 15: Power Dissipation from Cold LNAs

| MIC Amplifiers | | | | MMIC Amplifiers | | | |
|-------------------------------------|--------------------|-------------------|------------------------|-----------------|--------------------|-------------------|------------------------|
| Stage | Drain Current (mA) | Drain Voltage (V) | Power Dissipation (mW) | Stage | Drain Current (mA) | Drain Voltage (V) | Power Dissipation (mW) |
| 1 | 1.5 | 0.8 | 1.2 | 1 | 9 | 1.1 | 9.9 |
| 2 | 1.5 | 0.8 | 1.2 | 2 | 28 | 1.2 | 33.6 |
| 3 | 4 | 1.0 | 4 | -- | -- | -- | -- |
| 4 | 5 | 1.5 | 7.5 | -- | -- | -- | -- |
| 5 | 12 | 1.7 | 20.4 | -- | -- | -- | -- |
| Total for each preamp: | | | 34.3 | | | | 43.5 |
| Total into 15K stage for both LNAs: | | | 68.6 | | | | 87 |

Table 16: Thermal Loading from Waveguide

| | | | |
|---|---|-----------------------|--------------------------|
| WR-12 0.122 ins x 0.061 ins | | | |
| Outside dims from dwg 0.141 ins x 0.081 ins | | | |
| | a dim | 3.0988 mm | 0.0030988 m |
| | b dim | 1.5494 mm | 0.0015494 m |
| | wall thickness | 0.254 mm | 0.000254 m |
| | area | 2.619 mm ² | 2.619E-06 m ² |
| SS Waveguide: 300K to 110K stage | Length | 13.3 cm | 0.133 m |
| | Thot | 300 K | |
| | Tcold | 80 K | |
| | Using vba integration with NIST 8-term equation | | |
| | k*ΔT | 2706 Wm ⁻¹ | |
| | P | 0.053 W | 53.3 mW |
| SS Waveguide: 110K to 15K stage | Length | 5.9 cm | 0.059 m |
| | Thot | 80 K | |
| | Tcold | 15 K | |
| | Using vba integration with NIST 8-term equation | | |
| | k*ΔT | 339 Wm ⁻¹ | |
| | P | 0.015 W | 15.0 mW |

<https://sharepoint.nrao.edu/cdl/Shared Documents/ALMA/Band 2/Background documents/ThermalAnalysis1.xlsm>


| | | |
|---|--|-------------------------------------|
|  | ALMA Project | Date: 2017-12-27 Page: 64 of 117 |
| | Design and testing of a Prototype Band 2 Cartridge Final Report | |

Table 17: Static and On-State Heat Loads from Waveguides and Wiring


LNA power dissipation is given in [Table 16](#) details of the waveguide thermal loads are shown in [Table 17](#)

| Thermal Loading Summary, Band 2 Cartridge | | | |
|---|-------------------|--------------------|------------|
| Loading (mW) | 15K | 110K | |
| Wiring (from below) | 15.2 | 113 | |
| Waveguide (from below) | 30.0 | 107 | |
| Totals | 45.2 | 219 | |
| Max Allow ed Static Loads [from (1)] | 95.0 | 450 | |
| Static Heat Load Margin (mW) | 49.8 | 231 | |
| | MMIC | MIC | |
| Additional Active Heat Load | 87.0 | 68.6 | 0 |
| Total Allow ed Active Heat Load [from (1)] | 90.0 | | 150 |
| Active Heat Load Margin (mW) | 3.0 | 21.4 | 150 |
| | | | |
| Loading Between Stages: | 15K - 110K | 110K - 300K | |
| Wiring: | | | |
| Length (mm) | 130 | 130 | |
| Loading [from (2)] (mW/w ire) | 0.16 | 1.17 | |
| Wires | 96 | 96 | |
| Totals (mW) | 15.2 | 113 | |
| Waveguide: | | | |
| 304 Stainless section | | | |
| Loading [from (3)] (mW) | 15.0 | 53.3 | |
| Num of WG's | 2 | 2 | |
| Totals (mW) | 30.0 | 106.6 | |
| | | | |
| Ref's | | | |
| (1) From "ALMA FE Thermal Budge", FEND-40.00.00.00-050-B-GEN, 2007-04-11 and Band 2 to Dew ar ICD, FEND-40.02.02.00-40.03.01.00-A-ICD | | | |
| (2) Loading from Anna Orlow ska's "Cryostat design report", FEND-40.03.00.00-007-A-REP, 2003-12-05 (assumes 125 um of BeCu, length parameter not used) | | | |
| (3) Effland, integrating NIST conductivities for 304 stainless steel | | | |
| | | | |
| http://sharepoint.nrao.edu/cdi/Shared Documents/ALMA/Band 2/Background documents/ThermalAnalysis1.xlsm | | | |

7.12. Wiring and cabling

The M&C electronics interfaces with the cryogenic wiring harness through the hermetic connectors in the cartridge base plate as specified in [\[RD 41\]](#). Protection circuits in the vacuum space of the cartridge next to the base-plate protect the mixers and preamplifiers when the bias module and Warm Cartridge Assembly are removed from the base-plate [\[RD 42\]](#).

The two hermetic connectors providing bias voltage and currents and temperature sensor information are attached to a single carrier plate mounted on the 300 K base plate of the cartridge and are drawn in [\[RD 43\]](#) and [\[RD 44\]](#).

| | | |
|---|--|-------------------------------------|
|  | ALMA Project | Date: 2017-12-27 Page: 65 of 117 |
| | Design and testing of a Prototype Band 2 Cartridge Final Report | |

7.12.1. Electronic Interface

The Band 2 cold LNAs use a multi-wire bias scheme to supply the gate and drain voltages for the five stages with a separate wire for ground return. Connector pin assignments and voltage ranges for the mixer and preamplifier are given in the ICD [\[RD 52\]](#). Cold LNA bias connections are made through the MDM connector mounted on LNA block.

7.12.2. Wiring Diagram

The Band 2 cartridge uses the standard ALMA cartridge wiring harness drawn in [\[RD 20\]](#). Phosphor bronze 36 AWG wire is used, twisted in pairs and then woven into a ribbon of 12 pairs (24 wires). The wiring diagram of the harness for the Band 2 cartridge is shown in [Figure 52](#) (source document is [\[RD 20\]](#)) and the pigtail, which connects the 15-K heat sinks to the cold LNAs and temperature sensors is shown in [Figure 54](#) (source document is [\[RD 21\]](#)).

To reduce the risk of electrostatic discharge damaging the mixers, protection circuits identical to those used for Band 6 cartridges are mounted in the vacuum space of the cartridge. A schematic diagram of the bias protection board is given in [Figure 56](#).

All wiring is heat sunk on the 110K stage to reduce thermal loading using the harness clamp design identical to the Band 6 heat sinks as drawn in [\[RD 45\]](#). The 15K heatsink is identical to the Koller 4K design from Band 6 cartridges, shown in [Figure 53](#), drawn in [\[RD 46\]](#), and is assembled using the procedures in [\[RD 47\]](#). The pigtails from the 9-pin MDM connectors on the 15-K heat sinks to the various components are shown in [Figure 54](#).

7.13. Vacuum Considerations

Vacuum seals for the Band 2 cartridge are made using (Fluoroelastomer, FKM) Viton O-rings, which appear to be the best choice short of using metal O-rings with knife-edges in the grooves. Slides 7, 10, 12, 14, and 15 in [\[RD 64\]](#) review O-ring choices. NASA's measurements [\[RD 65\]](#) show that outgassing properties of nearly all Viton seals meet ALMA specs of Total Mass Loss (TML) < 1.0 % and Collected Volatile Condensable Material (CVCM) < 0.1 % ([Figure 51](#)) while the more traditional Buna-N O-ring material does not as shown in [Figure 50](#).

| MATERIAL | % TML | % CVCM | CURE TIME | CURE TEMP | AT- MOS | % WVR | DATA REF | APPLICATION | MFR CODE |
|------------------------------------|----------|-----------|--------------|--------------|------------|----------|-------------|------------------|-------------|
| BUNA-S RUBBER DIAPHRAGM | 12.79 | 6.41 | | | | 0.14 | GSC32719 | RUBBER DIAPHRAGM | DEB |
| EC 2126 BUNA N ADHESIVE | 9.48 | 1.32 | 72H | 25 | AIR | | GSFC3584 | ADHESIVE | MMM |
| PARKER O-RING N-219-7 BUNA N | 4.49 | 2.24 | | | | | GSFC0686 | O-RING | PSC |
| PARKER O-RING N-299-5 BUNA-N | 14.74 | 6.25 | | | | | GSFC0680 | O-RING | PSC |
| PARKER O-RING N-674-70 BUNA N | 4.99 | 2.40 | | | | | GSFC2875 | O-RING | PSC |
| PARKER O-RING N674-70 BLACK BUNA-N | 7.70 | 4.12 | 8H | 71 | AIR | 0.26 | GSC20902 | O-RING | PSC |

Figure 50: NASA Outgassing properties for Buna-N

| MATERIAL | % TML | % CVMC | CURE TIME | CURE AT- TEMP MOS | % WVR | DATA REF | APPLICATION | MFR CODE |
|--|----------|-----------|--------------|----------------------|----------|-------------|------------------|-------------|
| BLACK VITON GASKET MATERIAL | 0.21 | 0.00 | | | 0.06 | GSC28399 | VACUUM GASKET | ASG |
| FLURAN F5005 VITON A RED TUBING | 0.53 | 0.00 | | | | GSFC4582 | TUBING | NPC |
| O-RING - VITON A | 0.21 | 0.03 | | | | GSFC5657 | O-RING | AMI |
| O-RING BLACK VITON 360.07078142 | 0.15 | 0.00 | 24H | 66 AIR | 0.07 | GSC20887 | O-RING | DUP |
| PARKER O-RING 77-545 VITON A | 0.35 | 0.02 | | | | GSFC0683 | O-RING | PSC |
| PARKER O-RING V-0835 BLACK VITON FLUOROCARBON | 0.64 | 0.00 | | | 0.38 | GSC19833 | O-RING | PSC |
| PARKER O-RING V-0894 BROWN VITON CPND | 0.11 | 0.01 | | | 0.08 | GSC19723 | O-RING | PSC |
| PARKER O-RING V-747-75 VITON DUP E60C FLUOROCARBON | 0.10 | 0.00 | | | | GSFC3375 | O-RING | PSC |
| PRESRAY EXTRUDED VITON P-STRIP | 0.50 | 0.08 | | | 0.08 | GSC27010 | SEAL | PRS |
| SR 2702-75 VITON PER MIL R83248 TYPE 2 CLASS 1 | 0.16 | 0.00 | | | | GSFC4474 | DUST SEAL | STI |
| SR 2724-75 VITON E-60 | 0.46 | 0.00 | 24H | 260 AIR | 0.28 | GSC11294 | SEAL | STI |
| VITON 4900 BLACK GENERAL PURPOSE 70 DURO | 0.68 | 0.04 | | | 0.18 | GSC19168 | GASKET | DUP |
| VITON 4912 BLACK MIL R-83248 TYPE 2 CLASS 1 75 DURO | 0.15 | 0.01 | | | 0.10 | GSC19171 | GASKET | DUP |
| VITON A | 0.21 | 0.02 | | | | GSFC2071 | SEAL | DUP |
| VITON A GASKET | 0.29 | 0.01 | | | 0.18 | GSC30202 | GASKET | WCG |
| VITON A O-RING NAS 1593-012 | 0.21 | 0.02 | | | | GSFC2434 | O-RING | DUP |
| VITON A SHEET PER MIL-R-25897 TYPE II CLASS 1 1/16 INCH | 2.45 | 0.43 | | | 0.09 | GSC24635 | ELASTOMER | DUP |
| VITON B | 0.89 | 0.00 | | | | GSFC4382 | GROMMET | AGI |
| VITON B DUPONT | 0.86 | 0.04 | | | | GSFC1696 | SEAL | DUP |
| VITON C HOSE | 0.30 | 0.03 | | | | GSFC2422 | TUBING | DUP |
| VITON CABLE CLAMP | 1.43 | 0.17 | | | 0.11 | GSC30130 | CLAMP ELASTOMER | JAM |
| VITON CABLE CLAMP (VACUUM BAKED) | 0.18 | 0.01 | 24H | 160 AIR | 0.09 | GSC30178 | ELASTOMER | JMP |
| VITON GASKET MATERIAL | 0.14 | 0.01 | | | 0.04 | GSC28390 | VACUUM GASKET | THD |
| VITON IMPREGNATED DACRON DUPONT 84-001 | 0.85 | 0.09 | | | | GSFC2511 | DAMPER | DUP |
| VITON O-RING UHP (2-035-UHP) | 0.22 | 0.00 | | | 0.10 | GSC30208 | VACUUM SEAL RING | PSC2 |
| VITON O-RING, BLACK (2-035V747 LOT# 327528) | 0.18 | 0.00 | | | 0.09 | GSC27991 | O-RING | VAS |
| VITON O-RING, BLACK (2-035V747 LOT# 327528) WASHED IN SIMPLE GRN | 0.14 | 0.00 | 24H | 150 E-2 | 0.09 | GSC27994 | O-RING | VAS |
| VITON PER AMS 3218C, VIBRATION CUSHION, ITT P/N 8222244-2 | 0.14 | 0.01 | | | 0.03 | GSC32386 | O-RING CUSHION | PSC |
| VITON RUBBER (TB-187-031-77009) | 0.21 | 0.00 | | | 0.16 | GSC29902 | TUBE | AAA |
| VITON RUBBER BOOT | 0.30 | 0.00 | | | 0.16 | GSC34096 | CONNECTOR | KIG |
| VITON TUBING | 0.14 | 0.03 | 24H | 120 AIR | 0.07 | GSC25258 | ELASTOMER | MCM |
| VITON V-70 O-RINGS (INTERNAL X-87689) | 0.19 | 0.01 | | | 0.11 | GSC29851 | O-RINGS | NAS |
| VITON V0747-75 | 0.21 | 0.00 | | | 0.11 | GSC31723 | O-RING | PAH |
| VITON V14 BLACK BATCH 64135 CARBON BLACK | 0.17 | 0.01 | | | 0.11 | GSC14362 | SEAL | FEM |
| VITON V31 WHITE BATCH 50592 ZNO | 0.46 | 0.05 | | | 0.16 | GSC14364 | SEAL | FEM |
| VITON V31 WHITE BATCH 50592 ZNO | 0.22 | 0.01 | | | 0.15 | GSC14366 | SEAL | FEM |

Figure 51: NASA Outgassing properties for Viton

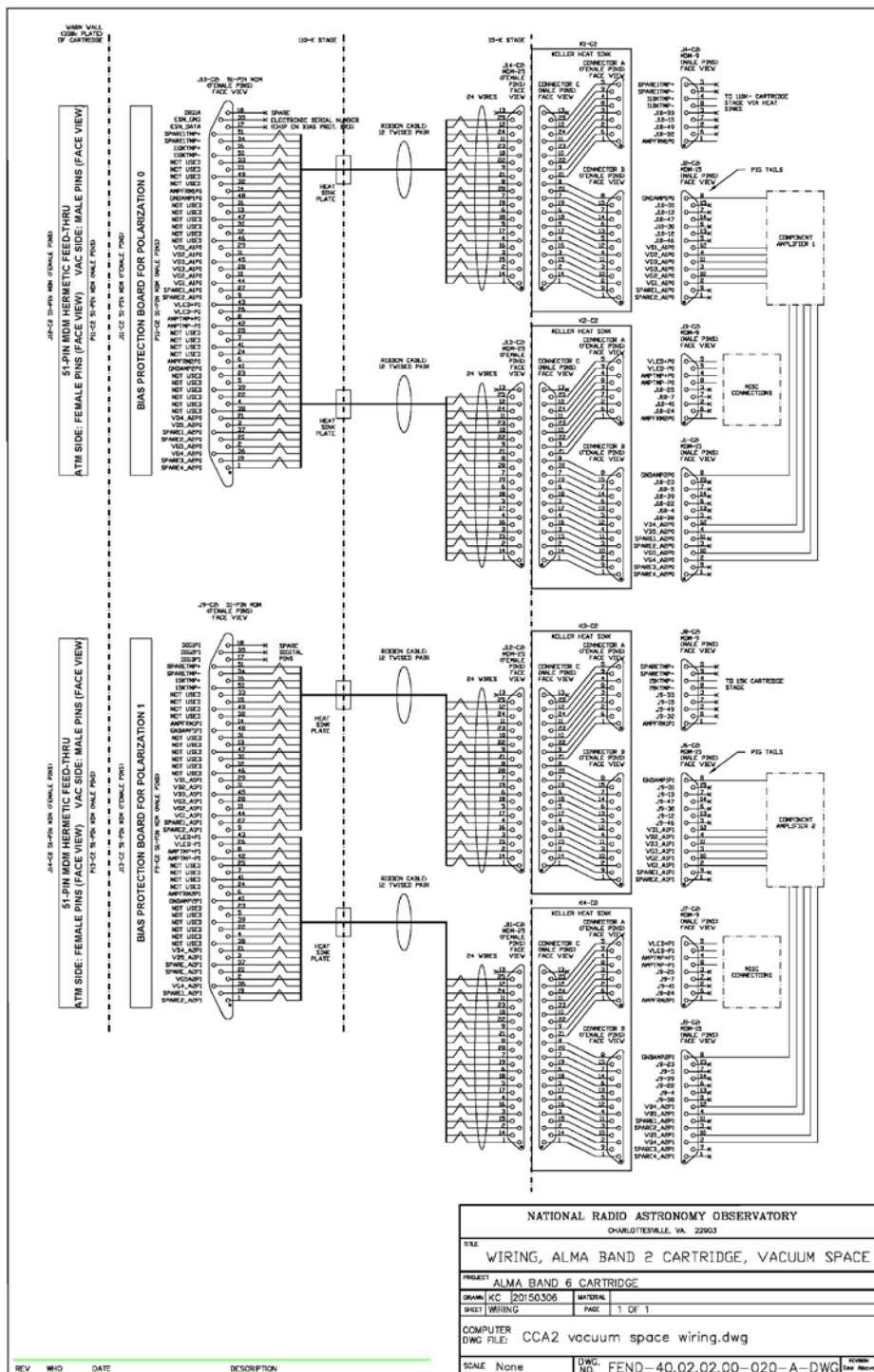


Figure 52: Band 2 Cartridge Wiring Diagram, from [\[RD 20\]](#)

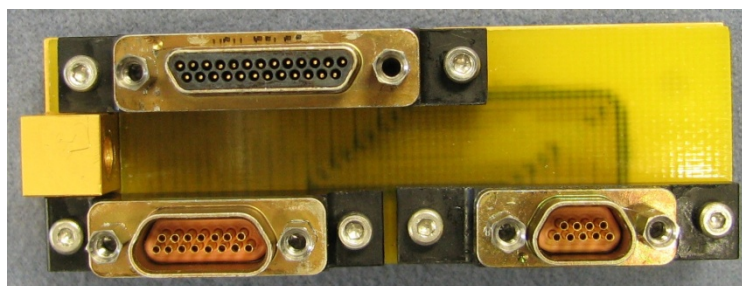


Figure 53: 15 K Wiring Koller Heat Sink

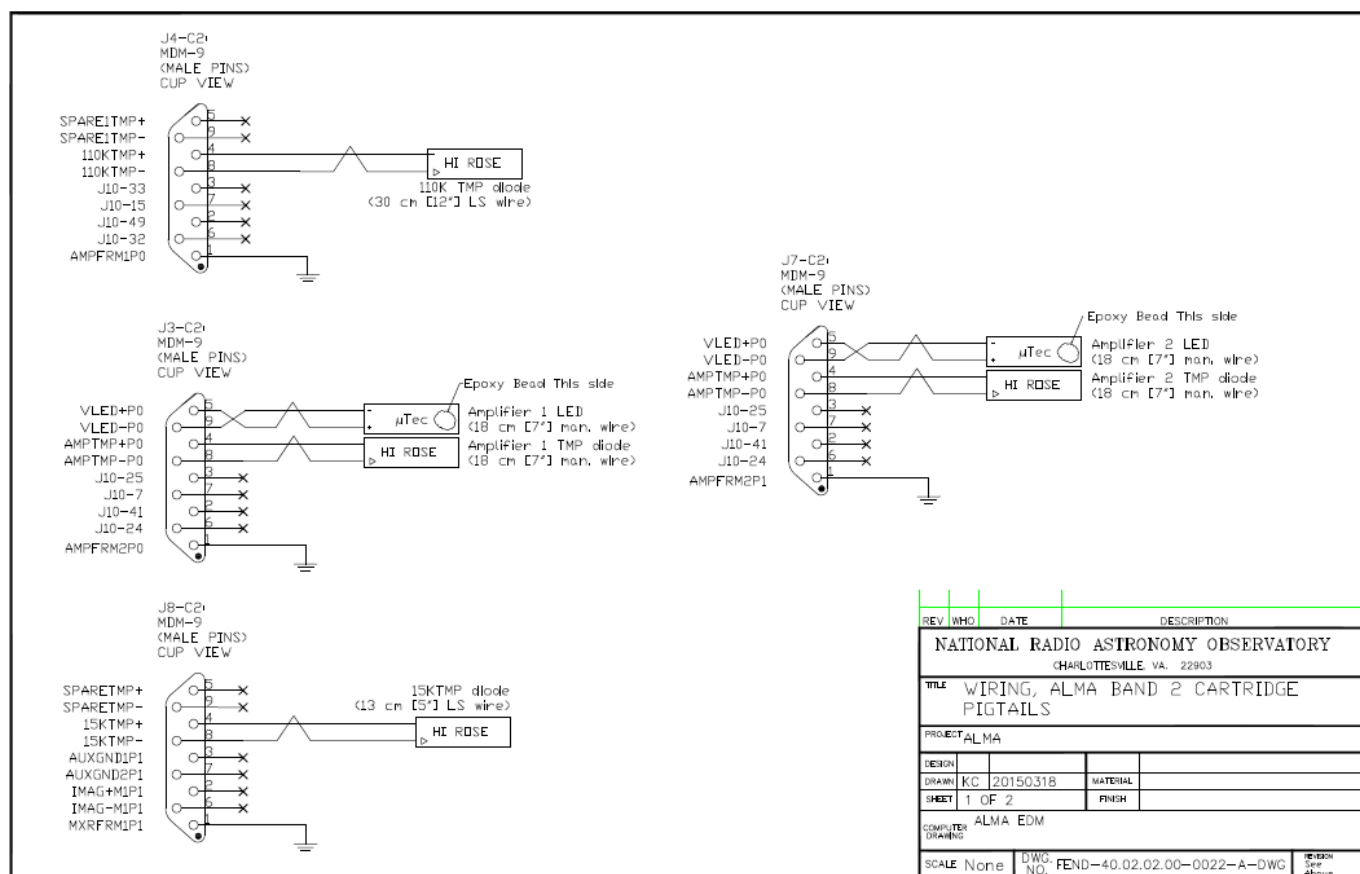


Figure 54: Band 2 Cartridge Pigtail Wiring, from [\[RD 21\]](#)

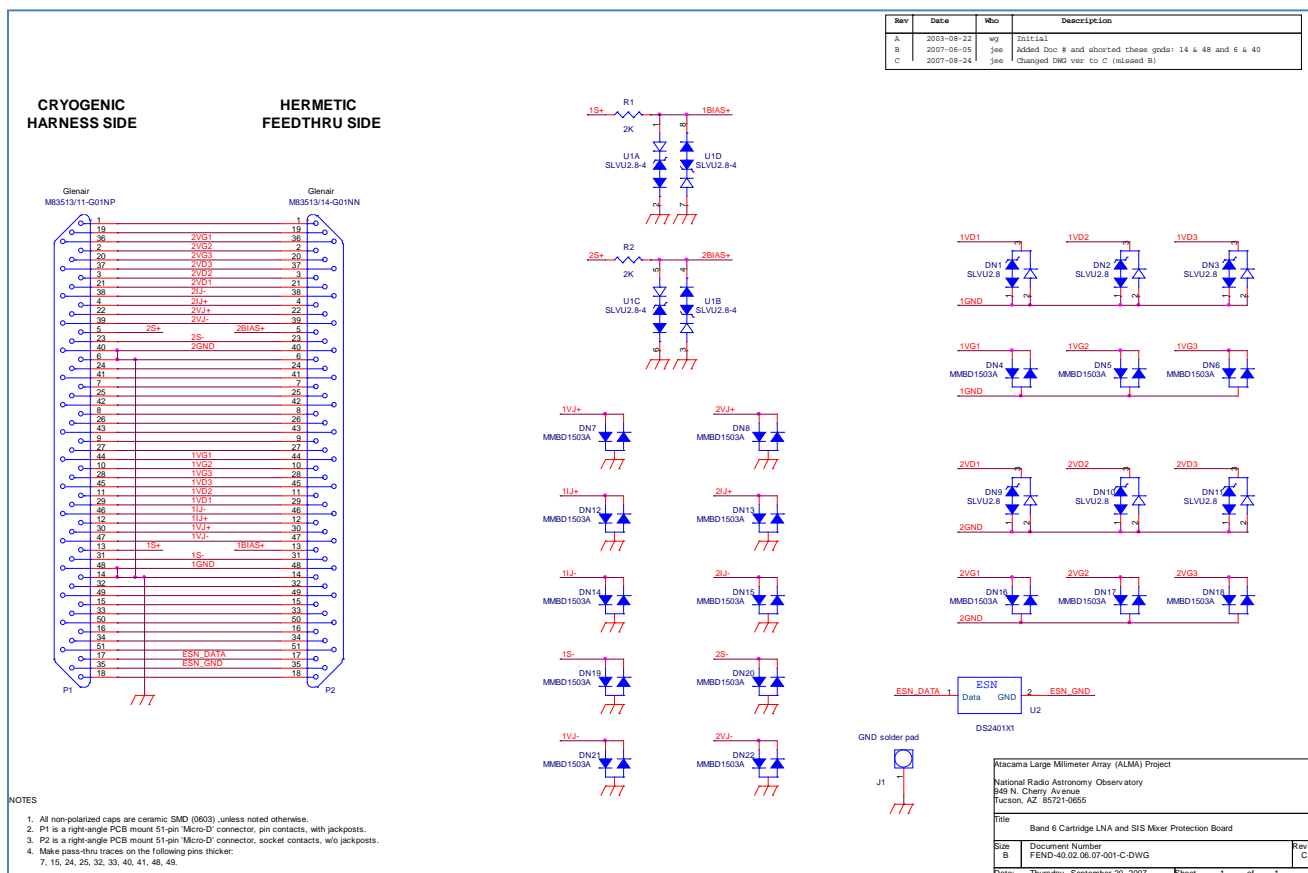


Figure 56: Schematic of the bias protection circuits (Reference only, from [RD 50])

8. Prototype Cartridge performance

This section shows typical Band 2 cartridge performance. Each section heading includes specification numbers from [RD 16].

8.1. Noise Performance (FEND-40.02.02.00-00180-00/T)

Figure 57 and Figure 58 show, for both polarizations, noise temperature over the 4-12 GHz IF band using the 80 nm gate length InP HEMT based MIC cryogenic amplifiers. Ripple at the lower end of the band results from interaction between the LNAs and the IR filters, as discussed in Section 7.2.8.

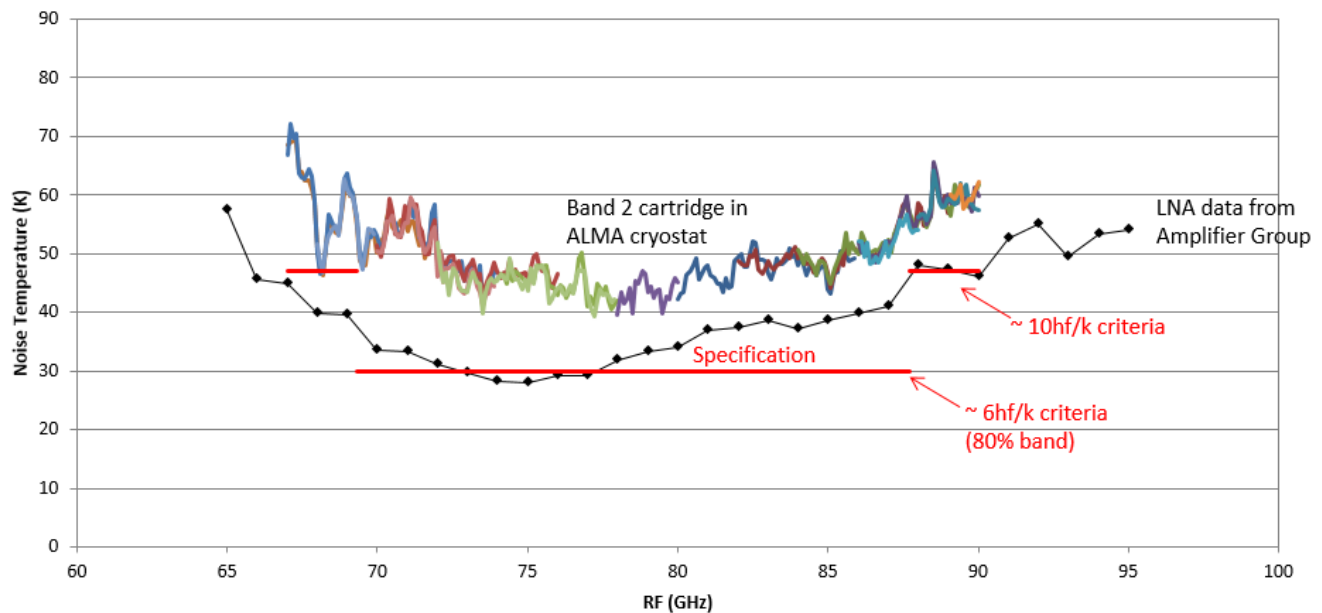


Figure 57: Noise Temperature for Polarization-0, using the 80 nm gate length InP HEMT based MIC cryogenic amplifier.

The data are not corrected for Image Rejection

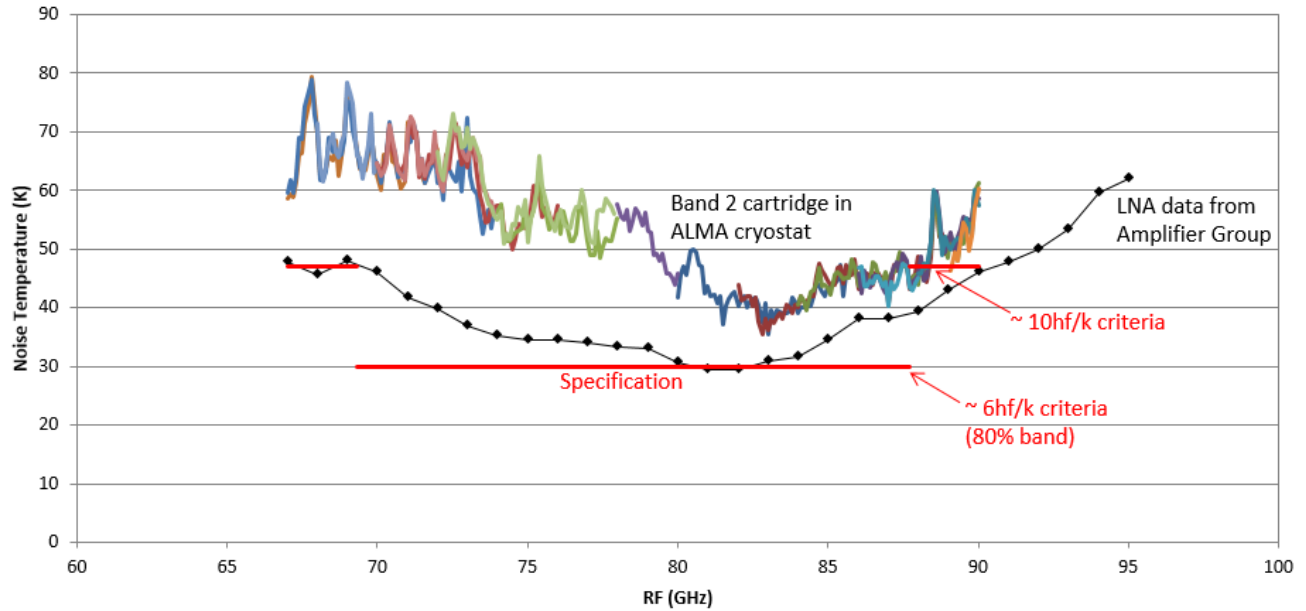


Figure 58: Noise Temperature for Polarization-1, using the 80 nm gate length InP HEMT based MIC cryogenic amplifier.

Data is not corrected for Image Rejection

In order to diagnose the ripple at the low end of the frequency band in the measured receiver temperature data, the reflection coefficient of the OMT and feed horn was measured with and without the 15 K IR filter. The 15 K filter was also placed at different distances from the feed horn aperture. [Figure 59](#) shows the ripple caused by the 15K filter placed at a distance of 5 mm from the feed horn. This experiment confirmed that 15 K IR filter most likely interacts with the rest of the receiver optics and with the LNA input, which might account for the noise ripple in the lower portion of the frequency band.

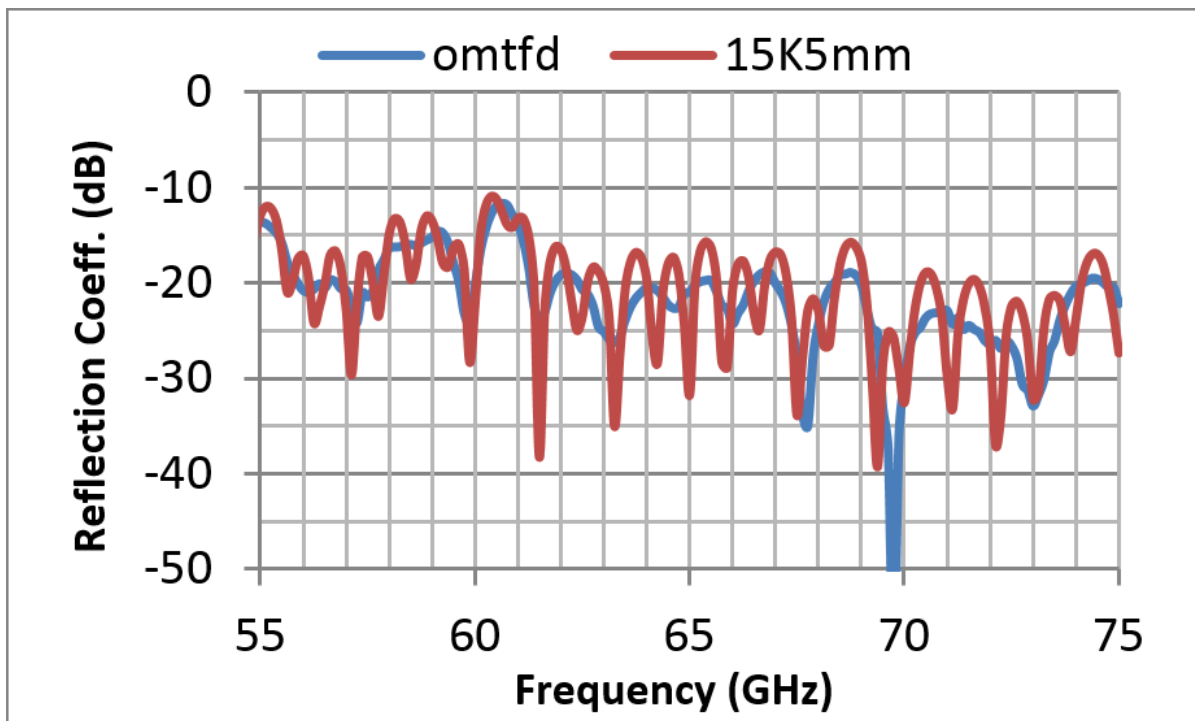


Figure 59: Measured Retn Loss of OMT+Feed with/without IR filter

Measured reflection coefficient of the OMT plus feed horn without IR filter (trace labeled “omtfd”) and that of the OMT plus feed horn with the 15 K IR filter placed 5 mm from the feed horn aperture (trace labeled “15K5mm”).

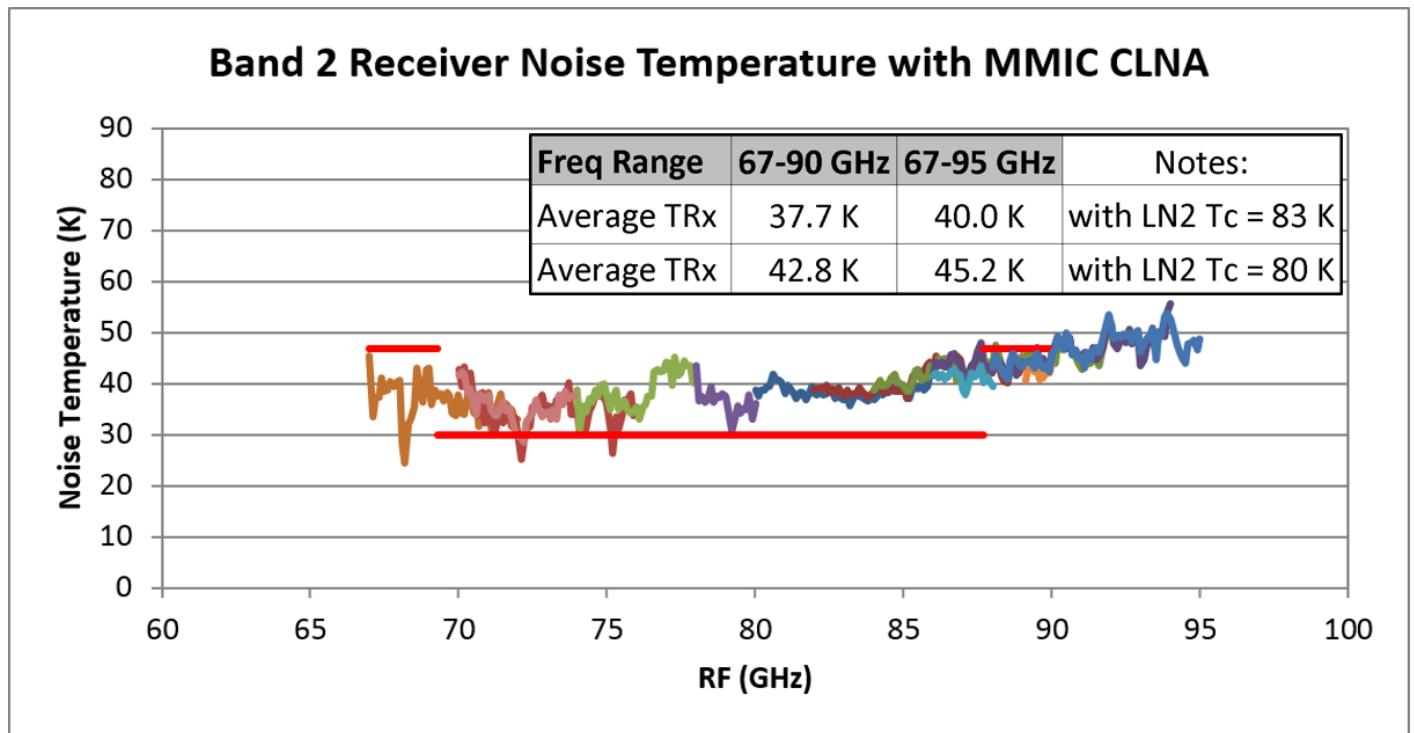


Figure 60: Receiver noise temperature of the Band 2 prototype cartridge using a MMIC based LNA
 Measured with state-of-the-art NGC 35 nm gate length MMICs produced under the Band 2 cartridge prototype project sub-contract with Cahill Radio Astronomy Laboratory (CRAL) at the California Institute of Technology. The numerical average of traces is close to predicted value of [Figure 5](#).

8.2. Image Rejection (FEND-40.02.02.00-00190-00/T)

Image rejection was measured for just the down converter assembly shown in [Figure 67](#).

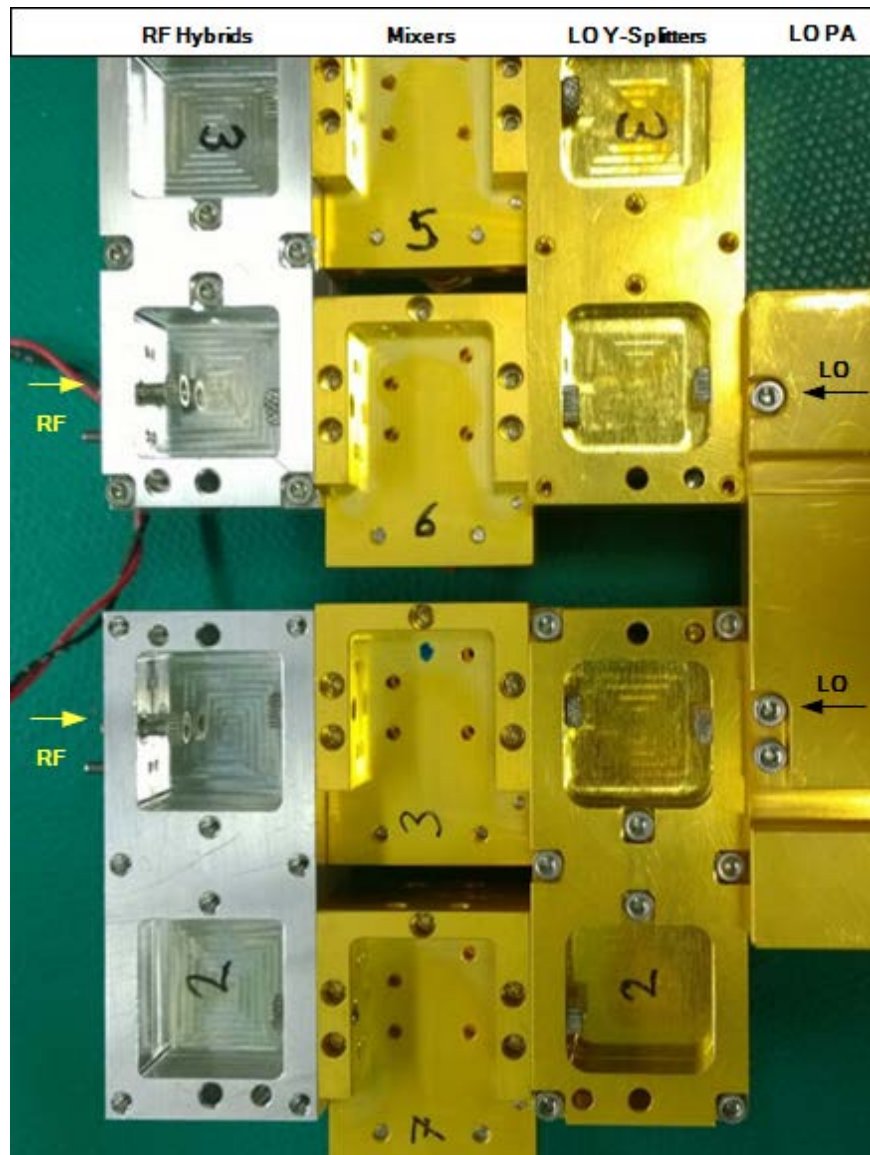


Figure 61: Photo of dual polarization 2SB downconverter

Downconverter for which test data is provided in the plots that follow. The I & Q outputs and the IF hybrid(s) are not seen in the picture.

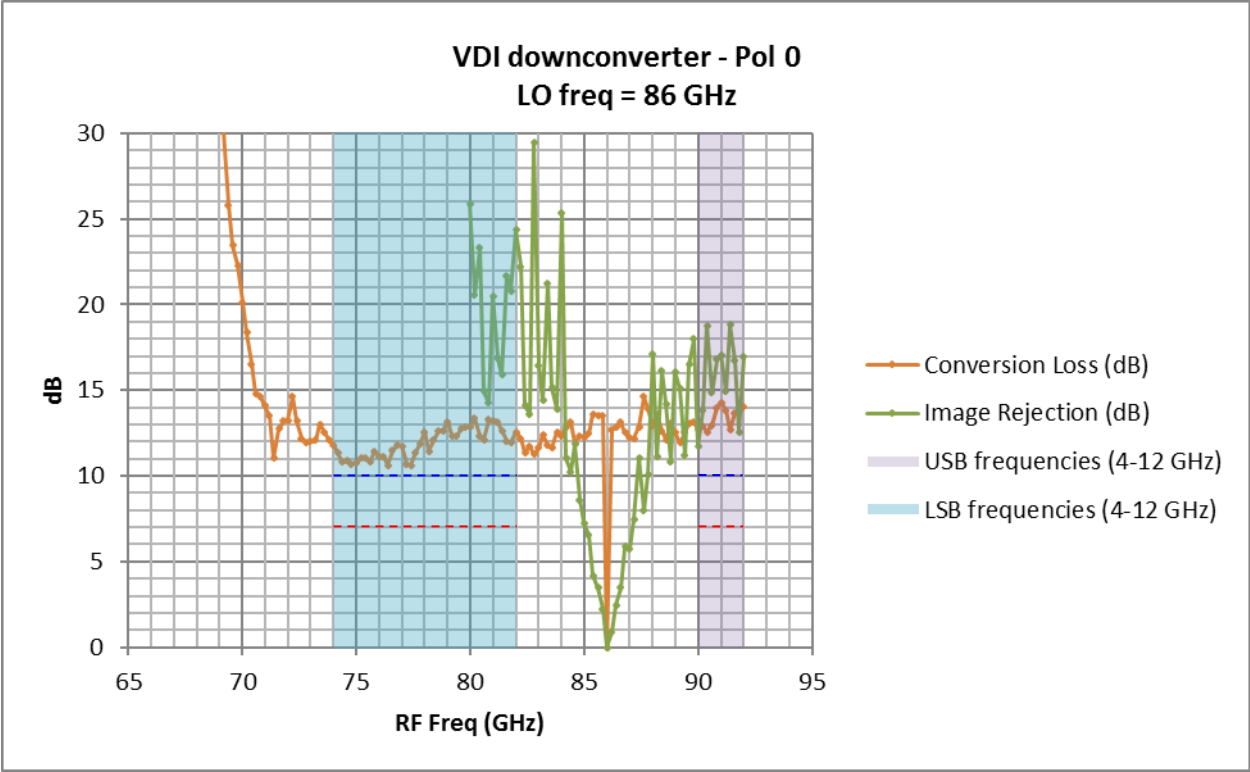


Figure 62: Image Rejection and Conversion Loss for LO = 86 GHz (Pol-0 channel).

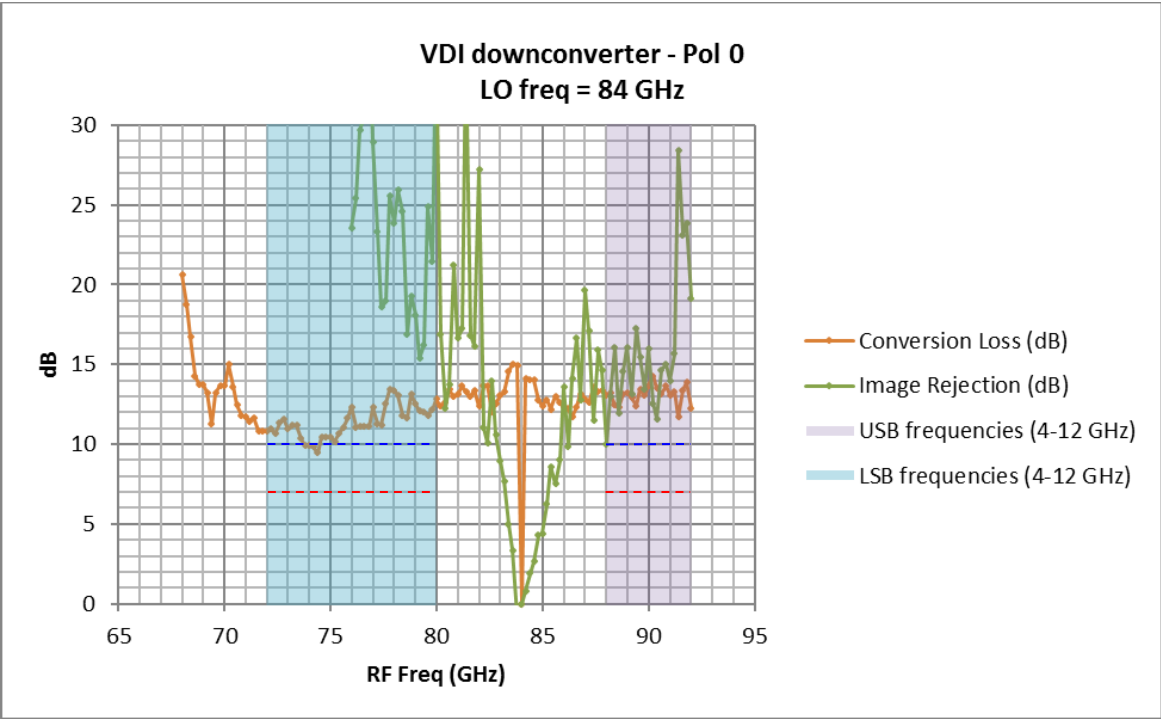


Figure 63: Image rejection and Conversion Loss for LO = 84 GHz (Pol-0 channel).

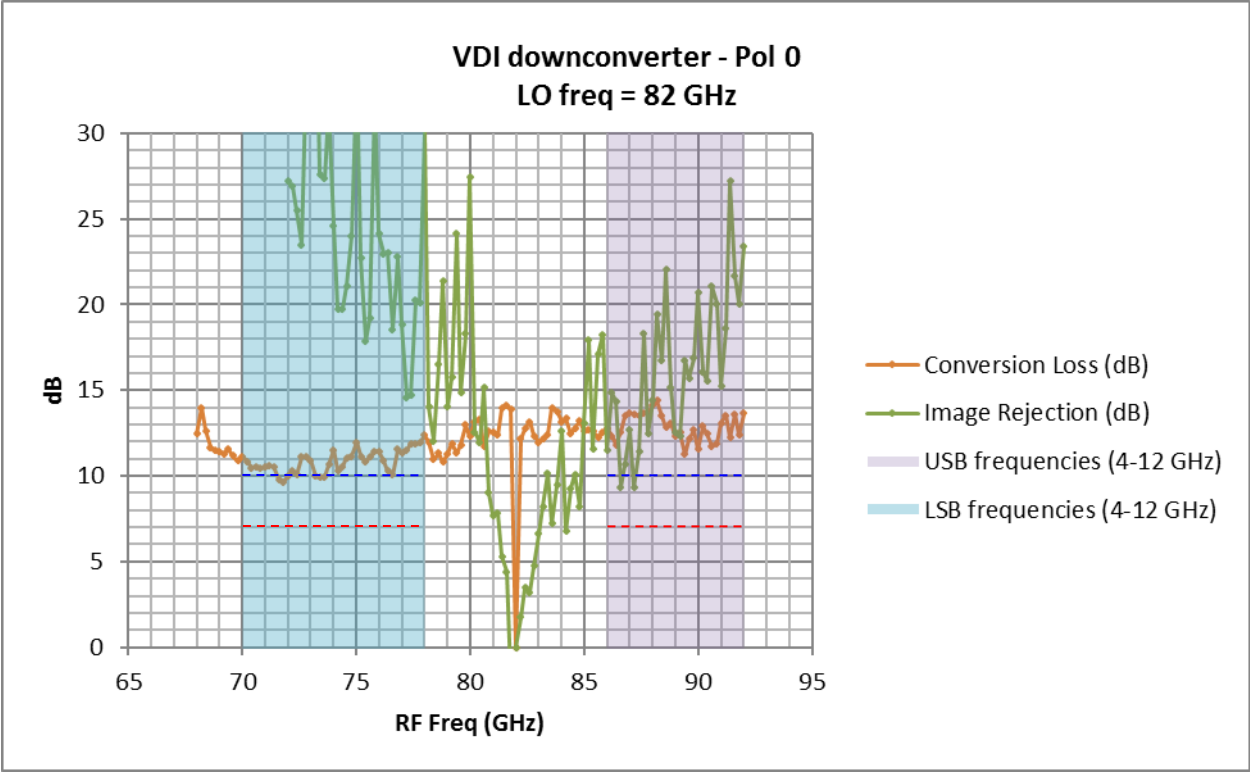


Figure 64: Image rejection and Conversion Loss for LO = 82 GHz (Pol-0 channel).

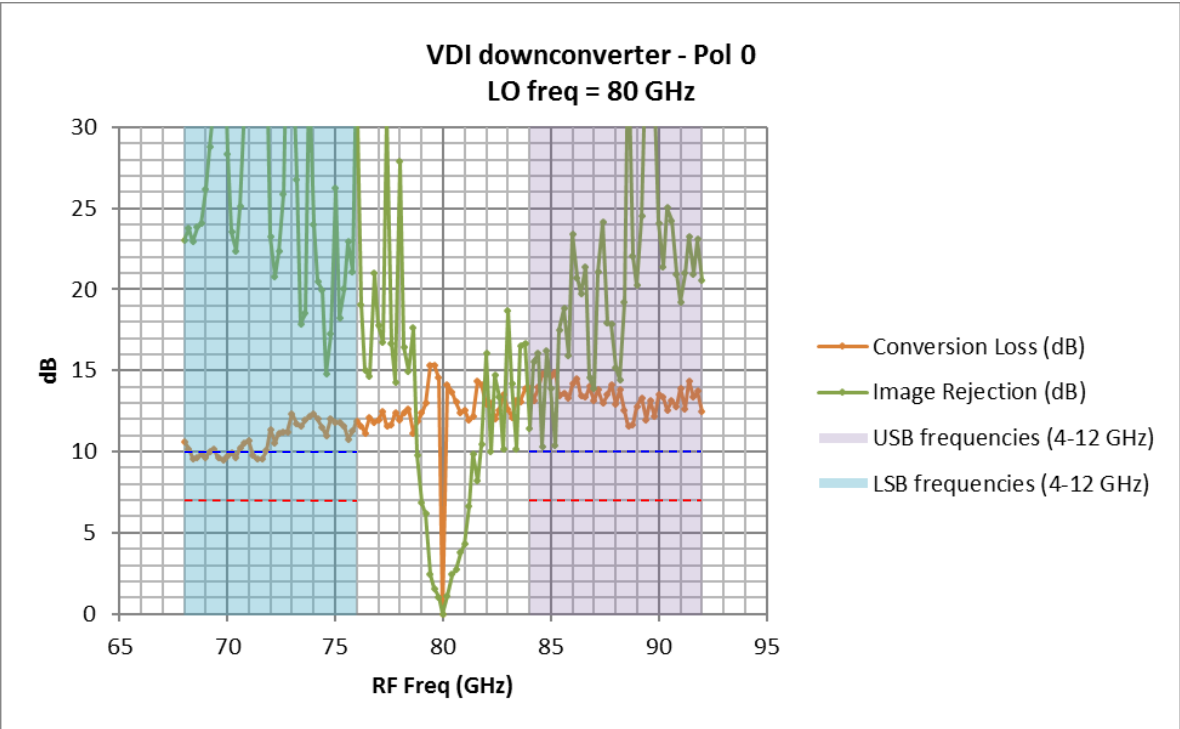


Figure 65: Image rejection and Conversion Loss for LO = 80 GHz (Pol-0 channel).

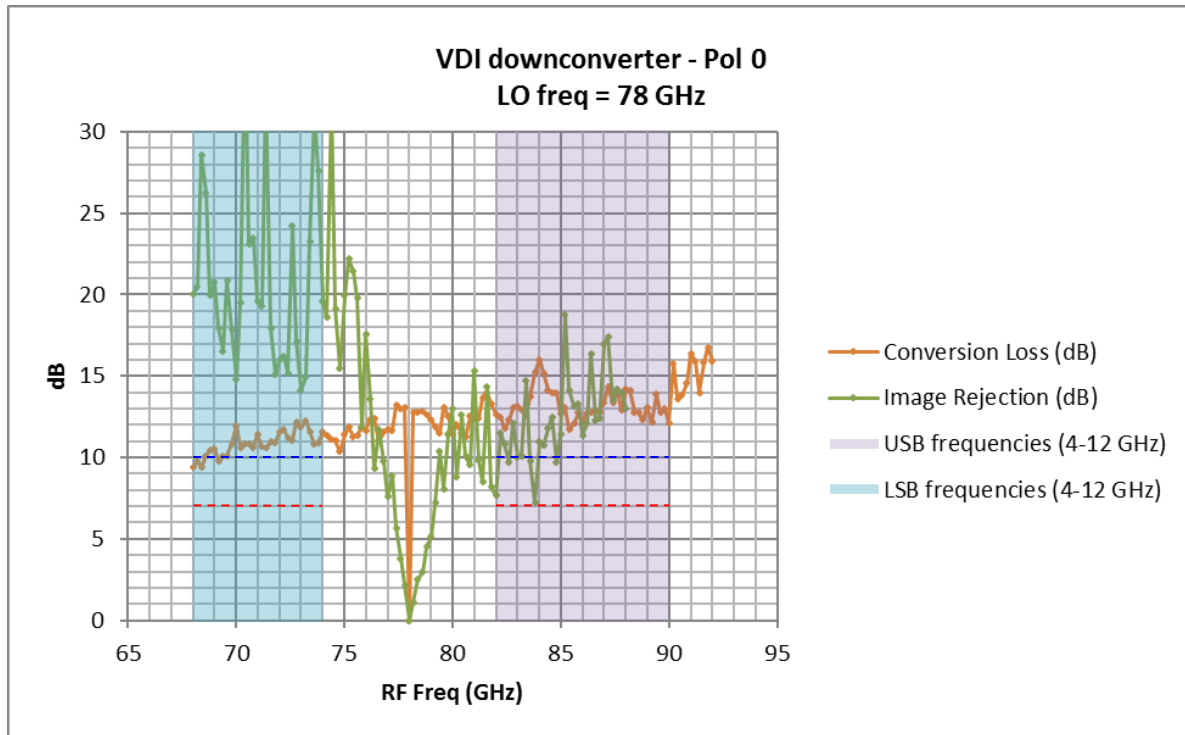


Figure 66: Image rejection and Conversion Loss for LO = 78 GHz (Pol-0 channel).

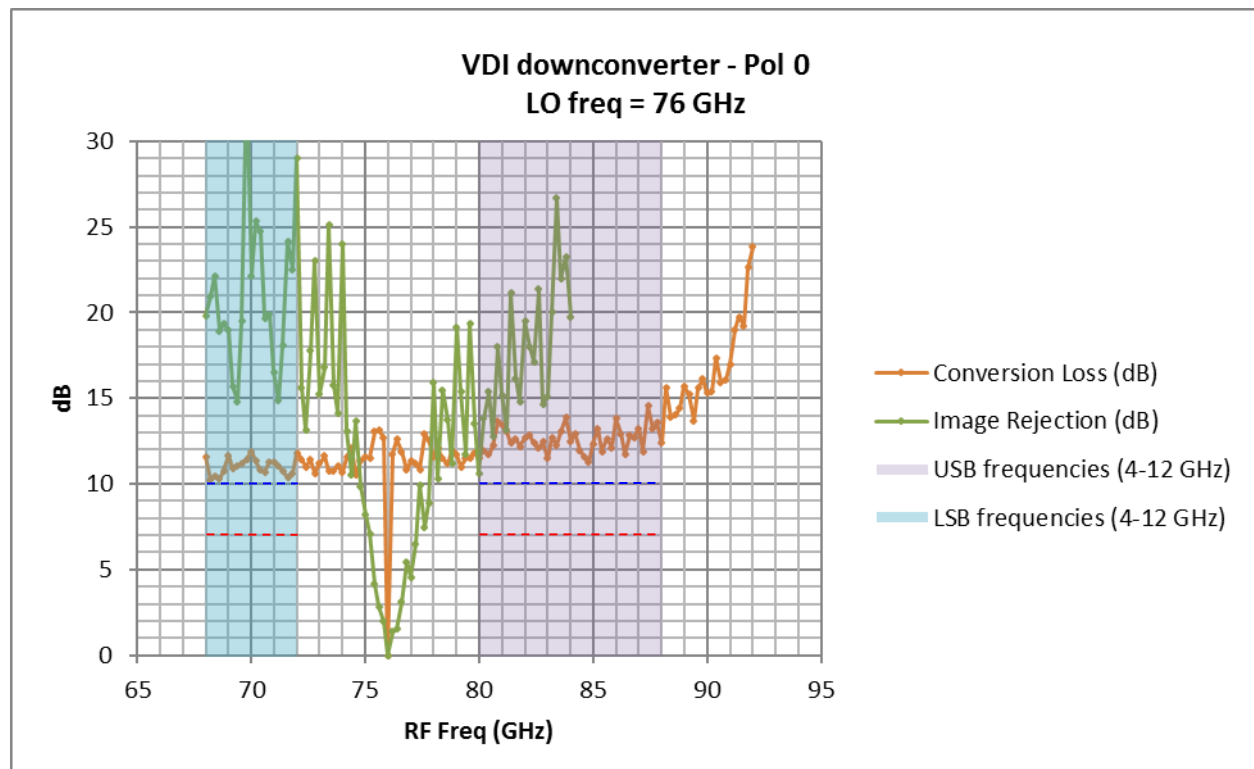


Figure 67: Image rejection and Conversion Loss for LO = 76 GHz (Pol-0 channel).

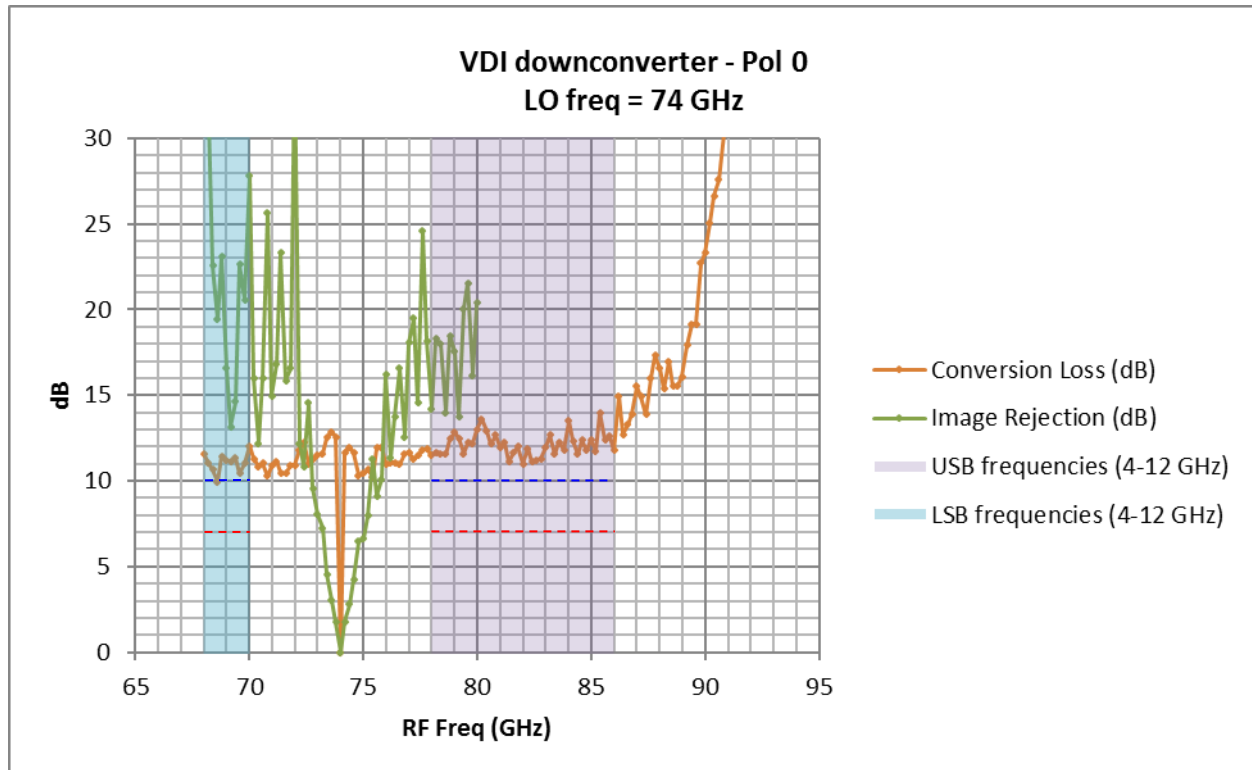


Figure 68: Image rejection and Conversion Loss for LO = 74 GHz (Pol-0 channel).

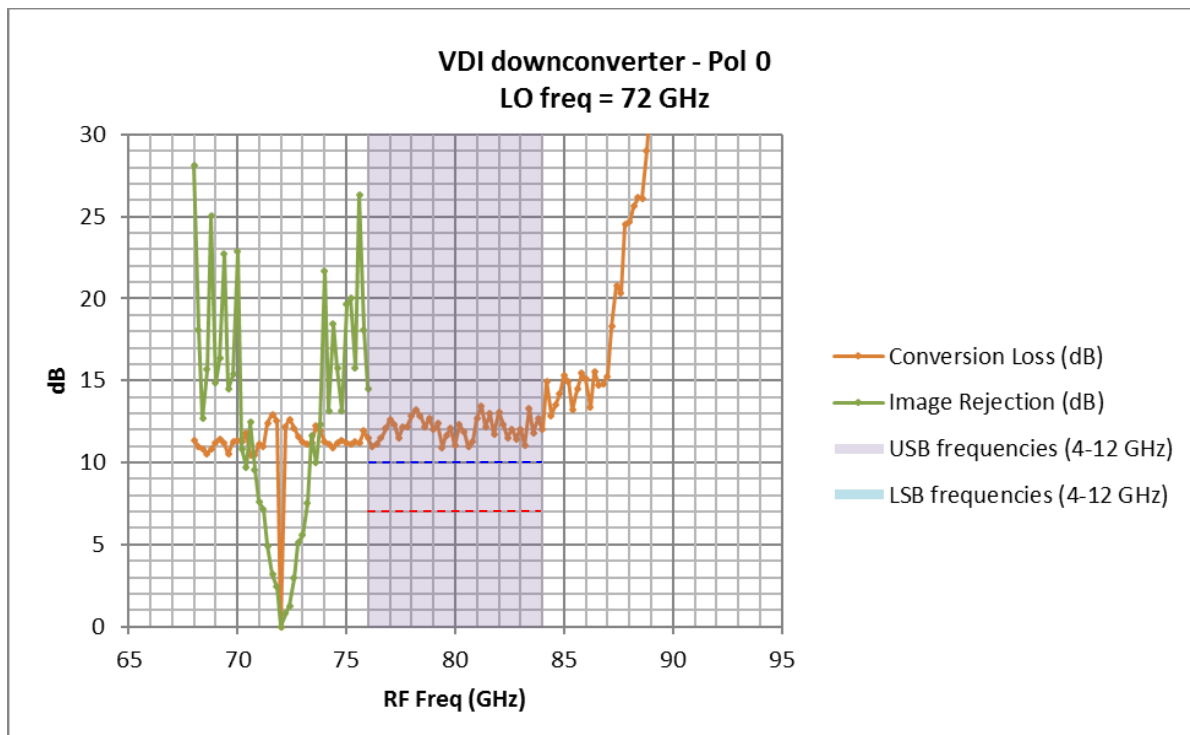


Figure 69: Image rejection and Conversion Loss for LO = 72 GHz (Pol-0 channel).

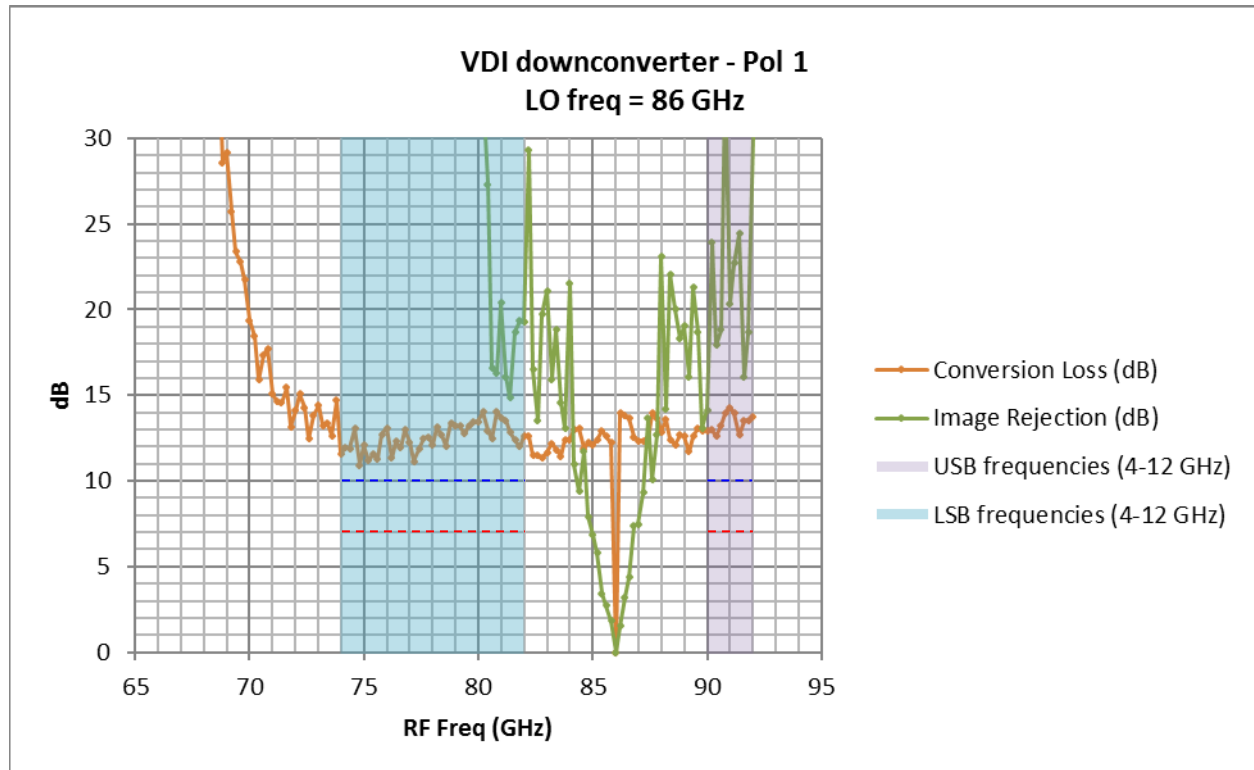


Figure 70: Image rejection and Conversion Loss for LO = 86 GHz (Pol-1 channel).

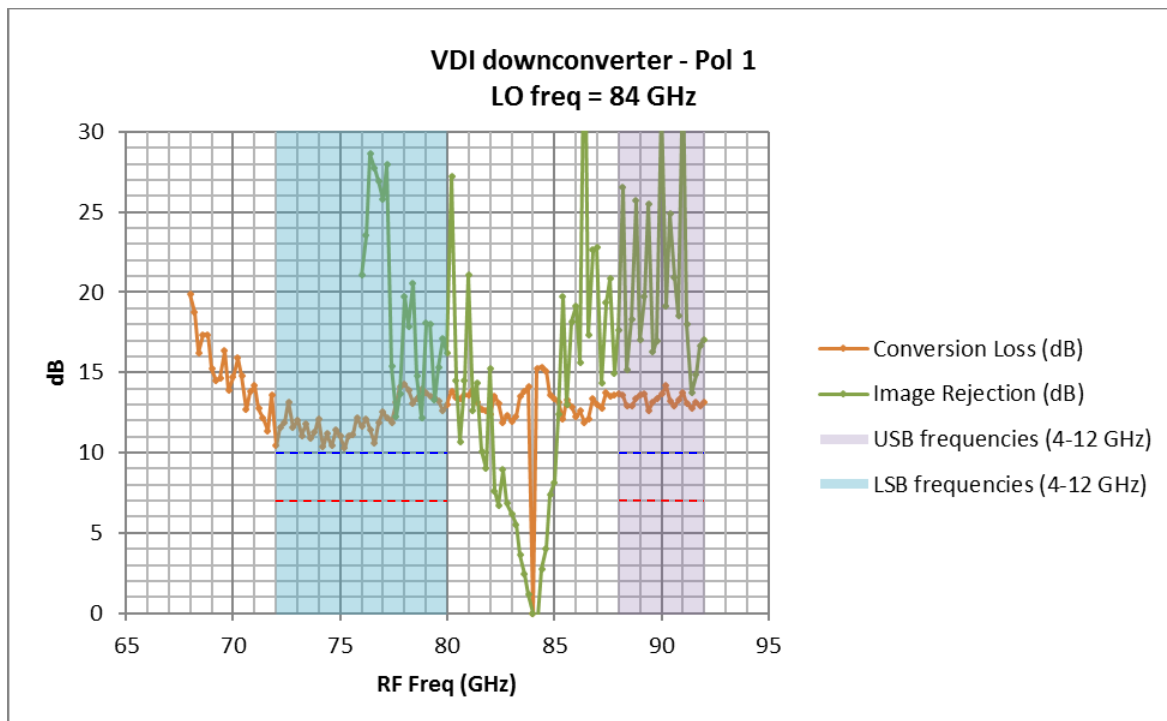


Figure 71: Image rejection and Conversion Loss for LO = 84 GHz (Pol-1 channel).

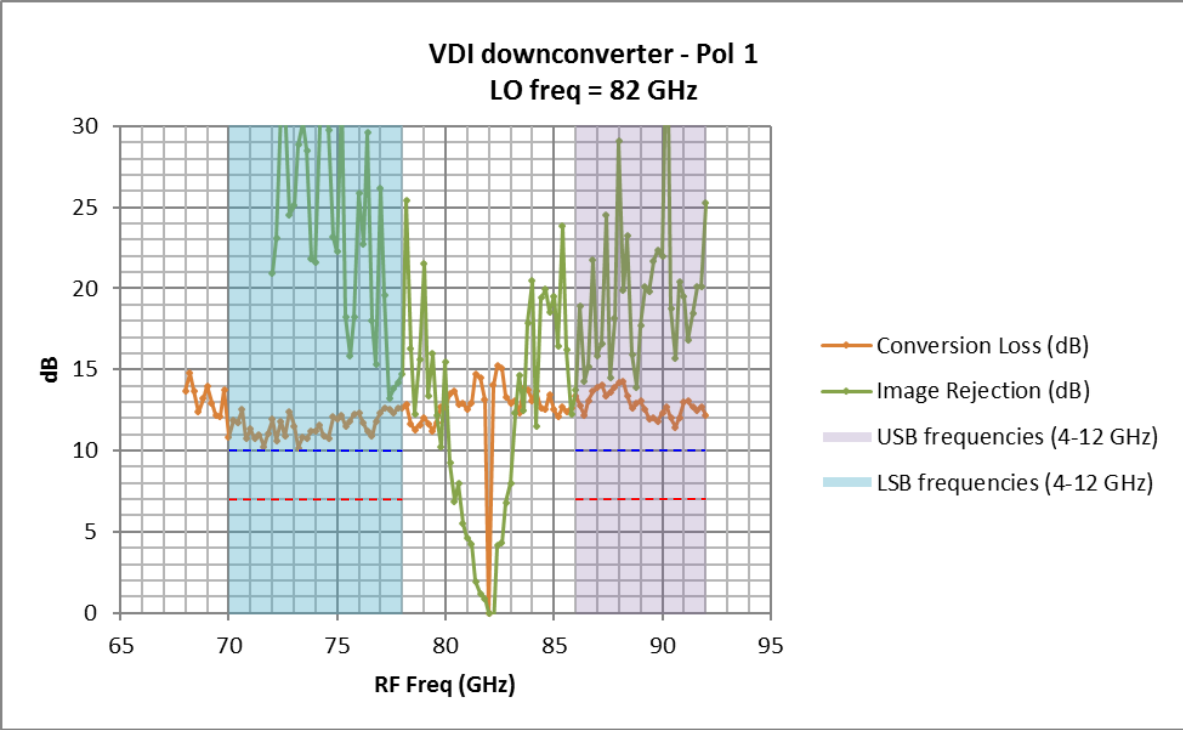


Figure 72: Image rejection and Conversion Loss for LO = 82 GHz (Pol-1 channel).

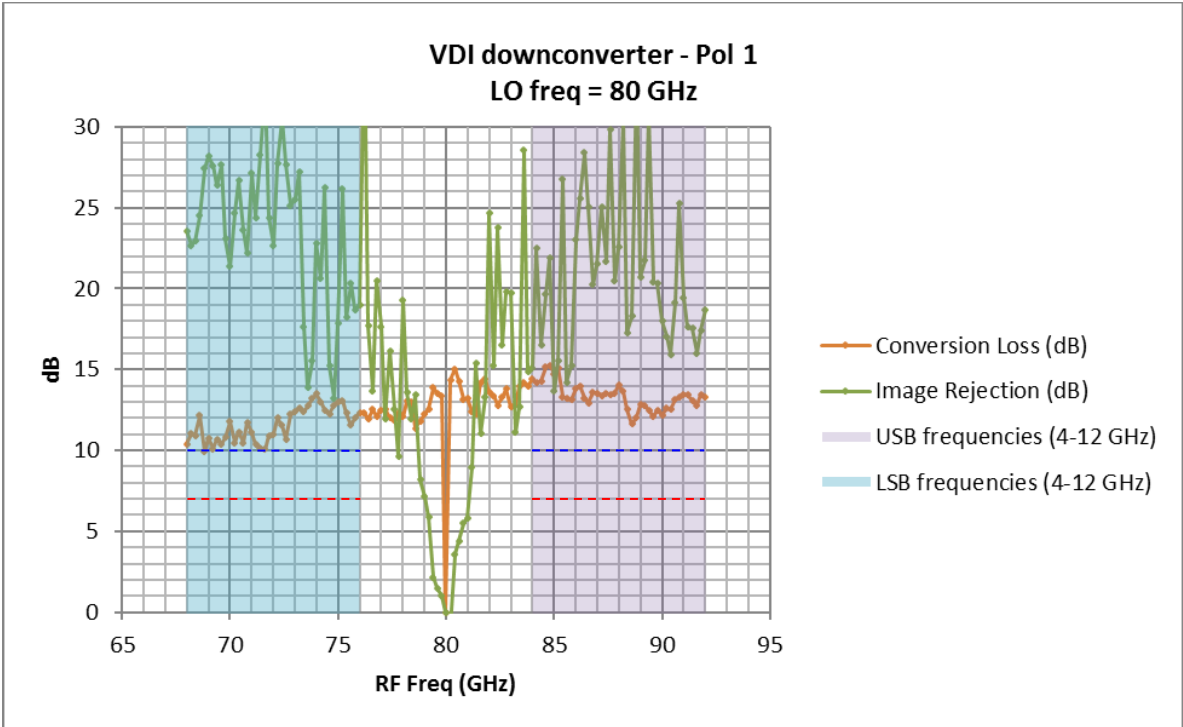


Figure 73: Image rejection and Conversion Loss for LO = 80 GHz (Pol-1 channel).

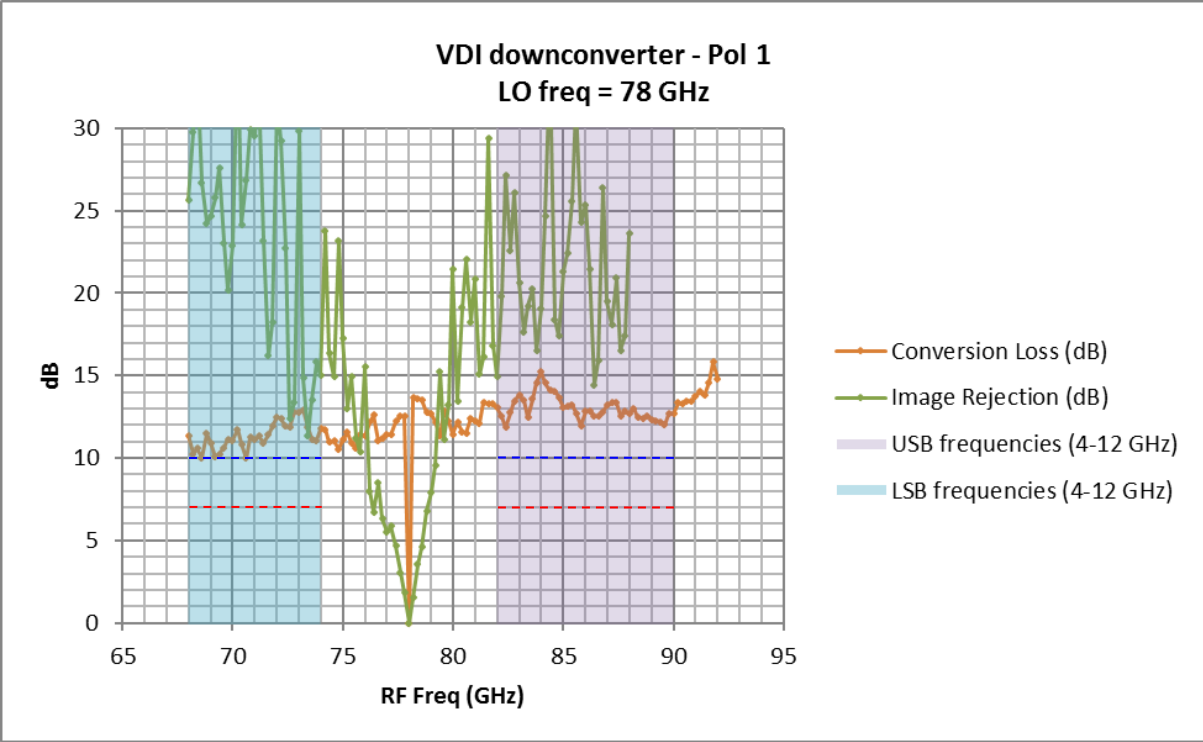


Figure 74: Image rejection and Conversion Loss for LO = 78 GHz (Pol-1 channel).

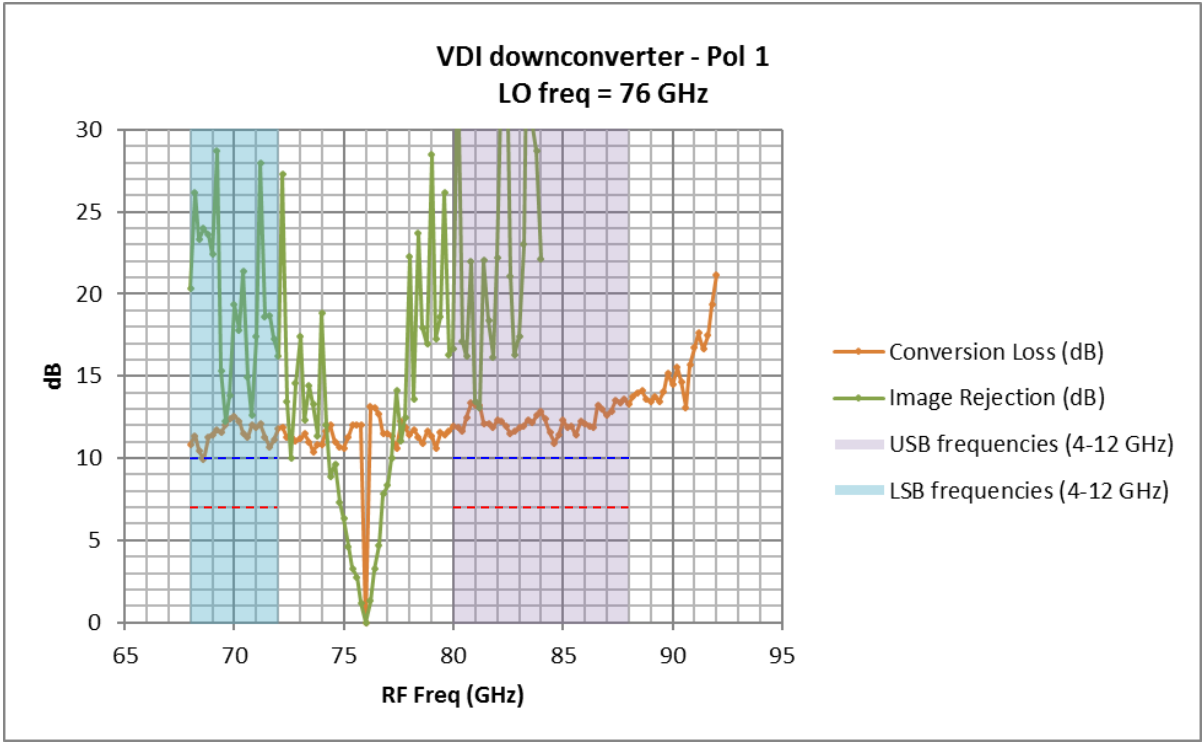


Figure 75: Image rejection and Conversion Loss for LO = 76 GHz (Pol-1 channel).

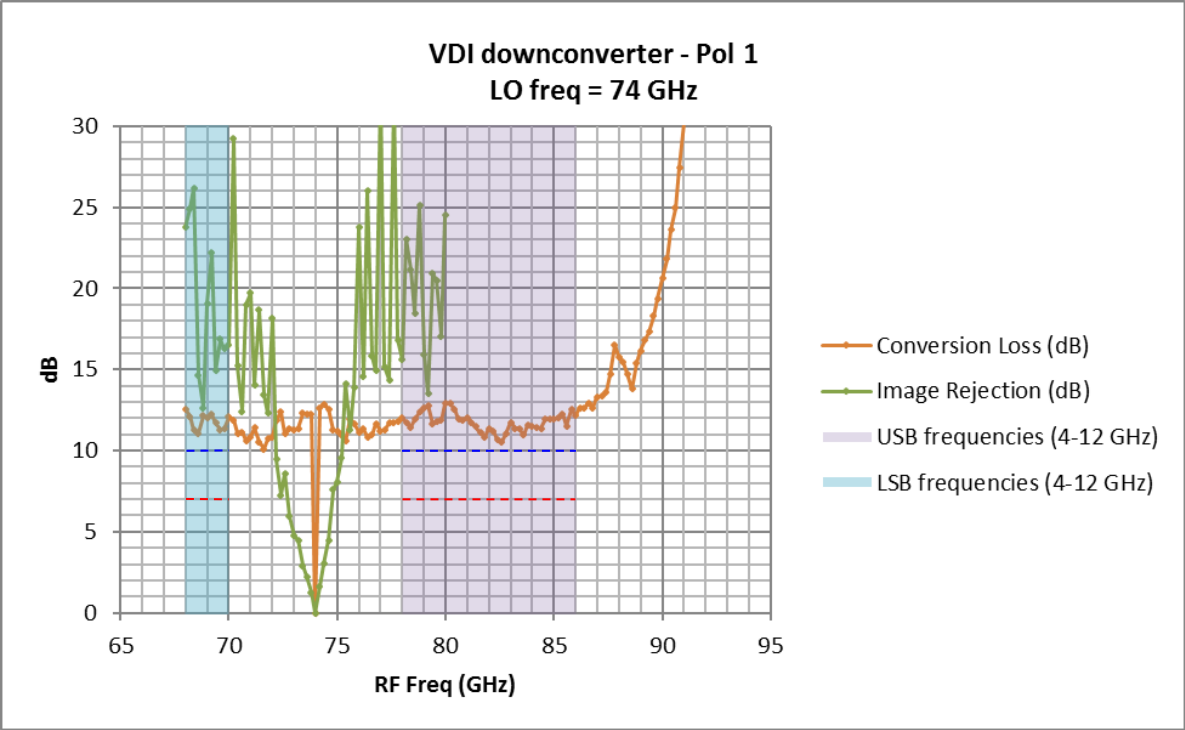


Figure 76: Image rejection and Conversion Loss for LO = 74 GHz (Pol-1 channel).

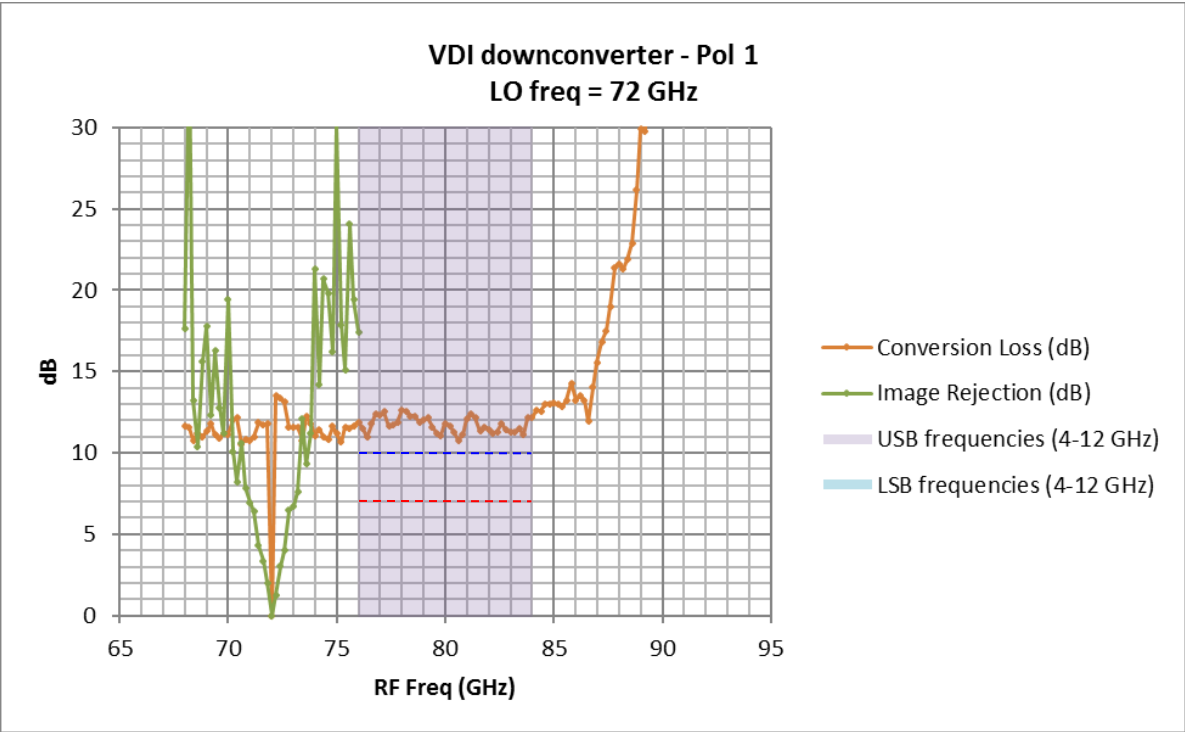


Figure 77: Image rejection and Conversion Loss for LO = 72 GHz (Pol-1 channel).

8.3. Output Power and Power Density Slope (FEND-40.02.02.00-00200-00/T) (FEND-40.02.02.00-00210-00/T)

Output power requirements are given in the ICD between the cartridge and IF switch in [\[RD 49\]](#).

Power density graphs are given in [Figure 78](#) and [Figure 81](#) and power density slopes are plotted in [Figure 82](#) through [Figure 85](#). Power variation in a 31 MHz window is shown in [Figure 86](#) through [Figure 89](#). Power variation across the entire IF band is shown in [Figure 90](#) while total and in-band power is tabulated in [Figure 91](#) and [Figure 92](#).

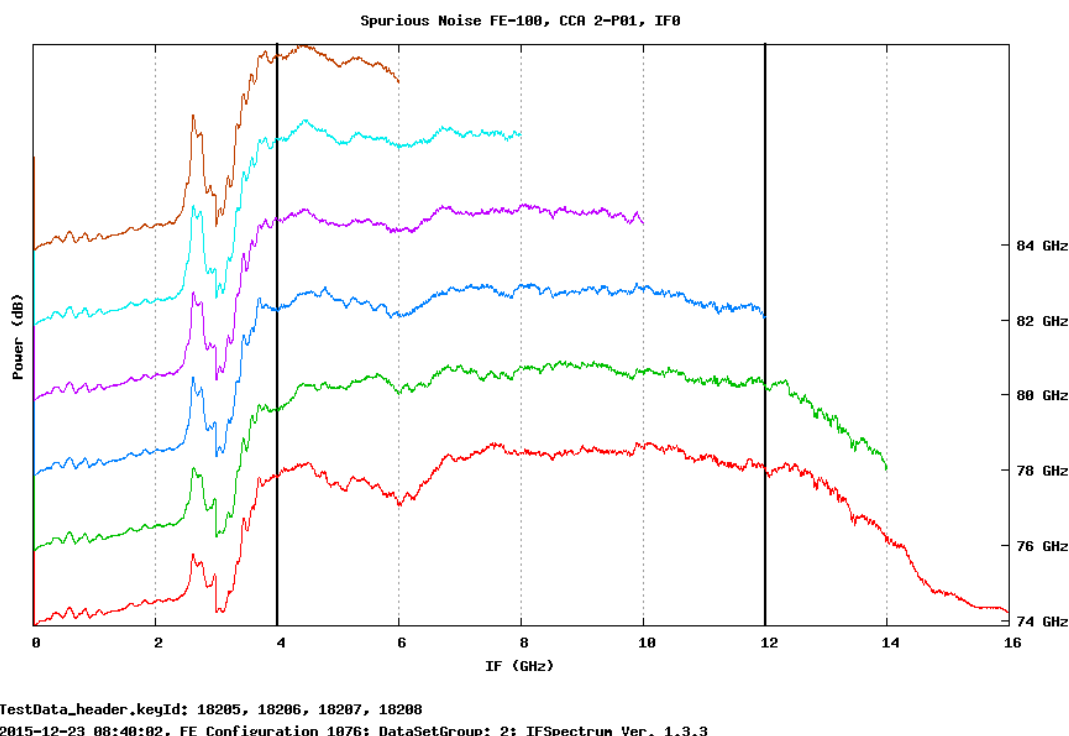
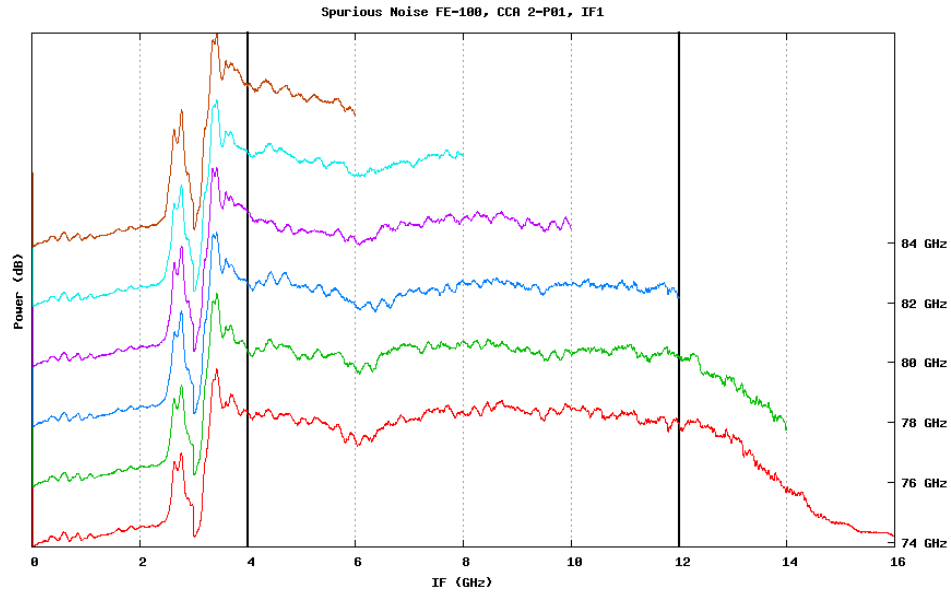


Figure 78: Output Power Density, Pol 0 USB

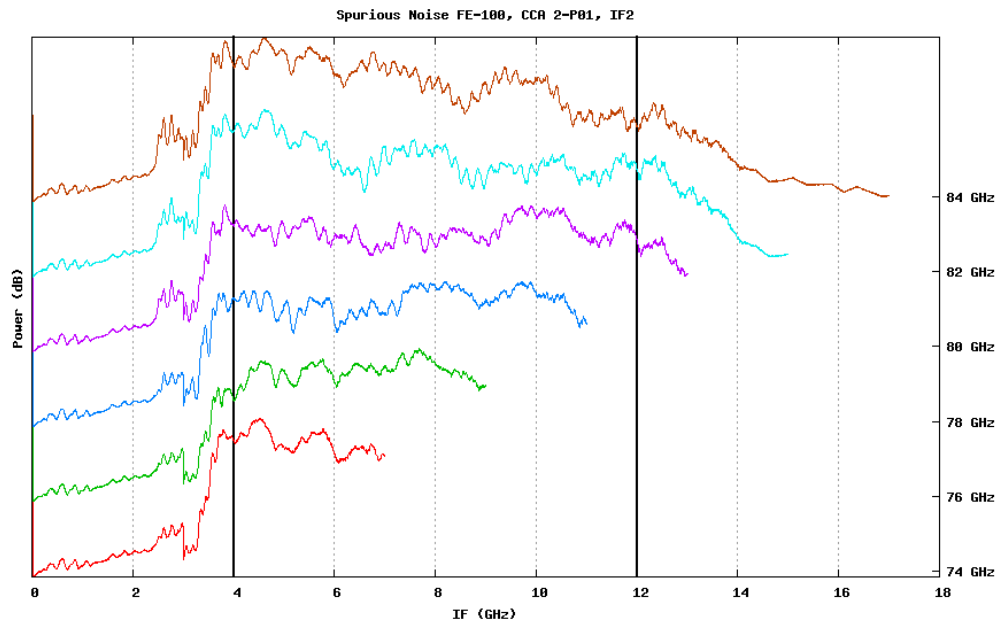
Measured with 80 nm gate length InP HEMT based MIC cryogenic amplifier. Final design will use MMIC amplifier that will impact this result.



TestData_header.keyId: 18205, 18206, 18207, 18208
2015-12-23 08:40:02, FE Configuration 1076; DataSetGroup: 2; IFSpectrum Ver. 1.3.3

Figure 79: Output Power Density, Pol 1 USB

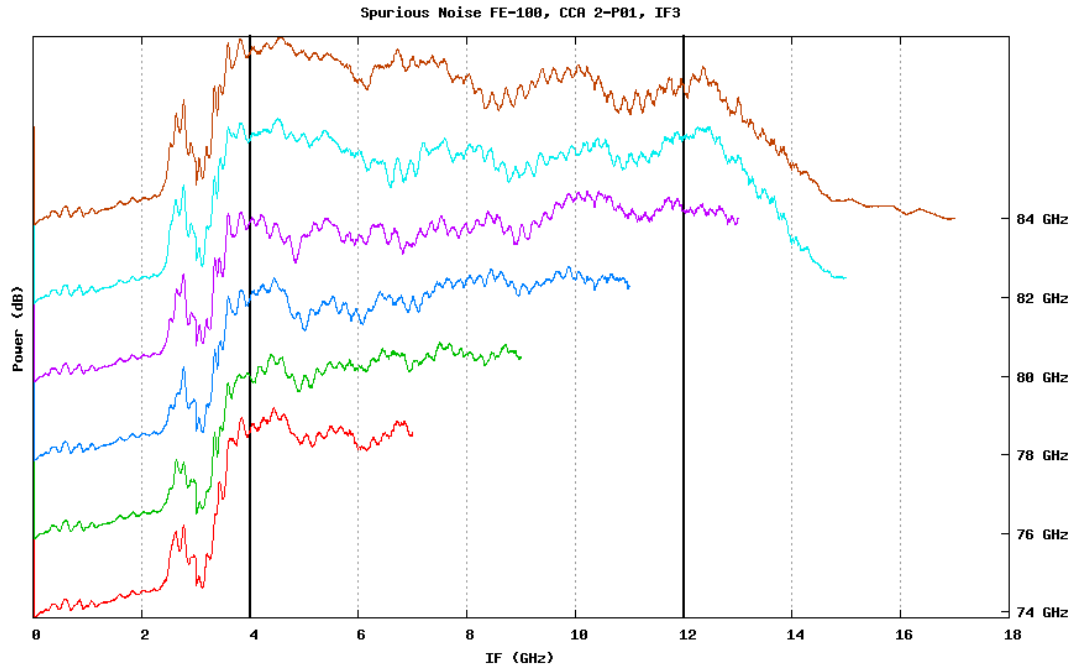
Measured with 80 nm gate length InP HEMT based MIC cryogenic amplifier. Final design will use MMIC amplifier that will impact this result.



TestData_header.keyId: 18205, 18206, 18207, 18208
2015-12-23 08:40:02, FE Configuration 1076; DataSetGroup: 2; IFSpectrum Ver. 1.3.3

Figure 80: Output Power Density, Pol 0 LSB

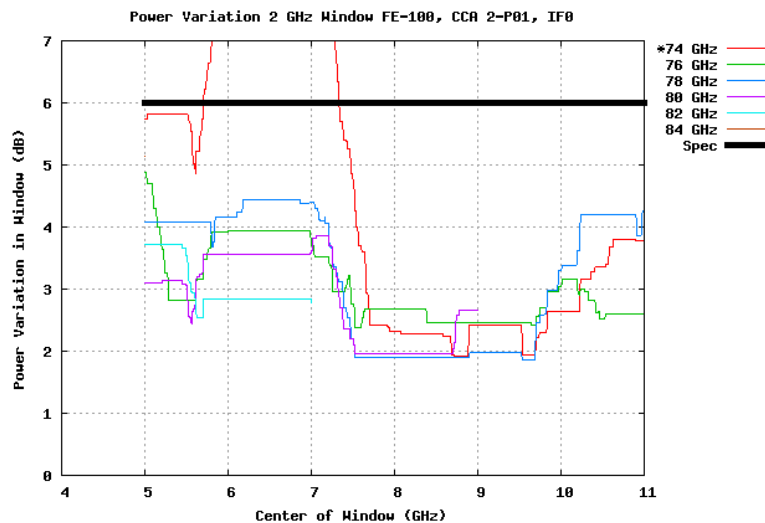
Measured with 80 nm gate length InP HEMT based MIC cryogenic amplifier. Final design will use MMIC amplifier that will impact this result.



TestData_header.keyId: 18205, 18206, 18207, 18208
2015-12-23 08:40:02, FE Configuration 1076; DataSetGroup: 2; IFSpectrum Ver. 1.3.3

Figure 81: Output Power Density, Pol 1 LSB

Measured with 80 nm gate length InP HEMT based MIC cryogenic amplifier. Final design will use MMIC amplifier that will impact this result.



TestData_header.keyId: 18205, 18206, 18207, 18208
2015-12-23 08:40:02, FE Configuration 1076; DataSetGroup: 2; IFSpectrum Ver. 1.3.3
Max Power Variation: 8.39 dB * indicates out-of-spec trace

Figure 82: Power Density Slope, Pol 0 USB

Measured with 80 nm gate length InP HEMT based MIC cryogenic amplifier. Final design will use MMIC amplifier that will impact this result.

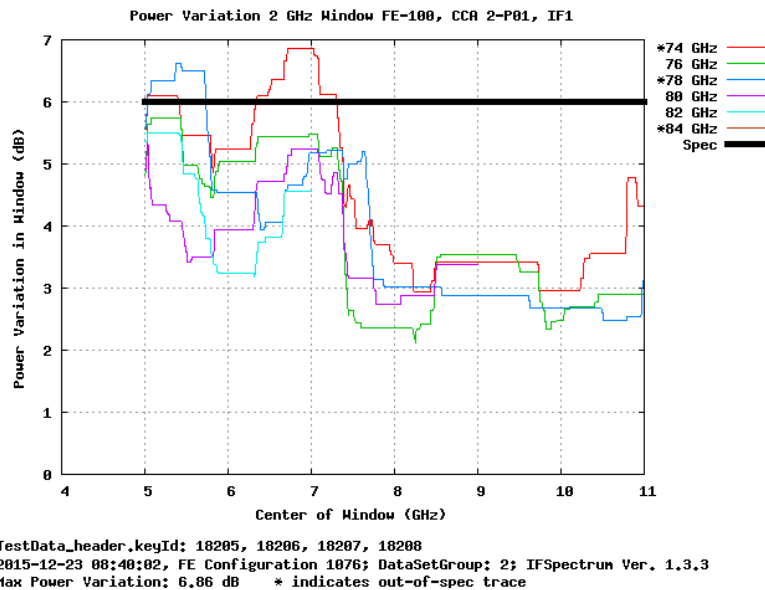


Figure 83: Power Density Slope, Pol 1 USB

Measured with 80 nm gate length InP HEMT based MIC cryogenic amplifier. Final design will use MMIC amplifier that will impact this result.

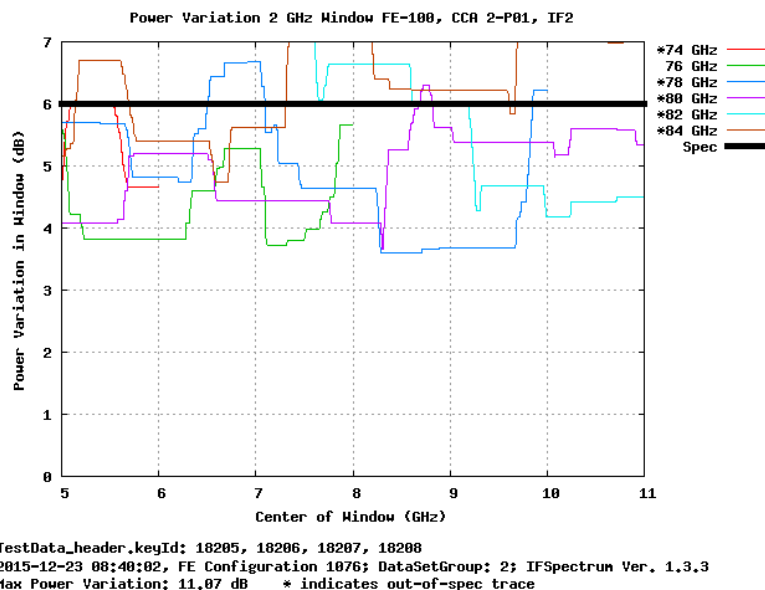


Figure 84: Power Density Slope, Pol 0 LSB

Measured with 80 nm gate length InP HEMT based MIC cryogenic amplifier. Final design will use MMIC amplifier that will impact this result.

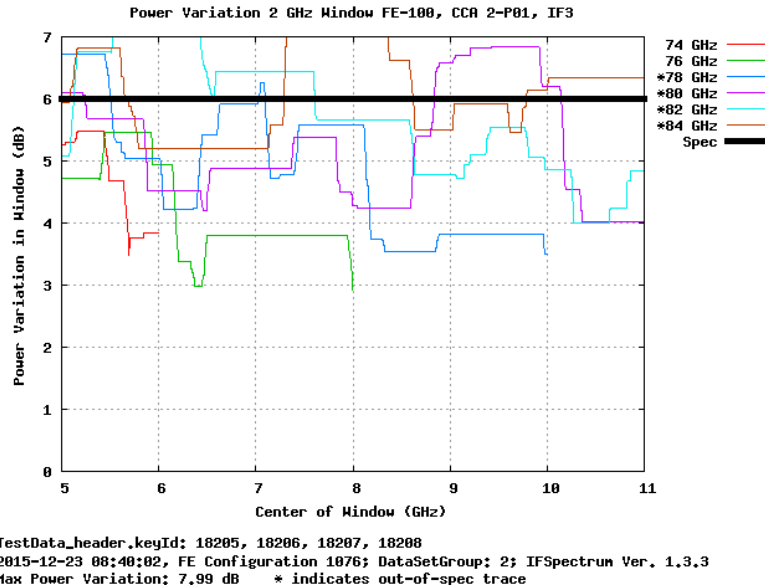


Figure 85: Power Density Slope, Pol 0 LSB

Measured with 80 nm gate length InP HEMT based MIC cryogenic amplifier. Final design will use MMIC amplifier that will impact this result.

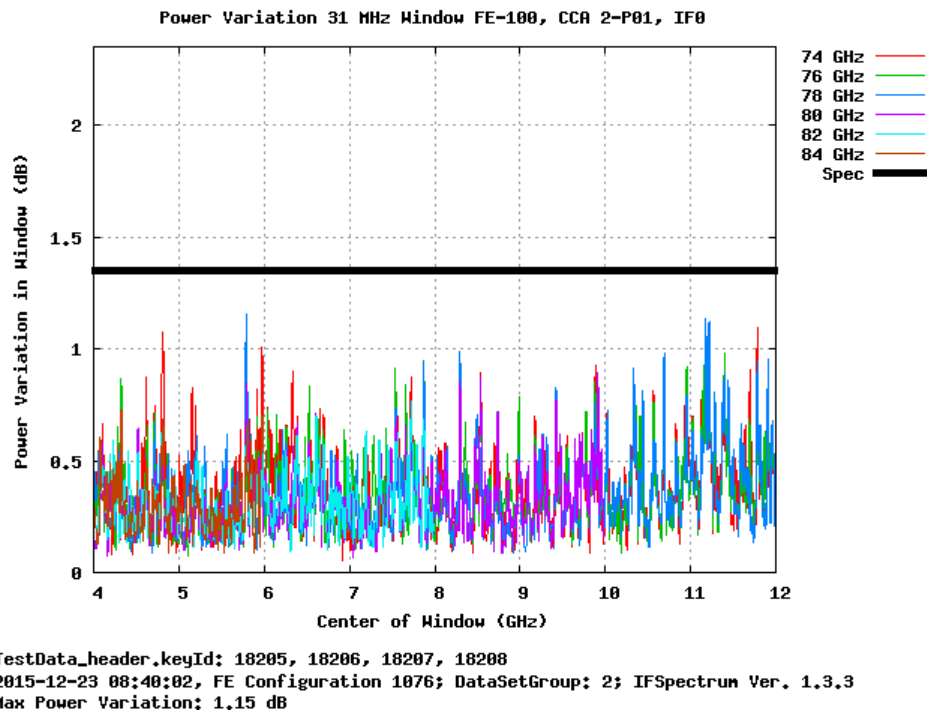


Figure 86: Power variation in 31 MHz window, Pol 0 USB

Measured with 80 nm gate length InP HEMT based MIC cryogenic amplifier. Final design will use MMIC amplifier that will impact this result.

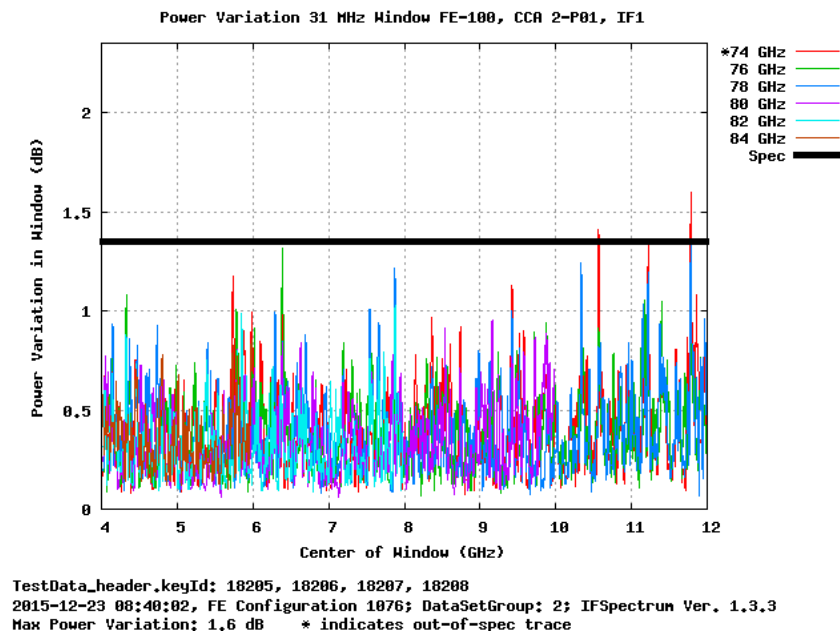


Figure 87: Power variation in 31 MHz window, Pol 1 USB

Measured with 80 nm gate length InP HEMT based MIC cryogenic amplifier. Final design will use MMIC amplifier that will impact this result.

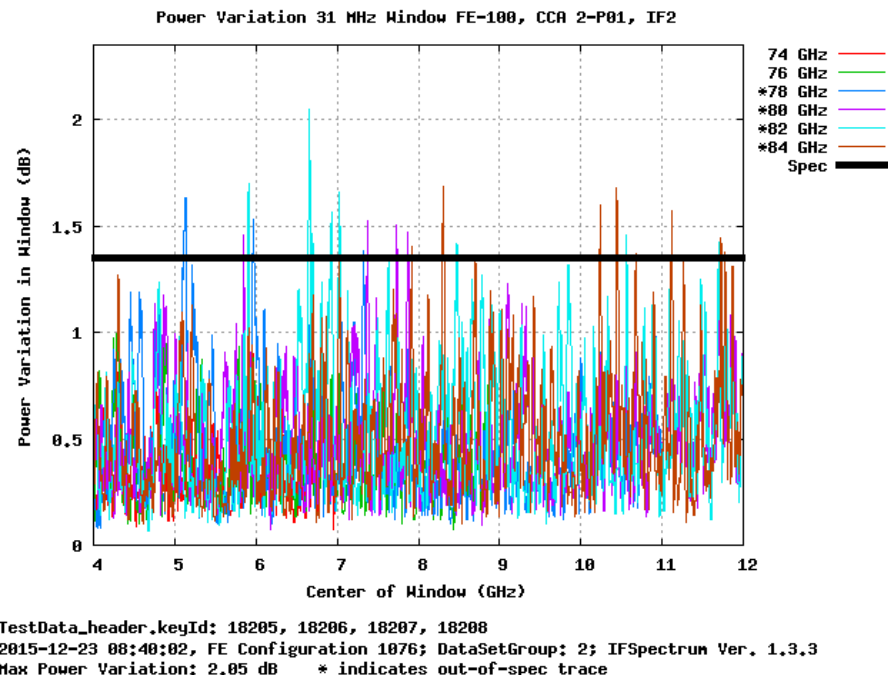


Figure 88: Power variation in 31 MHz window, Pol 0 LSB

Measured with 80 nm gate length InP HEMT based MIC cryogenic amplifier. Final design will use MMIC amplifier that will impact this result.

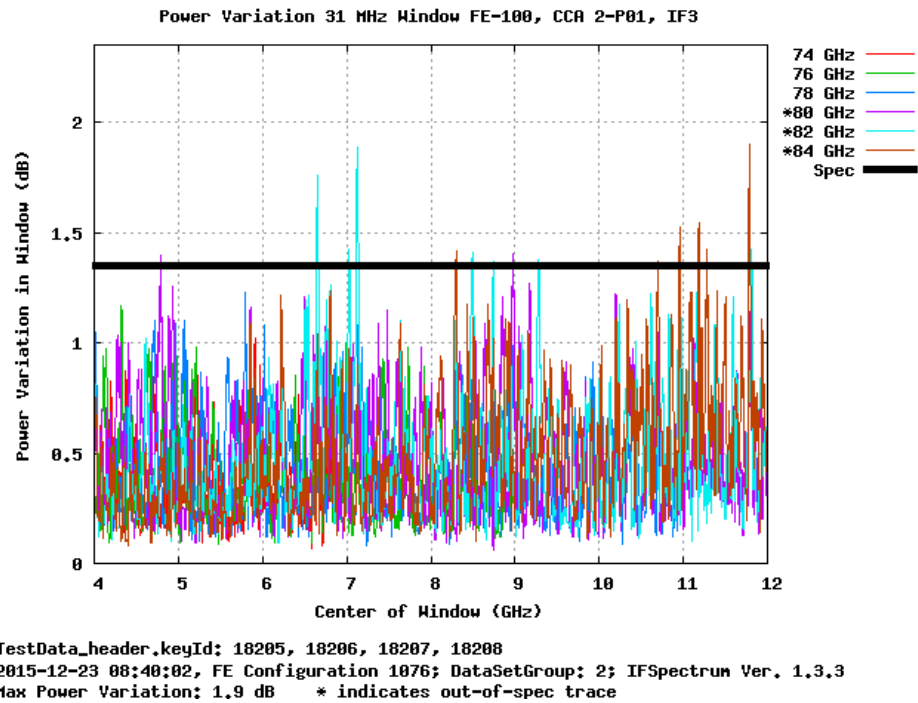


Figure 89: Power variation in 31 MHz window, Pol 1 LSB

Measured with 80 nm gate length InP HEMT based MIC cryogenic amplifier. Final design will use MMIC amplifier that will impact this result.

| Band 2 Power Variation Full Band | | | | |
|----------------------------------|------|------|------|------|
| LO (GHz) | IF0 | IF1 | IF2 | IF3 |
| 74 | 8.5 | 7.6 | 19.1 | 21.6 |
| 76 | 6.6 | 5.7 | 16.3 | 12.3 |
| 78 | 4.6 | 6.6 | 7.7 | 8.3 |
| 80 | 5.5 | 5.6 | 6.7 | 9.1 |
| 82 | 12.4 | 10.1 | 11.1 | 8.9 |
| 84 | 12.1 | 12.1 | 12.6 | 9.9 |

TestData_header.keyId: 18205, 18206, 18207, 18208
2015-12-23 08:40:02, FE Configuration 1076, DataSetGroup: 2, IFSpectrum Ver. 1.3.6

Figure 90: Power variation across the entire IF band

Measured with 80 nm gate length InP HEMT based MIC cryogenic amplifier. Final design will use MMIC amplifier that will impact this result.

| Band 2 Total and In-Band Power | | | | |
|--|---------------|---------------|-------------|-----------------|
| IF Channel 0 | | | | |
| 0 dB Gain | | 15 dB Gain | | |
| LO (GHz) | In-Band (dBm) | In-Band (dBm) | Total (dBm) | Total - In-Band |
| 76 | -25 | -10.2 | -9.6 | 0.6 |
| 78 | -23.9 | -9 | -8.5 | 0.5 |
| 80 | -23.3 | -8.4 | -7.9 | 0.5 |
| 82 | -22.9 | -8.1 | -7.7 | 0.4 |
| 84 | -22.8 | -8.8 | -8.3 | 0.5 |
| 84 | -22.8 | -8 | -7.6 | 0.4 |
| TestData_header.keyId: 18205, 18206, 18207, 18208 | | | | |
| 2015-12-23 08:40:02, FE Configuration 1076, DataSetGroup: 2, IFSpectrum Ver. 1.3.6 | | | | |

| Band 2 Total and In-Band Power | | | | |
|--|---------------|---------------|-------------|-----------------|
| IF Channel 1 | | | | |
| 0 dB Gain | | 15 dB Gain | | |
| LO (GHz) | In-Band (dBm) | In-Band (dBm) | Total (dBm) | Total - In-Band |
| 76 | -25.1 | -10.4 | -9.3 | 1.2 |
| 78 | -24.3 | -9.6 | -8.2 | 1.3 |
| 80 | -23.8 | -9 | -7.7 | 1.4 |
| 82 | -23.3 | -8.5 | -7.1 | 1.4 |
| 84 | -22.8 | -8.6 | -6.8 | 1.7 |
| 84 | -22.8 | -8 | -6.8 | 1.3 |
| TestData_header.keyId: 18205, 18206, 18207, 18208 | | | | |
| 2015-12-23 08:40:02, FE Configuration 1076, DataSetGroup: 2, IFSpectrum Ver. 1.3.6 | | | | |

Figure 91: Total and In-Band Power, Pol 0 (top) and Pol 1 (bottom), USB
Measured with 80 nm gate length InP HEMT based MIC cryogenic amplifier. Final design will use MMIC amplifier that will impact this result.

| Band 2 Total and In-Band Power | | | | |
|--|---------------|---------------|-------------|-----------------|
| IF Channel 2 | | | | |
| 0 dB Gain | | 15 dB Gain | | |
| LO (GHz) | In-Band (dBm) | In-Band (dBm) | Total (dBm) | Total - In-Band |
| 76 | -29.2 | -16.8 | -16.1 | 0.7 |
| 78 | -28.7 | -15.8 | -15.4 | 0.4 |
| 80 | -28.6 | -15.6 | -15.1 | 0.5 |
| 82 | -28.7 | -15.9 | -15.1 | 0.8 |
| 84 | -28.6 | -15.3 | -14.4 | 0.8 |
| 84 | -28.6 | -15.7 | -14.6 | 1 |
| In-band diffs not between 14 and 16 dB | | | | |
| TestData_header.keyId: 18205, 18206, 18207, 18208 | | | | |
| 2015-12-23 08:40:02, FE Configuration 1076, DataSetGroup: 2, IFSpectrum Ver. 1.3.6 | | | | |

| Band 2 Total and In-Band Power | | | | |
|--|---------------|---------------|-------------|-----------------|
| IF Channel 3 | | | | |
| 0 dB Gain | | 15 dB Gain | | |
| LO (GHz) | In-Band (dBm) | In-Band (dBm) | Total (dBm) | Total - In-Band |
| 76 | -22.9 | -9.2 | -8.8 | 0.4 |
| 78 | -23.3 | -9.4 | -8.9 | 0.4 |
| 80 | -24.1 | -10.2 | -9.6 | 0.5 |
| 82 | -25.3 | -11.6 | -10.5 | 1.1 |
| 84 | -26.2 | -12.6 | -11.7 | 0.9 |
| 84 | -26.2 | -12.7 | -11.4 | 1.3 |
| In-band diffs not between 14 and 16 dB | | | | |
| TestData_header.keyId: 18205, 18206, 18207, 18208 | | | | |
| 2015-12-23 08:40:02, FE Configuration 1076, DataSetGroup: 2, IFSpectrum Ver. 1.3.6 | | | | |

Figure 92: Total and In-Band Power, Pol 0 (top) and Pol 1 (bottom), LSB

Measured with 80 nm gate length InP HEMT based MIC cryogenic amplifier. Final design will use MMIC amplifier that will impact this result.

8.4. Gain Compression (FEND-40.02.02.00-00230-00/T)

Not yet measured.

8.5. Amplitude Stability (FEND-40.02.02.00-00240-00/T)

Amplitude stability was measured with a standard ALMA bias module, and the results are as shown in [Figure 93](#) and [Figure 94](#).

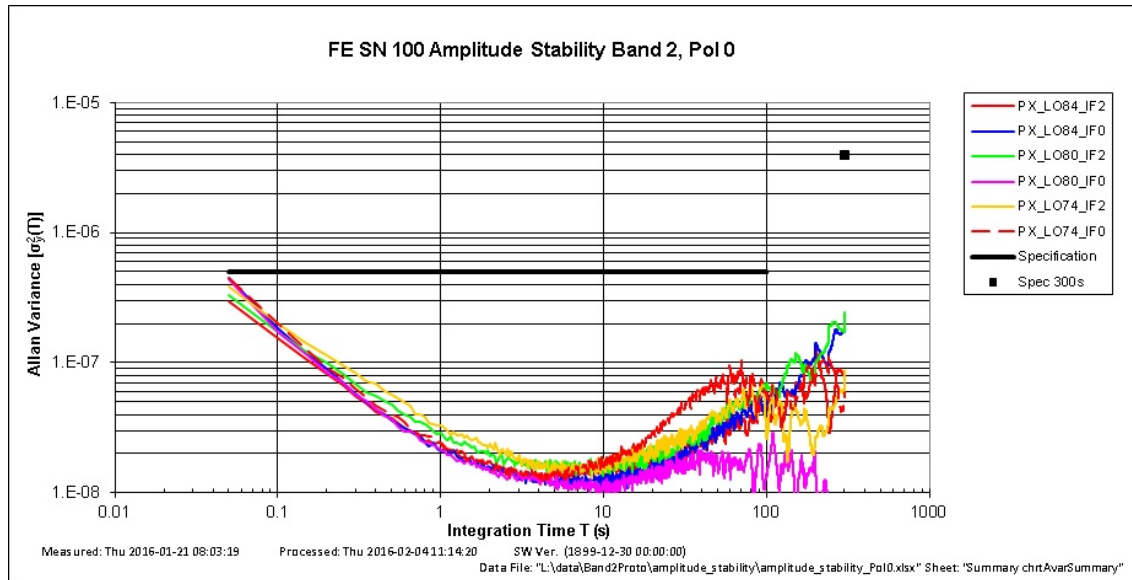


Figure 93: Amplitude Stability, Pol 0

Measured with 80 nm gate length InP HEMT based MIC cryogenic amplifier.

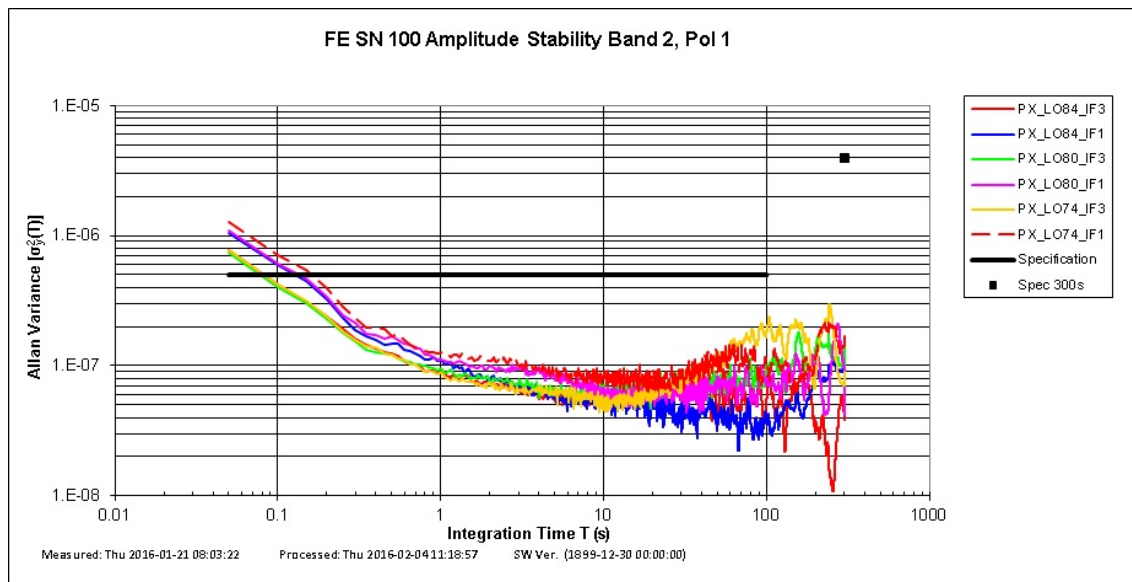



Figure 94: Amplitude Stability, Pol 1

Measured with 80 nm gate length InP HEMT based MIC cryogenic amplifier. Final design will use MMIC amplifier that meets specifications.

| | | |
|---|--|-------------------------------------|
|  | ALMA Project | Date: 2017-12-27 Page: 94 of 117 |
| | Design and testing of a Prototype Band 2 Cartridge Final Report | |

8.6. Signal Path Phase Stability (FEND-40.02.02.00-00250-00/T)

The current phase drift specification states the phase shall remain stable to within 0.2° (10 fs) on timescales up to 300 seconds. Rev B of the System Specifications [\[RD 01\]](#) requires the data be presented in the form of a 2-Point Allan Standard Deviation with a fixed averaging time of 10 second and intervals of 20 and 300 seconds.

The phase drift shown in [Figure 95](#) is the time sequence data converted to Allan Variance.

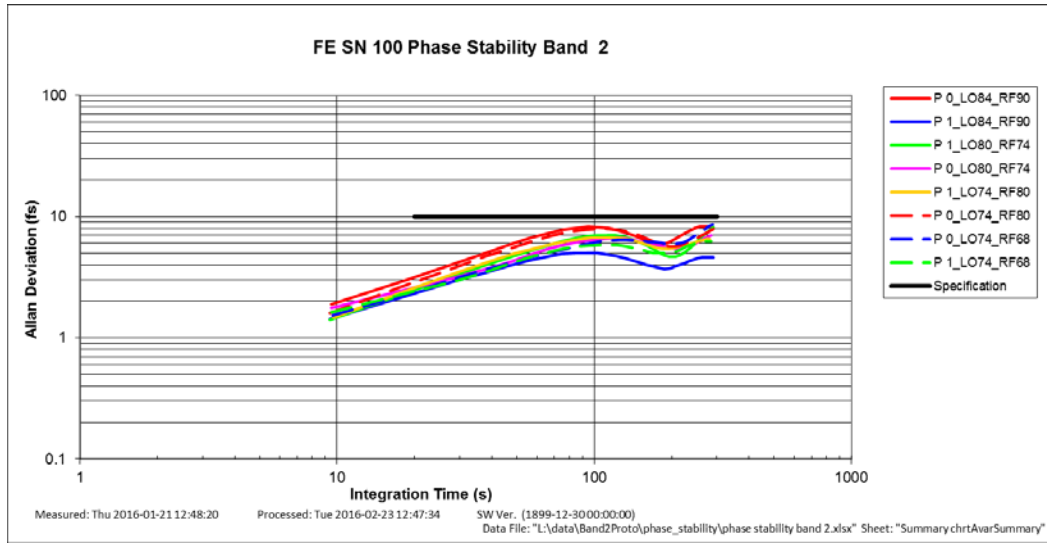


Figure 95: Phase Stability

Measured with 80 nm gate length InP HEMT based MIC cryogenic amplifier.

8.7. Beam Efficiency (FEND-40.02.02.00-00260-00/T)


Polarization efficiencies (η_{pol}) in earlier ALMA measurements were calculated with standard ALMA software as the ratio of cross-pol power ($|E_{cross}|^2$) to co-pol power ($|E_{co}|^2$) integrated over the entire scan area [\[RD 24\]](#):

$$\eta_{pol} = \frac{1}{1 + \frac{\sum_{all} |E_{cross}|^2}{\sum_{all} |E_{co}|^2}} \quad \text{Eq. 1}$$

That approach results in low polarization efficiencies for patterns exhibiting cross polar Condon lobes that essentially miss secondary, which is the case for the Band 2 design. The most recent version of ALMA Beam efficiency software (Ver. 2.0.4) calculates polarization efficiencies using the more conventional definition that sums power over just the secondary:

$$\eta_{pol} = \frac{1}{1 + \frac{\sum_{sec} |E_{cross}|^2}{\sum_{sec} |E_{co}|^2}} \quad \text{Eq. 2}$$

Although Eq. 1 was used during ALMA production, the use of Eq. 2 is not without precedent, since several cartridge groups calculated polarization efficiencies using this approach documented in [\[RD 24\]](#). For instance, see the Band 5 procedures of [\[RD 26\]](#) which also use Eq. 2. In these calculations the loss power to the cross polar peaks is captured in the spillover efficiency metric, and the overall beam efficiency is unchanged.

| | | |
|---|--|-------------------------------------|
|  | ALMA Project | Date: 2017-12-27 Page: 95 of 117 |
| | Design and testing of a Prototype Band 2 Cartridge Final Report | |

8.7.1. Test System

Beam patterns were measured with the same test system used to measure front ends during ALMA production. [Figure 96](#) shows the block diagram of the pattern measurement system, and outlines the phase locking scheme for the various sources in the test system. Two sources are required to cover the entire band.

8.7.2. Linearity

Linearity was confirmed for this series of measurements at several frequencies by comparing rectilinear beam patterns measured at different source power levels. To ensure consistency in power levels, the measurement software serves the transmit power to provide a fixed receive level at each frequency.



8.7.3. Measurements for Lens 3-2

To point the beam in the nominal secondary direction, beam position was measured for a series of lens translations to first determine the plate factor, and then find the appropriate lens offset at room temperature to optimize beam pointing for the cooled cryostat. A laser was mounted on the beam scanner to allow locating the center of the lens to about ± 0.3 mm. Fine positioning of the lens was available only from set screws on a frame, and provided about ± 0.3 mm adjustment precision. [Table 19](#) summarizes the results, and Row 42 shows the final room temperature lens position just prior to cool down.

The final beam centering results are shown in [Figure 97](#) with efficiencies graphed in [Figure 98](#) and [Figure 99](#) relative to the nominal secondary direction. [Figure 100](#) is the Pol 0 near and far-field patterns for this lens at 78 GHz where the polarization is nominal, while [Figure 101](#) is Pol 0 patterns at 85 GHz where there is a dip in polarization efficiency. For reference, [Figure 102](#) and [Figure 103](#) are efficiencies relative to the actual beam direction and are basically identical to efficiencies calculated in the nominal secondary direction which shows that the beam centering is essentially perfect.

Table 18: Room Temperature Pointing Compensation Calculations

| Row | | | | Pointing | | | | |
|-----|---|---------------|--------|----------|---------|---------|---------|-------------|
| | | Lens Position | | Az | | El | | |
| | | Az (m) | El (m) | Pol 0 | Pol 1 | Pol 0 | Pol 1 | |
| 1 | Spec Pointing | | | -1.7553 | | 1.7553 | | degs |
| 2 | Cryostat Cold | -0.18180 | 0.1877 | -0.5564 | -0.5398 | 1.6250 | 1.6794 | degs |
| 3 | Cryostat at Room Temp | | | -0.9369 | -0.8802 | 1.9049 | 1.9478 | degs |
| 4 | Room temp minus cold | | | -0.3805 | -0.3404 | 0.2800 | 0.2684 | degs |
| 5 | | | | | | | | |
| 6 | Cryostat at Room Temp | -0.18000 | 0.1877 | -2.0470 | -2.0165 | 1.7014 | 1.7535 | degs |
| 7 | El change with no intentional El movement of lens | | | | | -0.2035 | -0.1943 | degs |
| 8 | Centers, nominal minus room temp | | | 0.2917 | 0.2612 | 0.0539 | 0.0018 | degs |
| 9 | Average | | | 0.2764 | | 0.0278 | | degs |
| 10 | Plate scale at room temp | | | -0.6167 | -0.6313 | -0.6167 | -0.6313 | degs/m m |
| 11 | Average | | | -0.6240 | | -0.6240 | | degs/m m |
| 12 | | | | | | | | |
| 13 | Required pointing at room temperature | | | -2.1358 | -2.0957 | 2.0353 | 2.0237 | degs |
| 14 | | | | | | | | |
| 15 | Current pointing at room temperature | | | -2.0470 | -2.0165 | 1.7014 | 1.7535 | degs |
| 16 | Change in pointing required | | | -0.0889 | -0.0792 | 0.3338 | 0.2702 | degs |
| 17 | Lens movement required | | | 0.142 | 0.127 | -0.535 | -0.433 | mm |
| 18 | Average | | | 0.135 | | -0.484 | | mm |
| 19 | | | | | | | | |
| 20 | Required absolute position of lens | -0.1799 | 0.1872 | | | | | m |
| 21 | Tue 2016-02-09 16:53 | | | | | | | |
| 22 | Lens moved to | -0.1799 | 0.1872 | | | | | m |
| 23 | Measured Pointing | | | -2.3874 | -2.2345 | 2.0210 | 2.0498 | degs |
| 24 | Error from required pointing | | | 0.2516 | 0.1388 | 0.0143 | -0.0261 | degs |
| 25 | Lens movement required to match required pointing | | | -0.408 | -0.220 | -0.023 | 0.041 | mm |
| 26 | Average | | | -0.314 | | 0.009 | | mm |
| 27 | New Position of lens | -0.1796 | 0.1872 | | | | | m |
| 28 | Wed 2016-02-10 14:17 | | | | | | | |



Design and testing of a Prototype Band 2 Cartridge: Final Report

Date: 2017-12-27

Page: 98 of 117

| | | | | | | | | |
|----|---|---------|--------|---------|---------|---------|---------|-----|
| 29 | Lens moved to | -0.1796 | 0.1872 | | | | | m |
| 30 | Measured Pointing | | | -2.3751 | -2.2512 | 2.0472 | 2.0715 | deg |
| 31 | Error from required pointing | | | 0.2393 | 0.1555 | -0.0119 | -0.0478 | deg |
| 32 | Lens movement required to match required pointing | | | -0.383 | -0.249 | 0.019 | 0.077 | mm |
| 33 | Average | | | -0.316 | | 0.048 | | mm |
| 34 | New Position of lens | -0.1793 | 0.1872 | | | | | |
| 35 | | | | | | | | |
| 36 | Thu 2016-02-11 14:02 | | | | | | | |
| 37 | Lens at | -0.1796 | 0.1872 | | | | | m |
| 38 | Measured Pointing | | | -2.338 | -2.049 | 2.264 | 2.285 | deg |
| 39 | Error from required pointing | | | -0.2024 | 0.0472 | 0.2286 | 0.2613 | deg |
| 40 | Lens movement required to match required pointing | | | 0.328 | -0.075 | -0.371 | -0.414 | mm |
| 41 | Average | | | 0.127 | | -0.392 | | mm |
| 42 | Position of lens for perfect pointing | -0.1797 | 0.1876 | | | | | m |

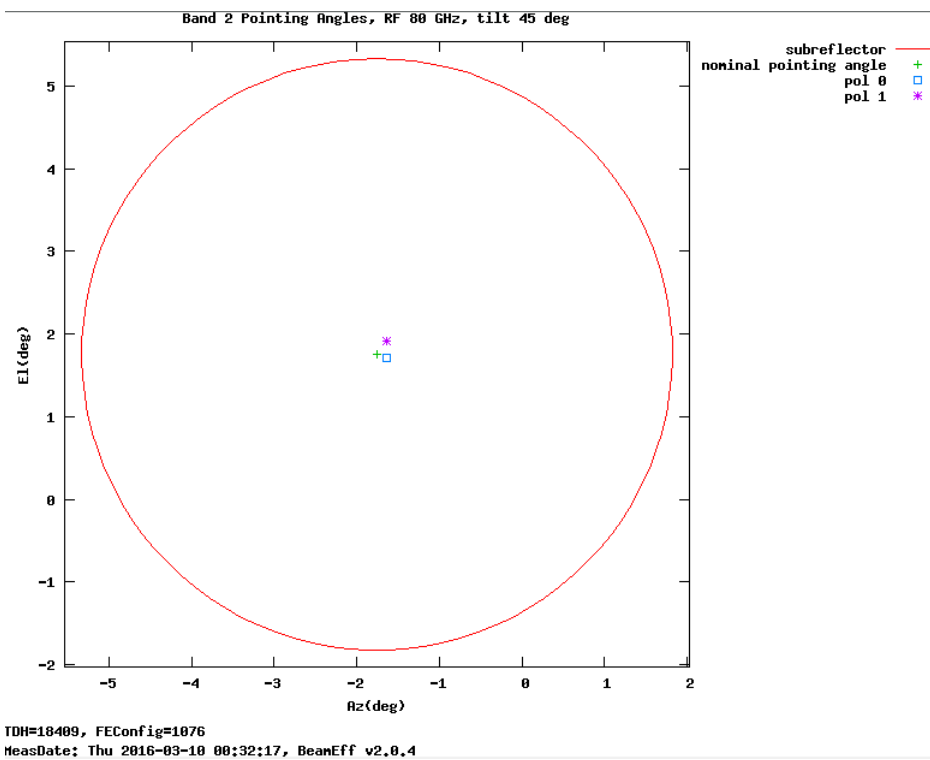


Figure 97: Final Beam Pointing with Lens 3-2, Cold Az = -0.1798m, El = 0.1876m



Design and testing of a Prototype Band 2 Cartridge: Final Report

Date: 2017-12-27

Page: 99 of 117

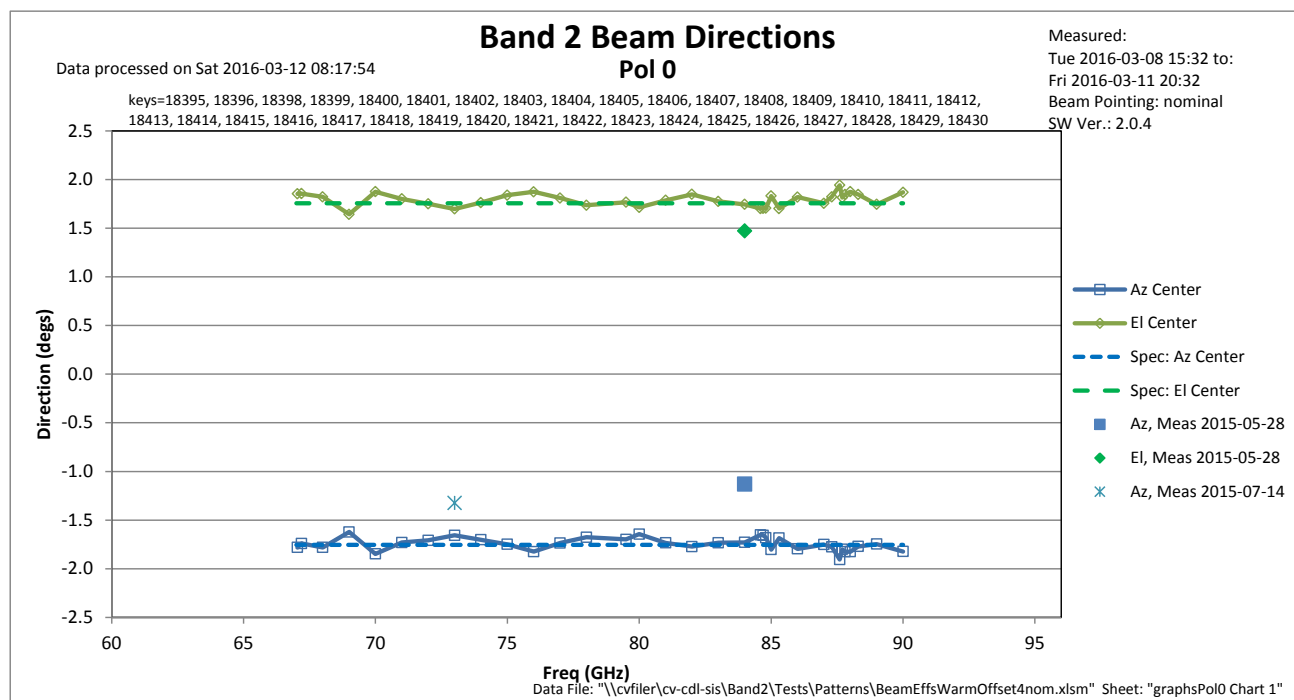
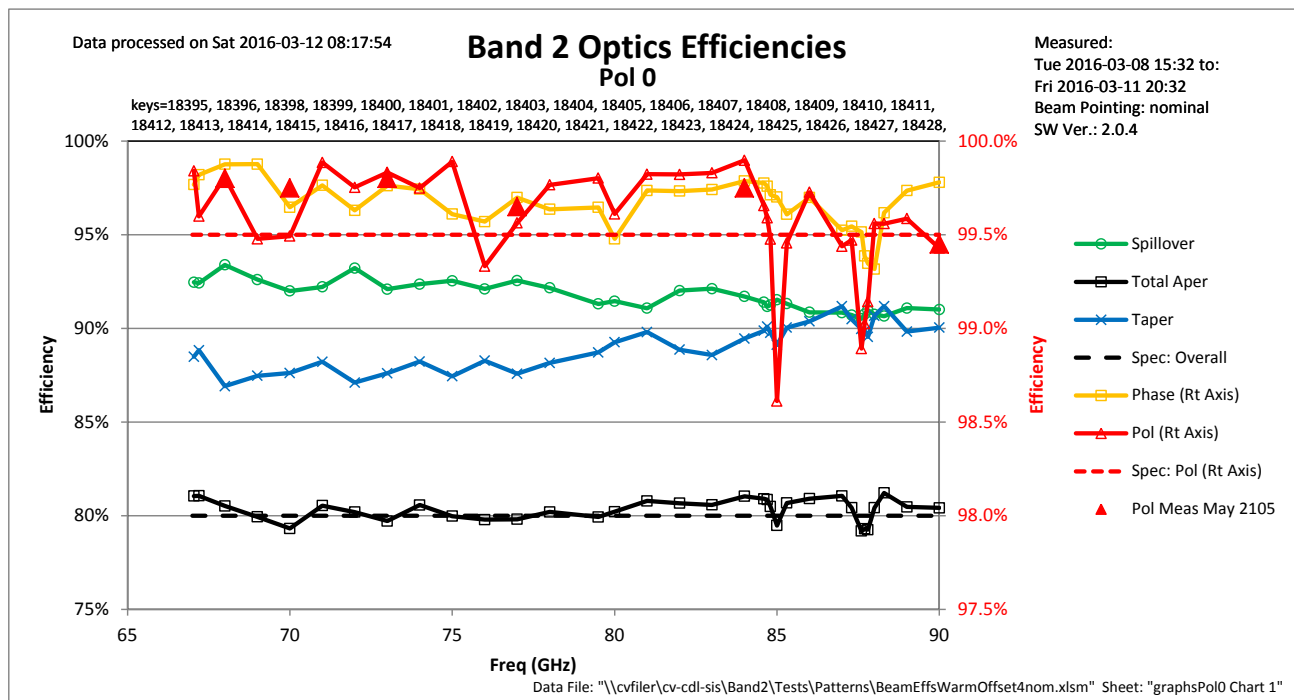


Figure 98: Efficiencies for Lens 3-2, Pol 0, cold, nominal secondary position.

Compare to efficiencies calculated relative to the direction of beam pointing in [Figure 102](#)



Design and testing of a Prototype Band 2 Cartridge: Final Report

Date: 2017-12-27

Page: 100 of 117

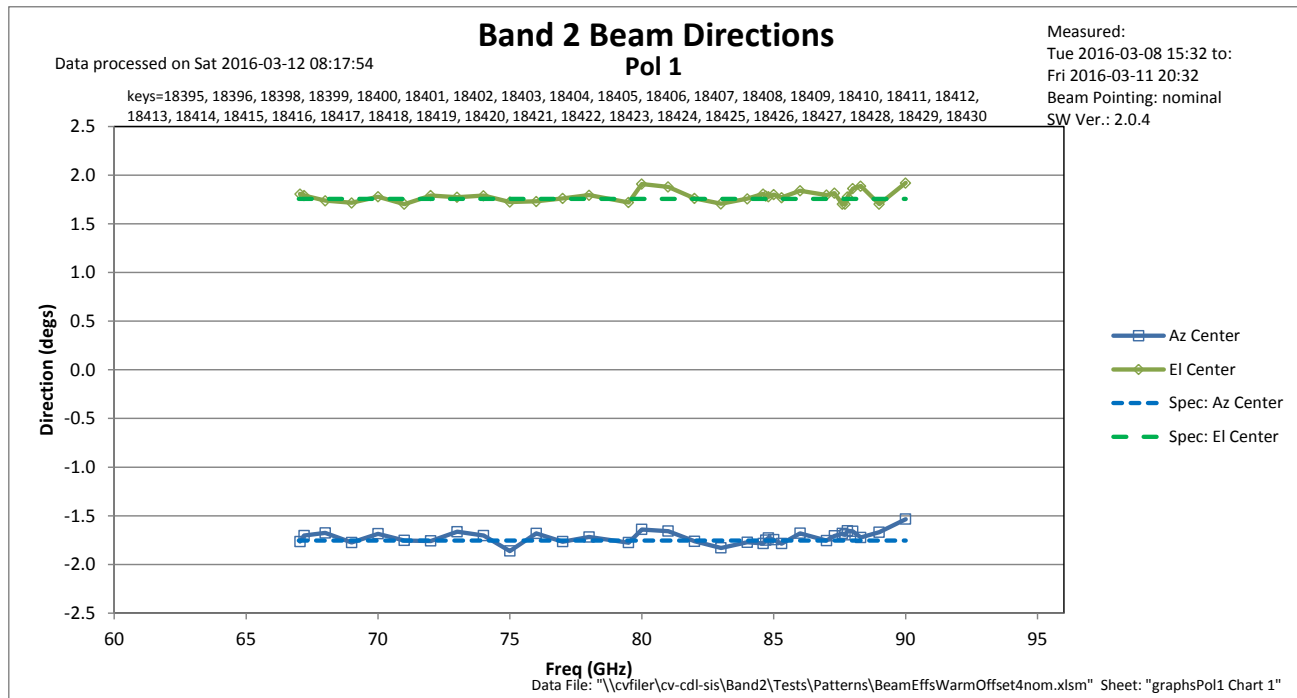
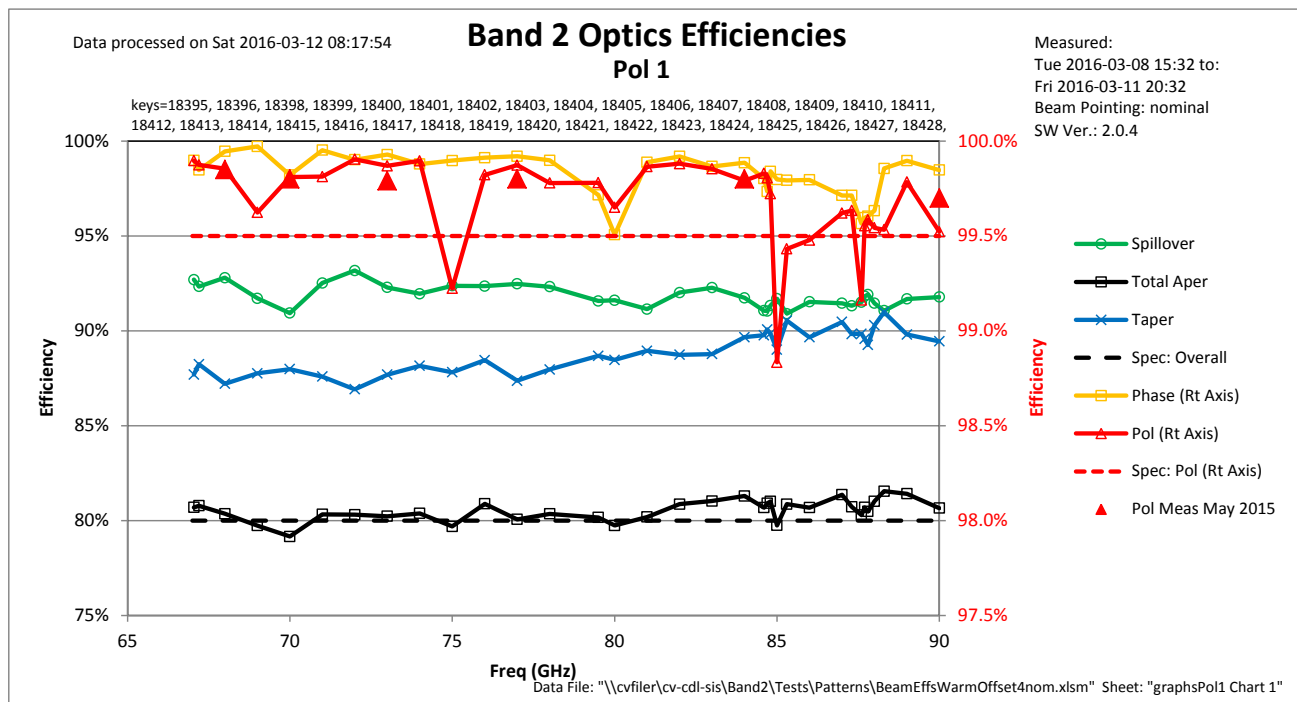


Figure 99: Efficiencies for Lens 3-2, Pol 1, cold, pointing: nominal secondary position.

Compare to efficiencies calculated relative to the direction of beam pointing in [Figure 103](#)



Design and testing of a Prototype Band 2 Cartridge: Final Report

Date: 2017-12-27

Page: 101 of 117

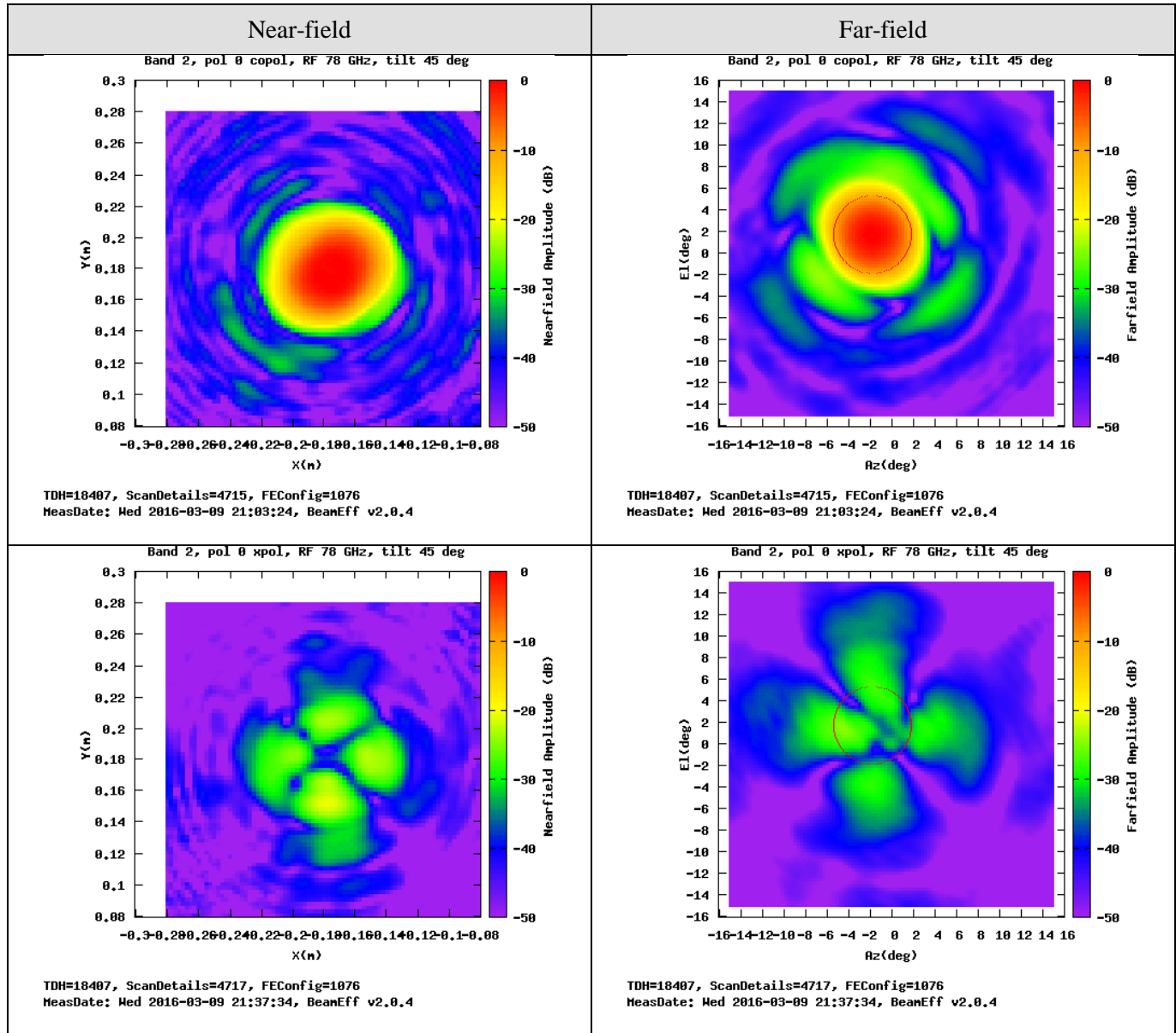


Figure 100: Pol 0 Near- and Far-field Patterns for 78 GHz: Lens 3-2



Design and testing of a Prototype Band 2 Cartridge: Final Report

Date: 2017-12-27

Page: 102 of 117

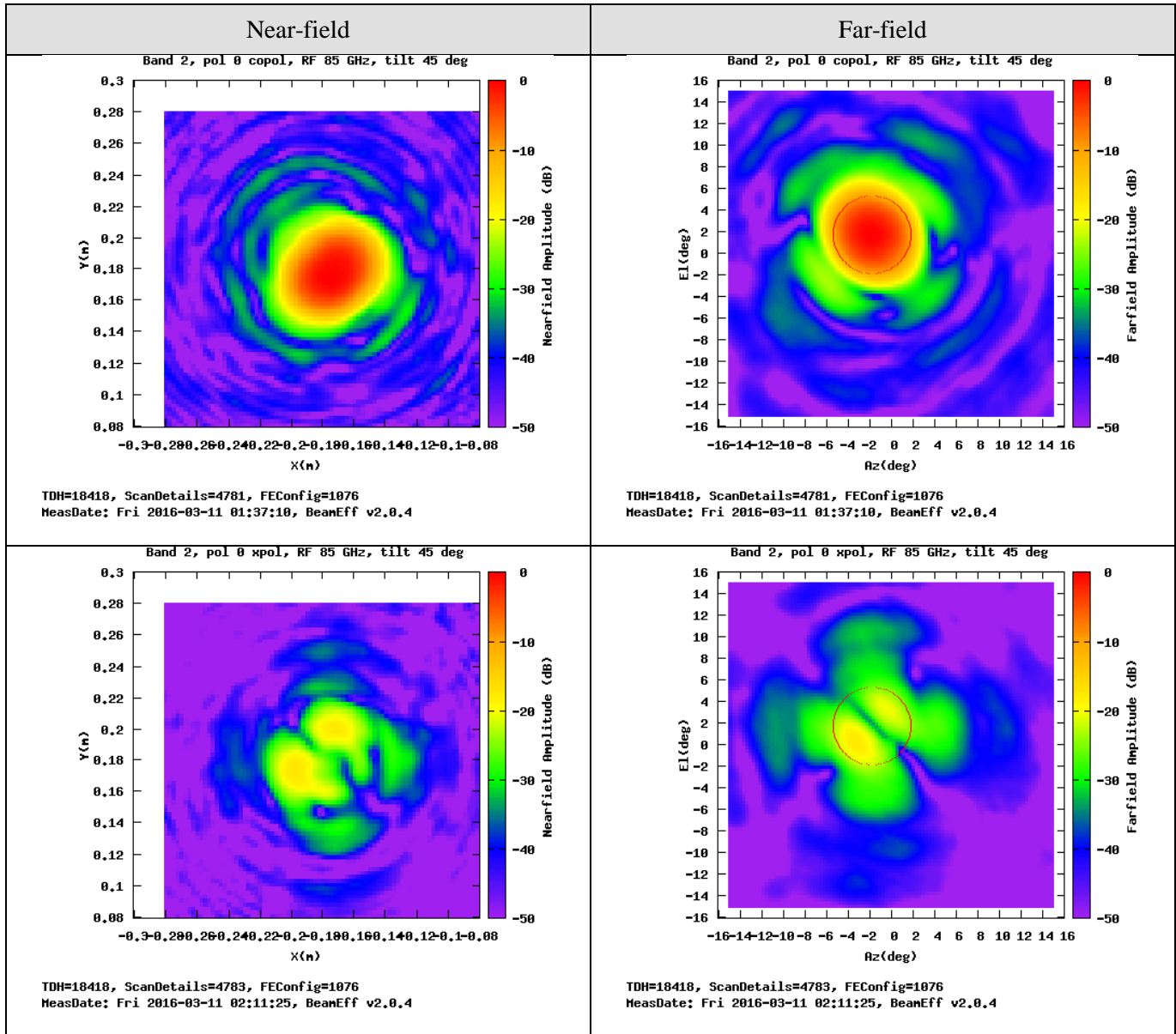


Figure 101: Pol 0 Near- and Far-field Patterns for 85 GHz: Lens 3-2, Pol Eff dip.



Design and testing of a Prototype Band 2 Cartridge: Final Report

Date: 2017-12-27

Page: 103 of 117

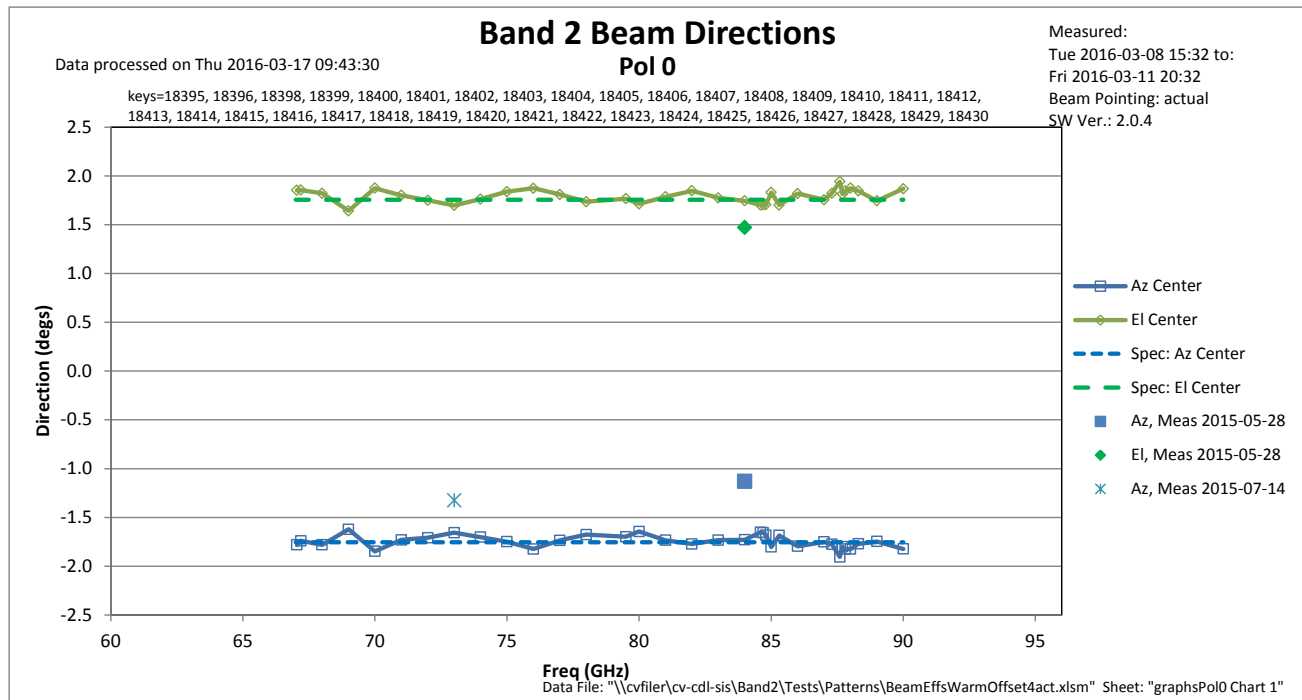
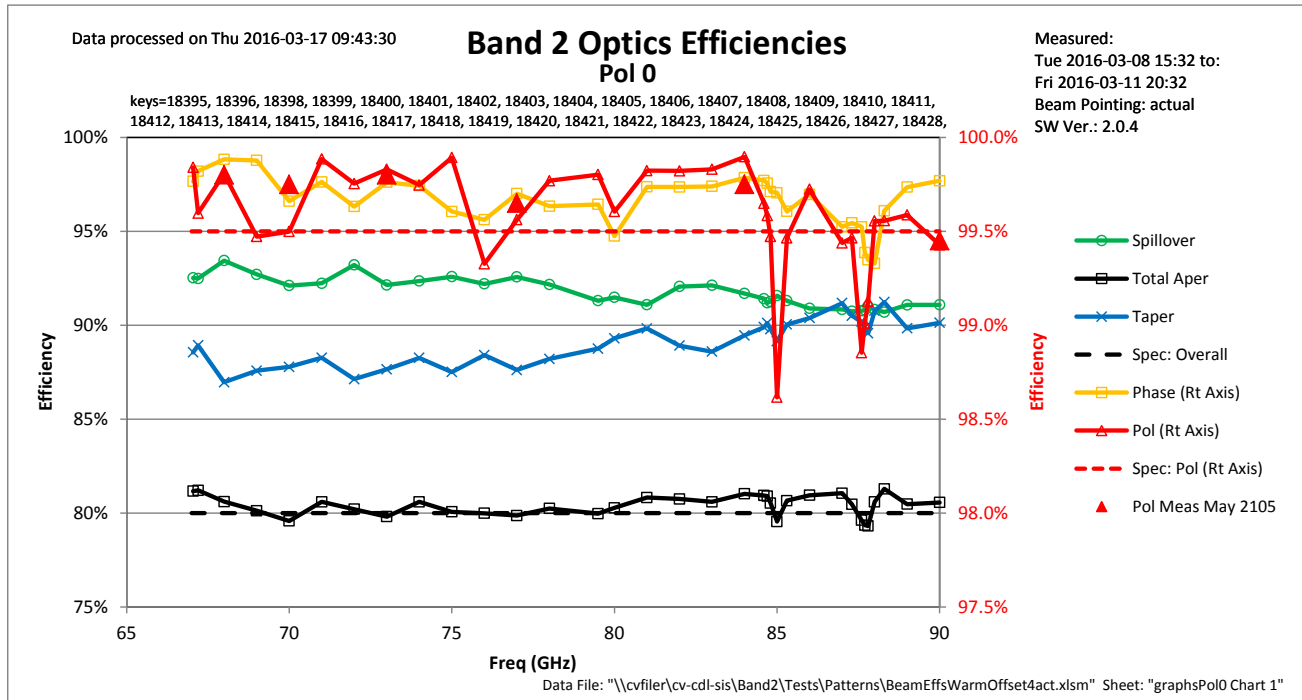


Figure 102: Final results for Lens 3-2, Pol 0, cold, pointing: actual beam direction.

Compare to measurements with the beam pointing towards the nominal subreflector direction in

[Figure 98](#)



Design and testing of a Prototype Band 2 Cartridge: Final Report

Date: 2017-12-27

Page: 104 of 117

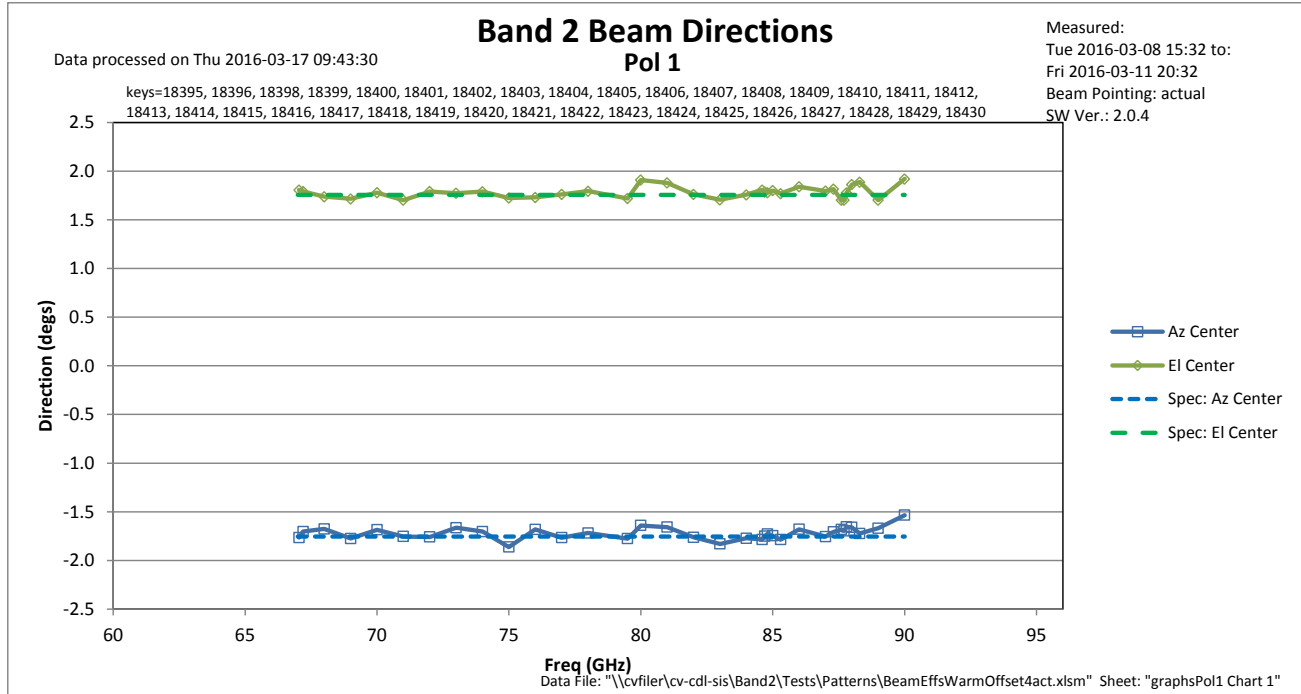
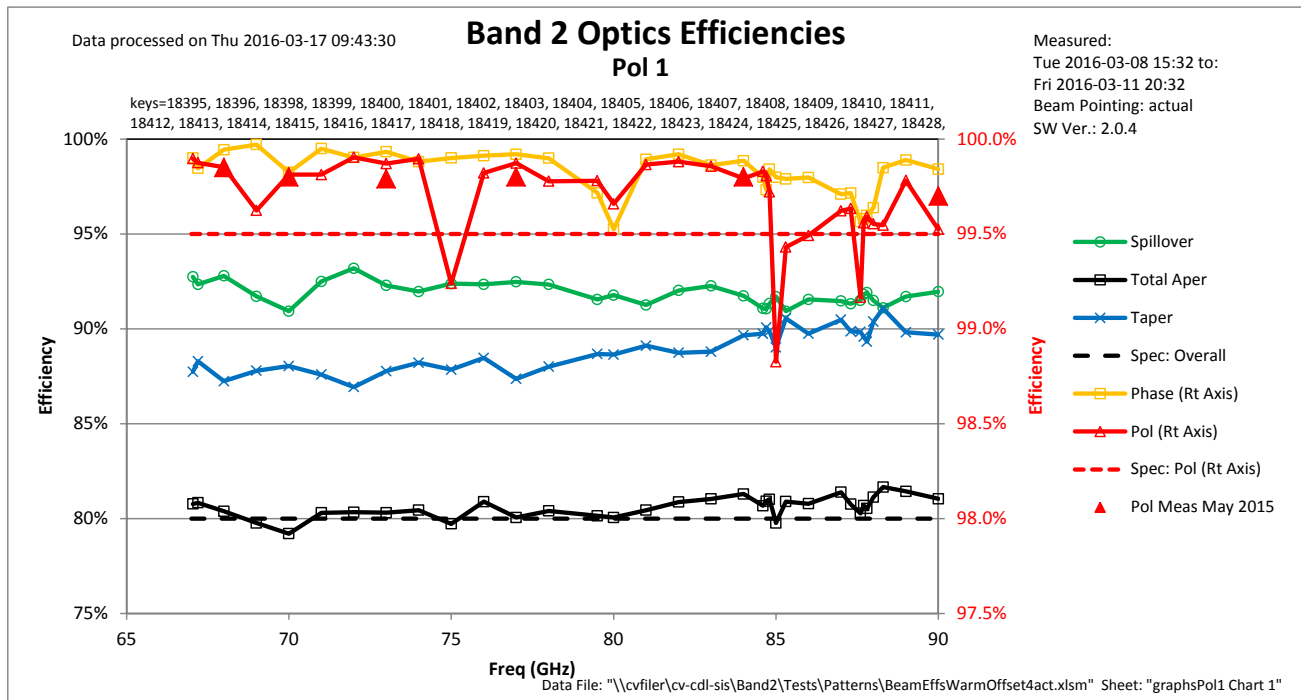


Figure 103: Efficiencies for Lens 3-2, Pol 1, cold, pointing: actual beam direction.

Compare to measurements with the beam pointing towards the nominal subreflector direction in
[Figure 99](#)

To study the effects of the IR filters on polarization efficiency, additional measurements were carried out in Green Bank's anechoic chamber. Measurements were done by introducing the IR filters and apertures representing the

openings in the cryostat at various stages, one at time. The filters were mounted at the appropriate angle with respect to the beam axis. Polarization efficiency was calculated using only two diagonal cuts, where the peaks of the cross-polarized pattern occur. Hence, the efficiency was expected to be lower than that calculated from 2D beam scans, as done in the NSI software. [Figure 104](#) shows polarization efficiency with and without the filters. This demonstrates that the 15 K IR filters cause deterioration of the cross-polarization and they are a significant contributor to cross-polarization degradation.

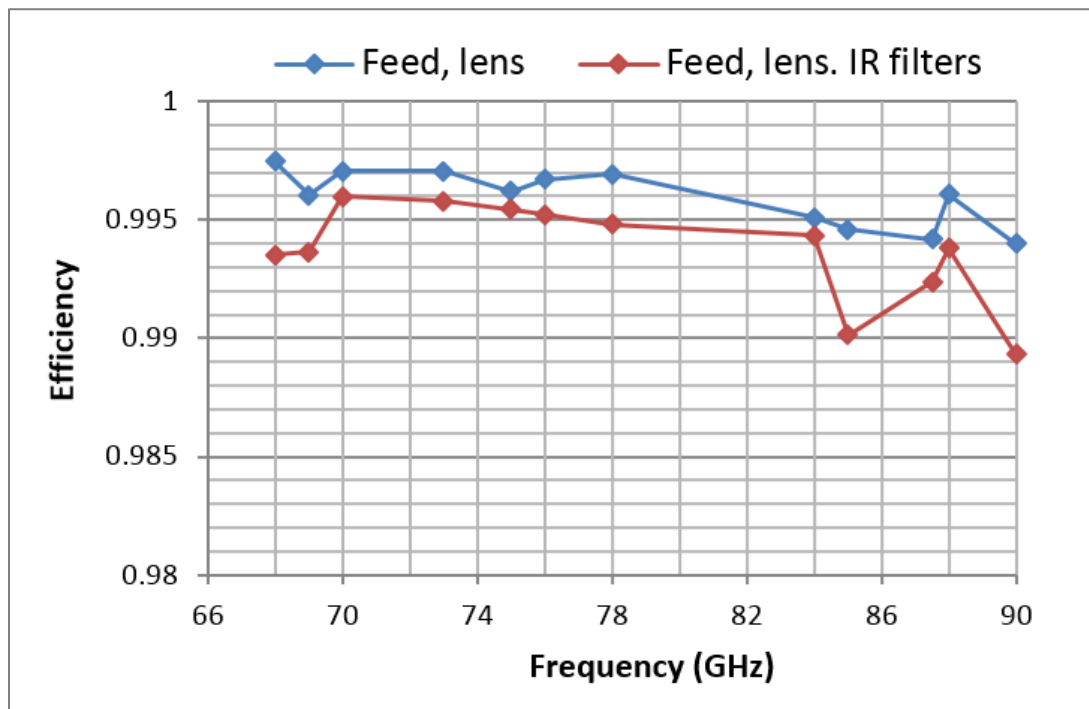


Figure 104: Measured polarization efficiency of feed horn & lens with and without the 15 K IR filter (Anechoic chamber measurements).

8.7.4. Measurements with Lens 1-1

Interaction between the 15K IR filter and the Band 1 feed horn is thought to be the cause of the polarization efficiency dips when using lens 3-2, ([Figure 98](#) and [Figure 99](#)). Therefore, efficiencies were measured for Lens 1-1 since the longer focal length of that lens places the horn 4 mm farther away from the 15 K IR filter. Lens 1-1 was initially positioned on the cryostat within ± 300 μ m of the location of lens 3-2, but the warm pointing direction differed significantly from the warm compensation position of lens 3-2. Consequently, the position of lens 1-1 was moved incrementally to make the warm beam direction the same as lens 3-2 by assuming the plate factors remained the same, and pointing results are shown in [Figure 105](#). Elevation pointing was not quite optimum as shown at the bottom graph in the efficiency plots, but the pointing is sufficiently close to check for polarization efficiency anomalies.

Beam efficiencies for lens 1-1 installed on a cold cryostat are given in [Figure 106](#) and [Figure 107](#). These figures show that the polarization dips remained despite the fact that lens was now 4 mm farther away from the 15 K IR filter. [Figure 108](#) shows the Pol 0 near and far-field patterns for this lens at 78 GHz where polarization efficiency is nominal.



Design and testing of a Prototype Band 2 Cartridge: Final Report

Date: 2017-12-27

Page: 106 of 117

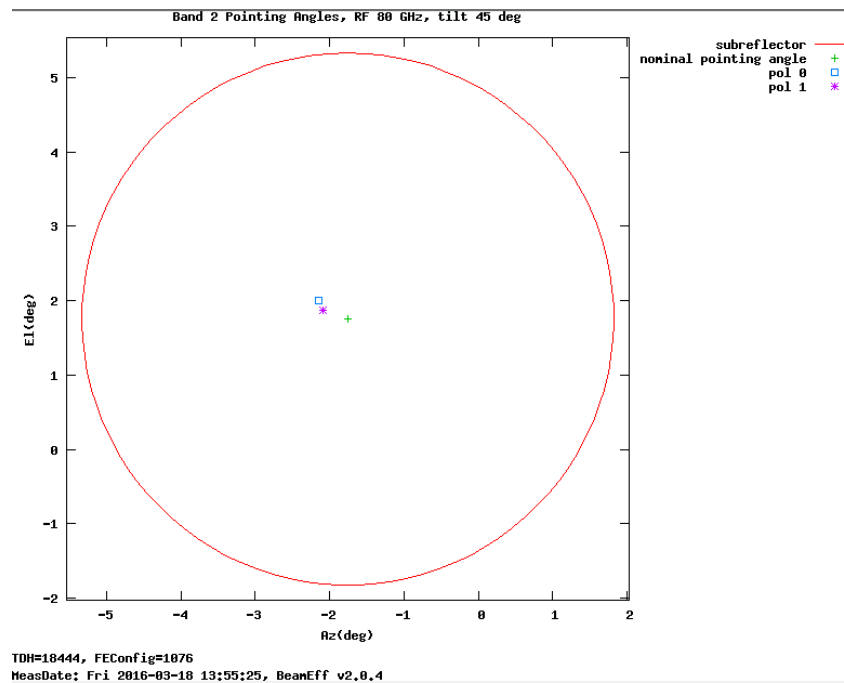


Figure 105: Final pointing of Lens 1-1, warm. Lens position was adjusted to match final warm pointing of Lens 3-2.



Design and testing of a Prototype Band 2 Cartridge: Final Report

Date: 2017-12-27

Page: 107 of 117

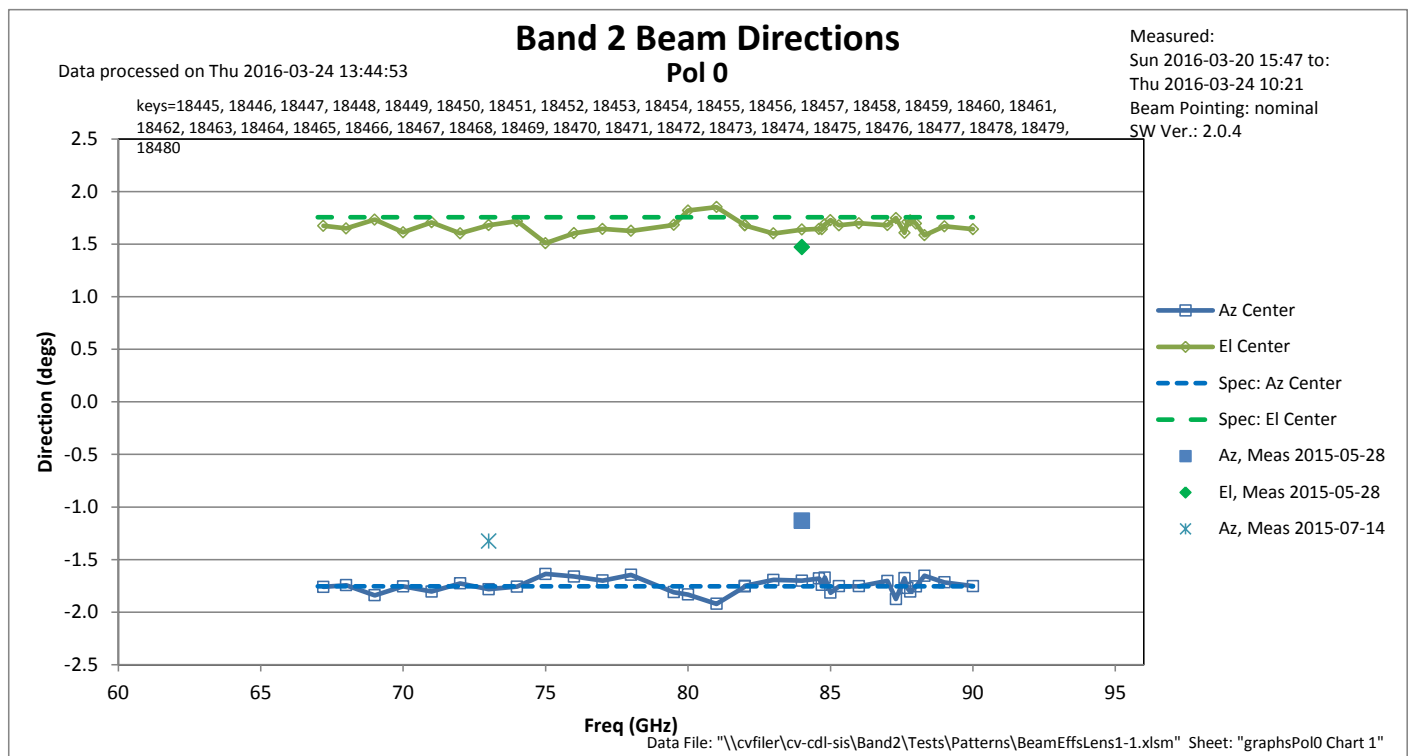
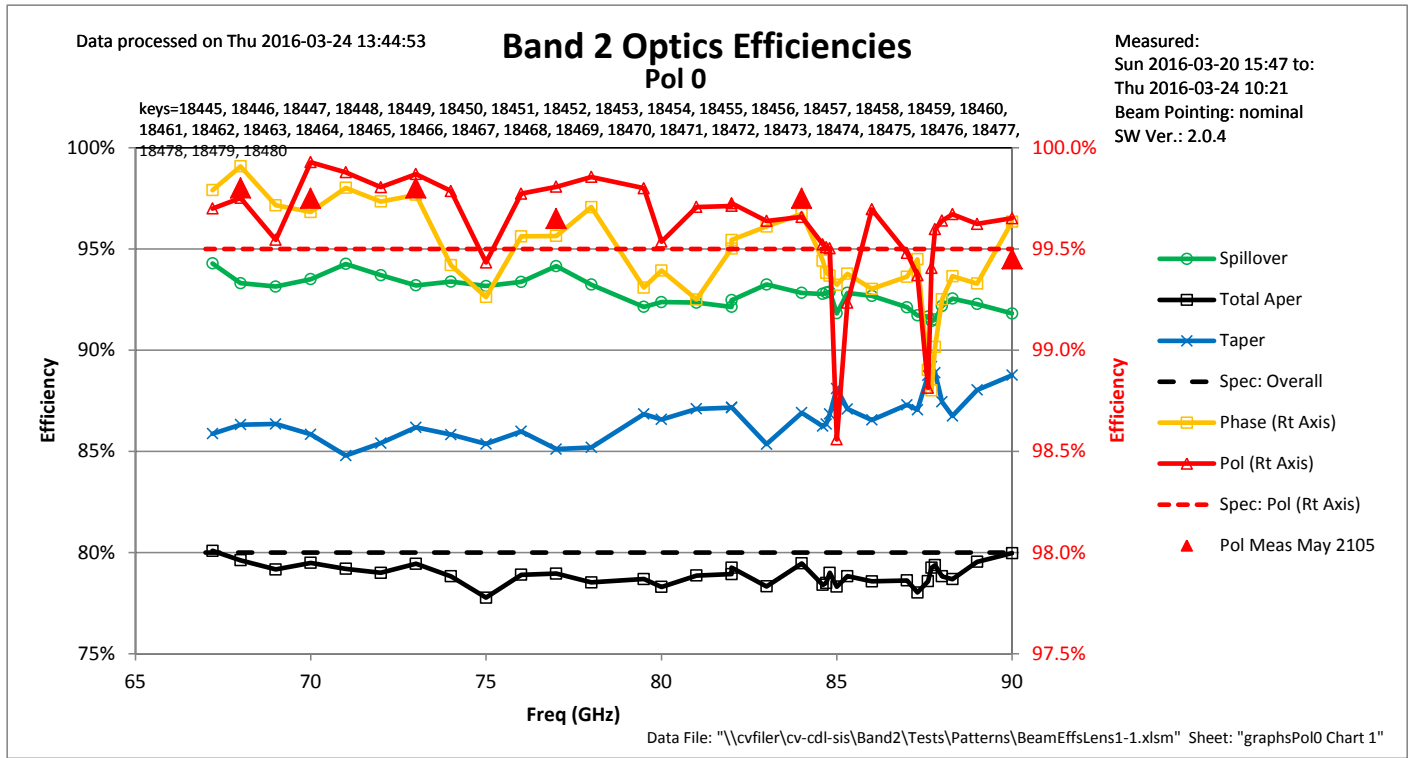


Figure 106: Lens 1-1, Pol 0, cold, nominal secondary position. Compare to Lens 3-2 in
[Figure 98](#)



Design and testing of a Prototype Band 2 Cartridge: Final Report

Date: 2017-12-27

Page: 108 of 117

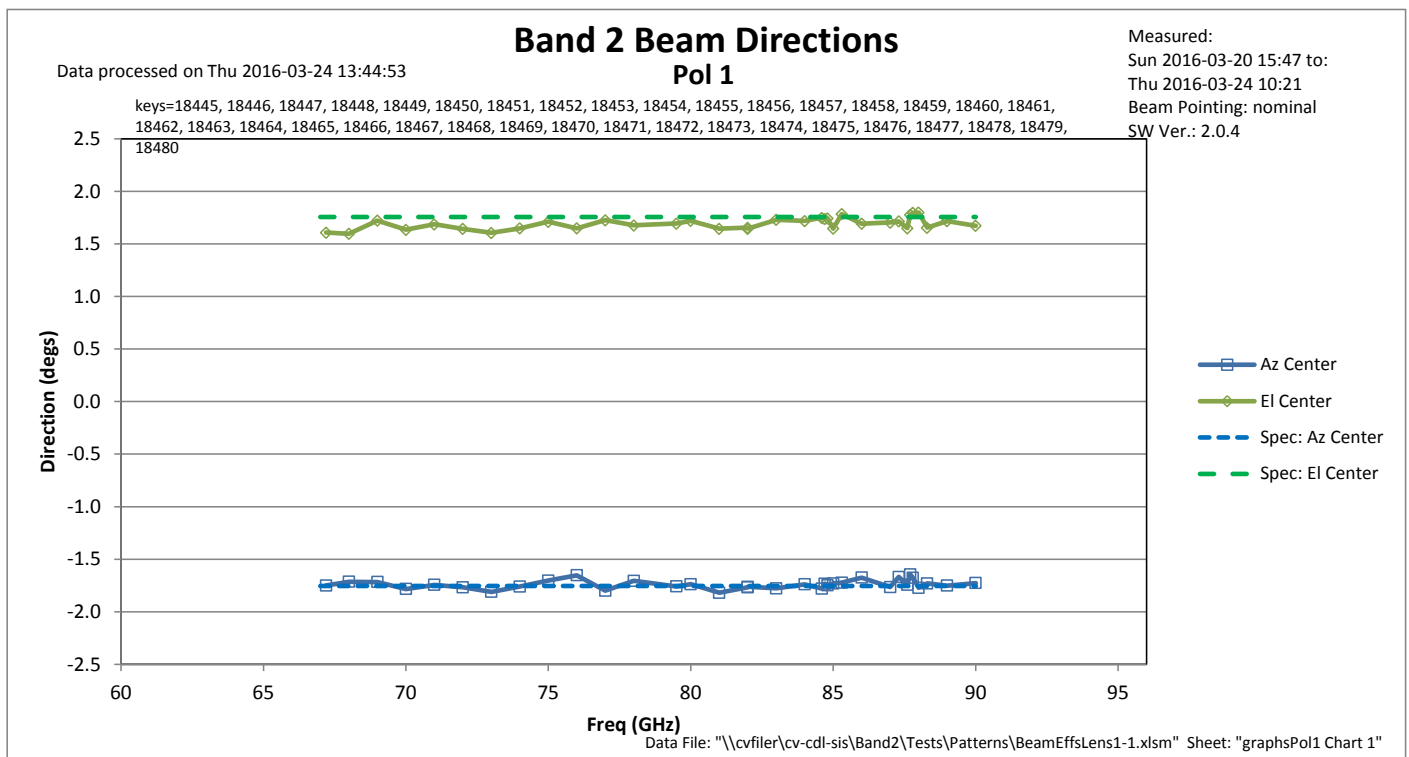
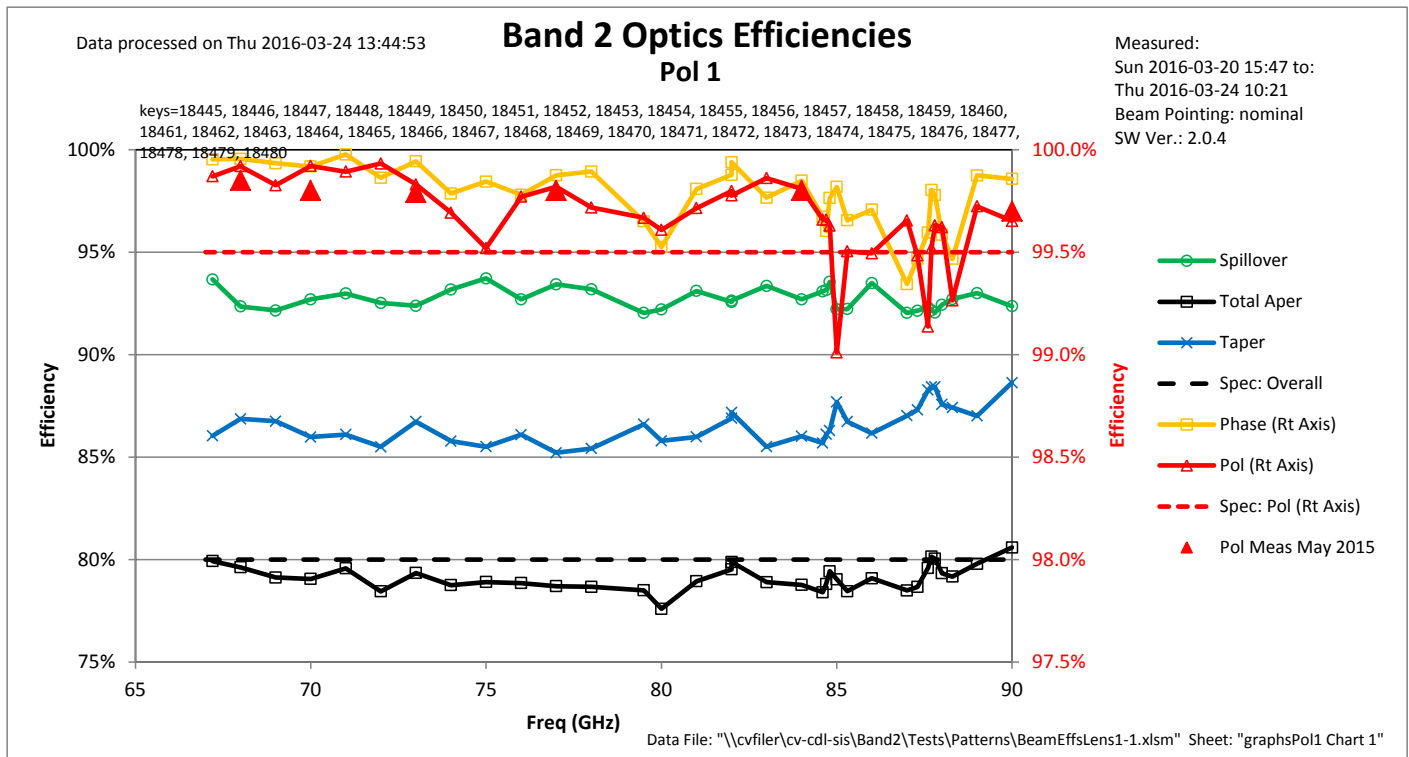


Figure 107: Lens 1-1, Pol 1, cold, nominal secondary position. Compare to Lens 3-2 in

[Figure 99.](#)

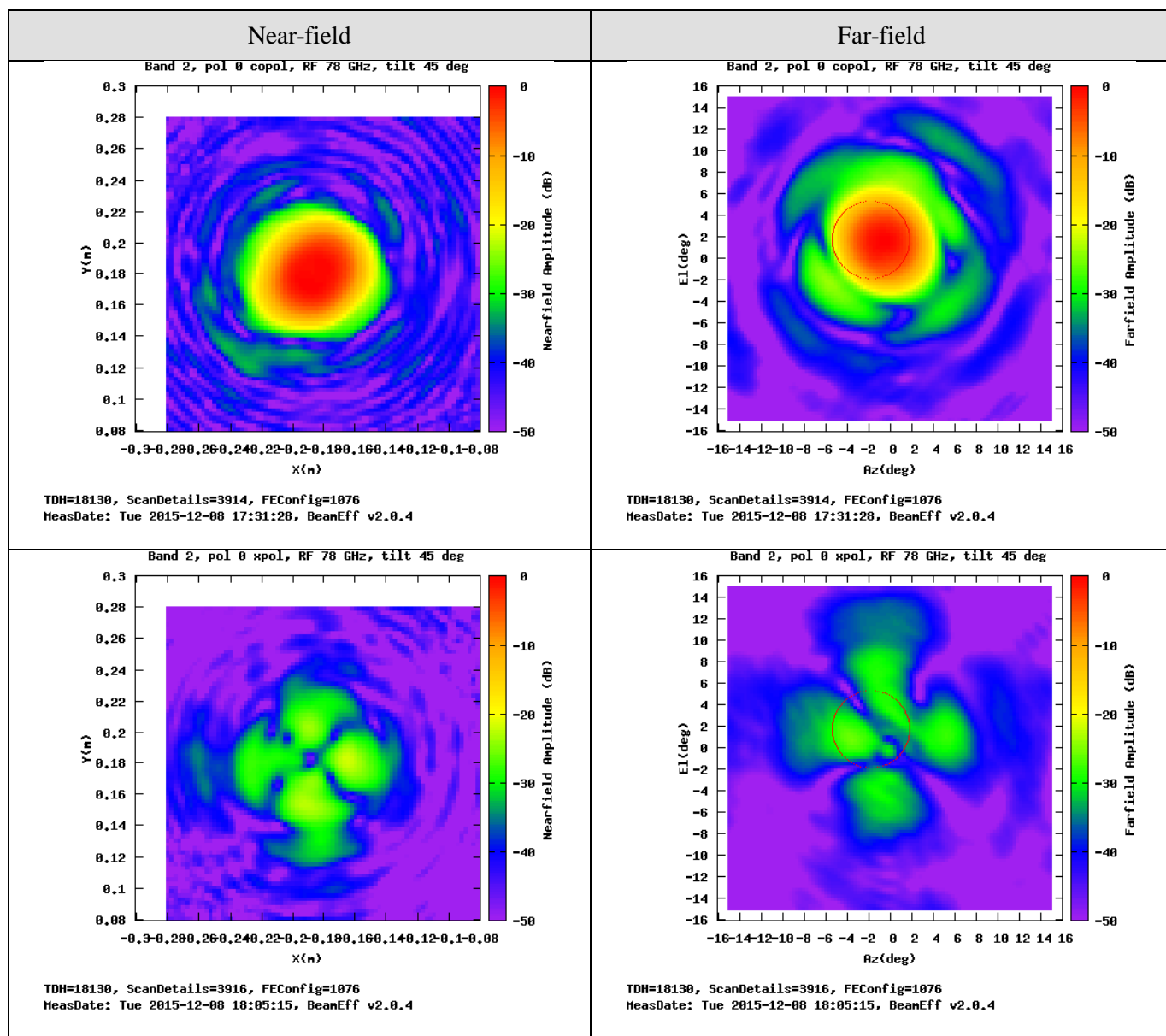


Figure 108: Pol 0 Near- and Far-field Patterns for 78 GHz: Lens 1-1

8.7.5. Measurements with Fresnel Lens

The cryostat mounting rings for the Fresnel lens (Section 7.2.9 above) severely constrained its lateral movement, so efficiencies were calculated relative to the absolute beam direction, rather than in the nominal direction of the secondary. Based on the measurements while centering lens 3-2 (Section 8.7.3 above), it was decided that it would not be useful to redesign the cryostat mounting rings to allow the zone lens to point in the nominal secondary direction. Rather, calculating efficiencies relative to the absolute beam direction would be sufficient to predict overall optics performance.



Design and testing of a Prototype Band 2 Cartridge: Final Report

Date: 2017-12-27

Page: 110 of 117

[Figure 109](#) and [Figure 110](#) are measured beam efficiencies for the Fresnel lens, and the overall efficiency, which averages 81.5%, is better than the 80.3% for lens 3-2 ([Figure 102](#) and [Figure 103](#)), primarily due to equal spillover and taper efficiencies, which is optimal for the Fresnel lens. [Figure 112](#) is the Pol 0 near and far-field patterns for this lens at 78 GHz where the polarization is nominal. The Fresnel lens exhibits the same dips in polarization efficiency as the other lenses, which supports the theory that these dips are caused by the IR filters.

Noise measurements showed that the Fresnel lens didn't significantly change compared to noise measured with lens 3-2, [Figure 57](#) and [Figure 58](#).



Design and testing of a Prototype Band 2 Cartridge: Final Report

Date: 2017-12-27

Page: 111 of 117

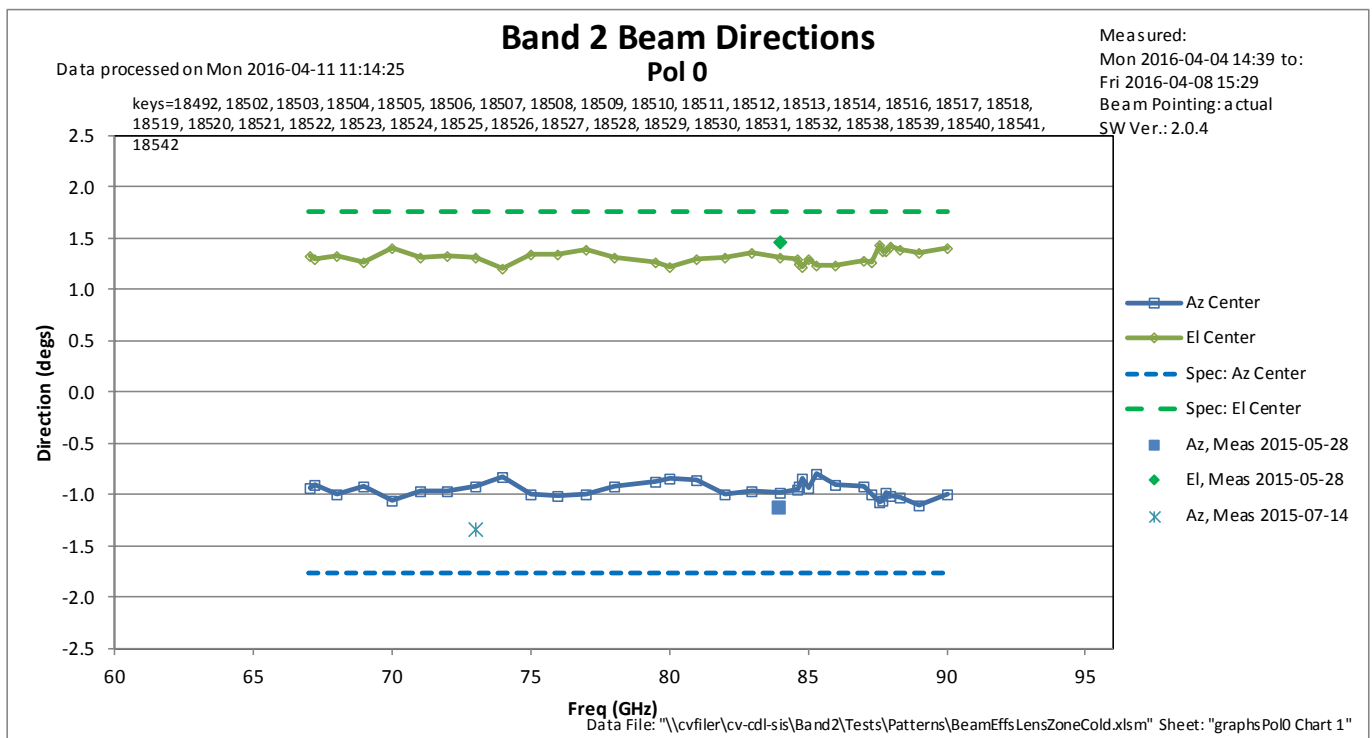
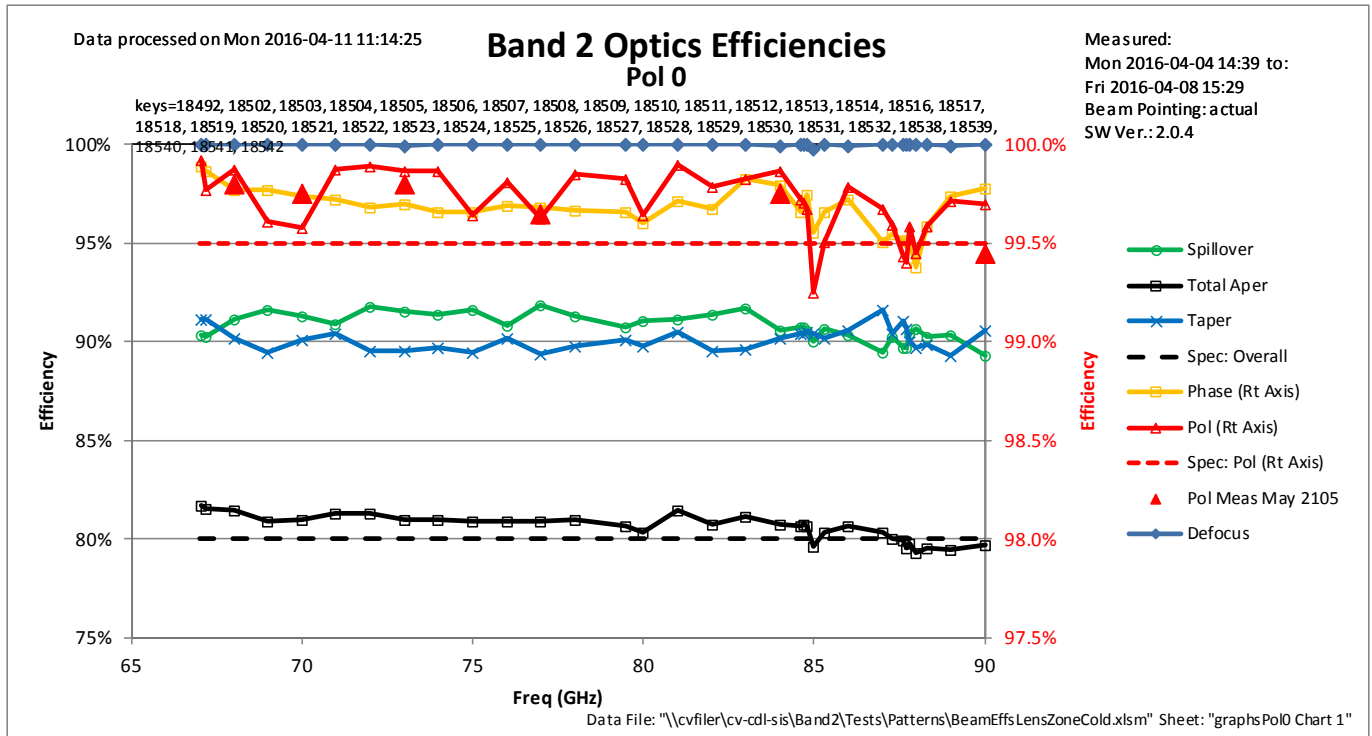


Figure 109: Fresnel lens, Pol 0, cold, actual beam pointing direction.

Compare with lens 3-2 in [Figure 102](#)



Design and testing of a Prototype Band 2 Cartridge: Final Report

Date: 2017-12-27

Page: 112 of 117

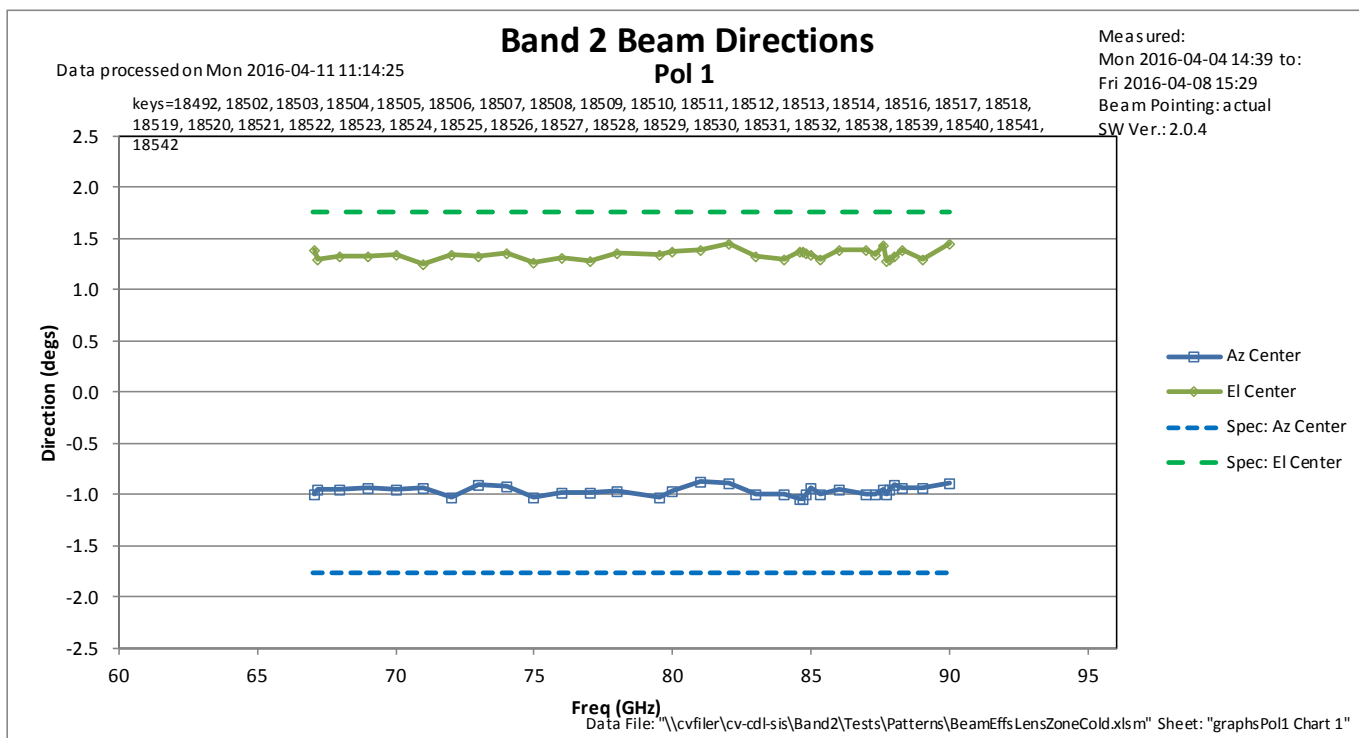
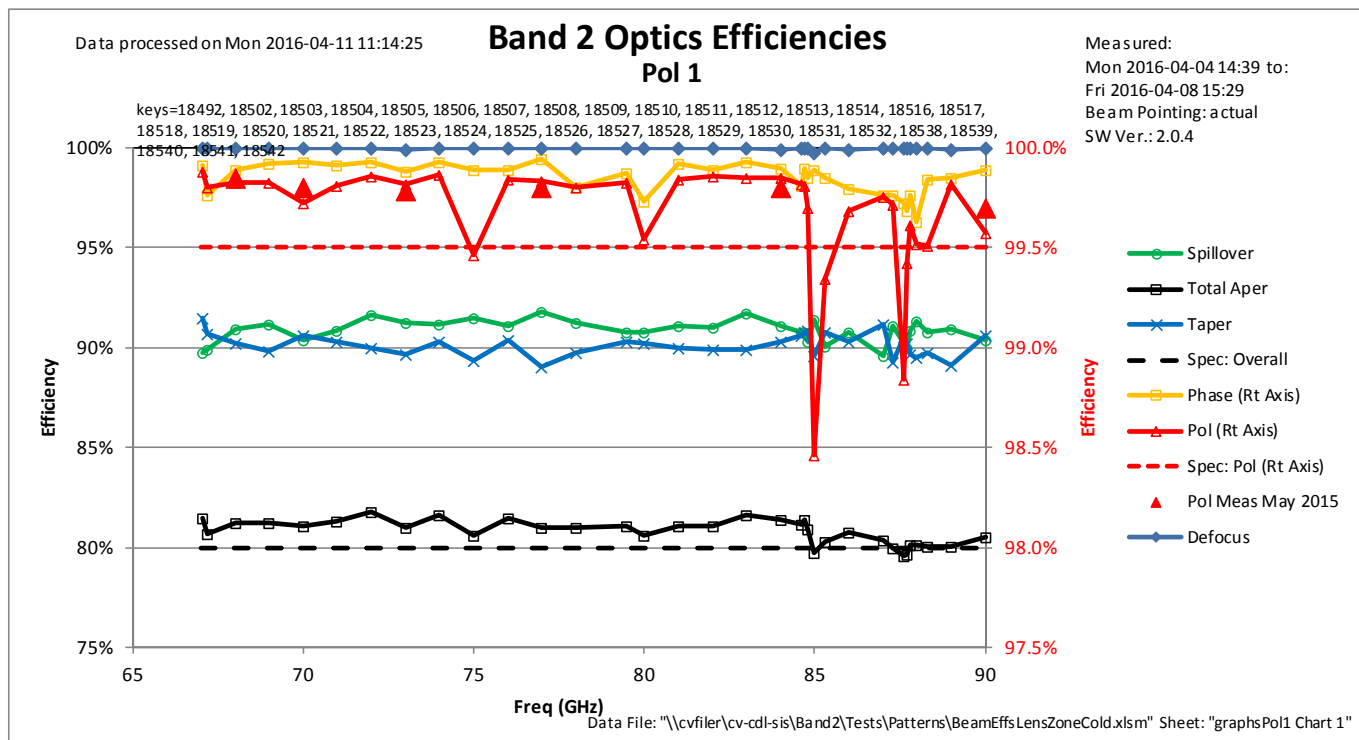


Figure 110: Fresnel lens, Pol 1, cold, actual beam pointing direction.

Compare with lens 3-2 in [Figure 103](#)



Design and testing of a Prototype Band 2 Cartridge: Final Report

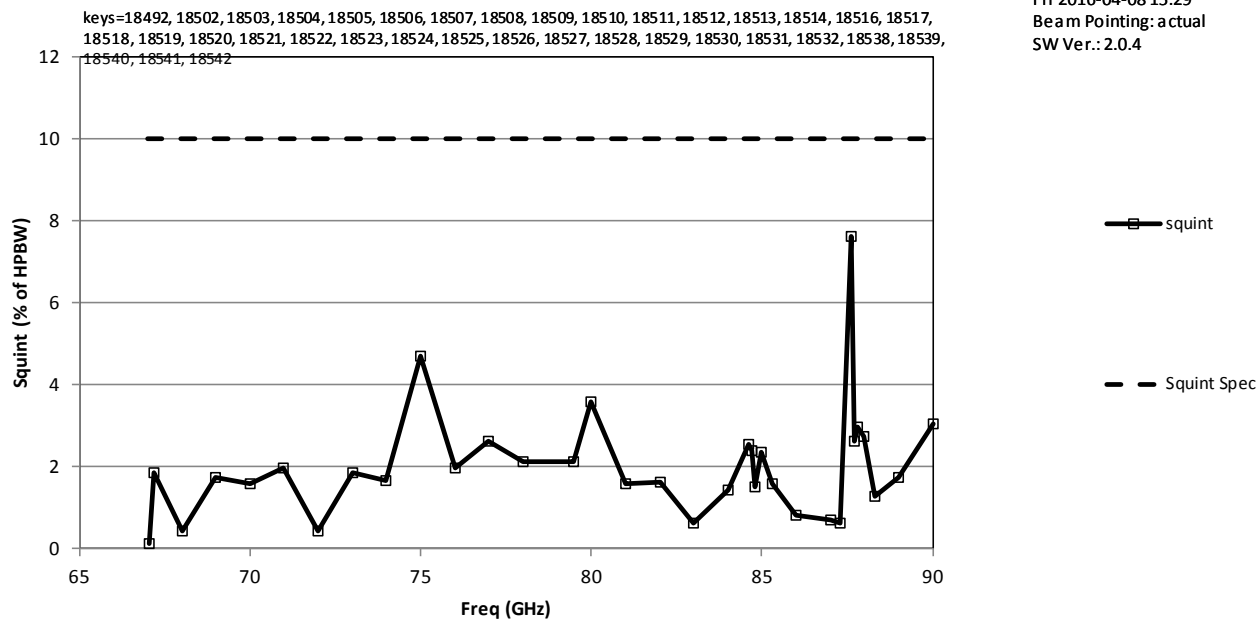
Date: 2017-12-27

Page: 113 of 117

Data processed on Mon 2016-04-11 11:14:25

Band 2 Beam Squint

Measured:
Mon 2016-04-04 14:39 to:
Fri 2016-04-08 15:29
Beam Pointing: actual
SW Ver.: 2.0.4



SW Ver: 2b9bdece (2016-11-14 15:05:22)

Data File: "I:\cvfiler\cv-cdl-sis\Band2\Tests\Patterns\BeamEffsLensZoneCold.xlsm" Sheet: "graphsPol0 Chart 7"

Figure 111: Fresnel lens, beam squint, actual beam pointing direction.

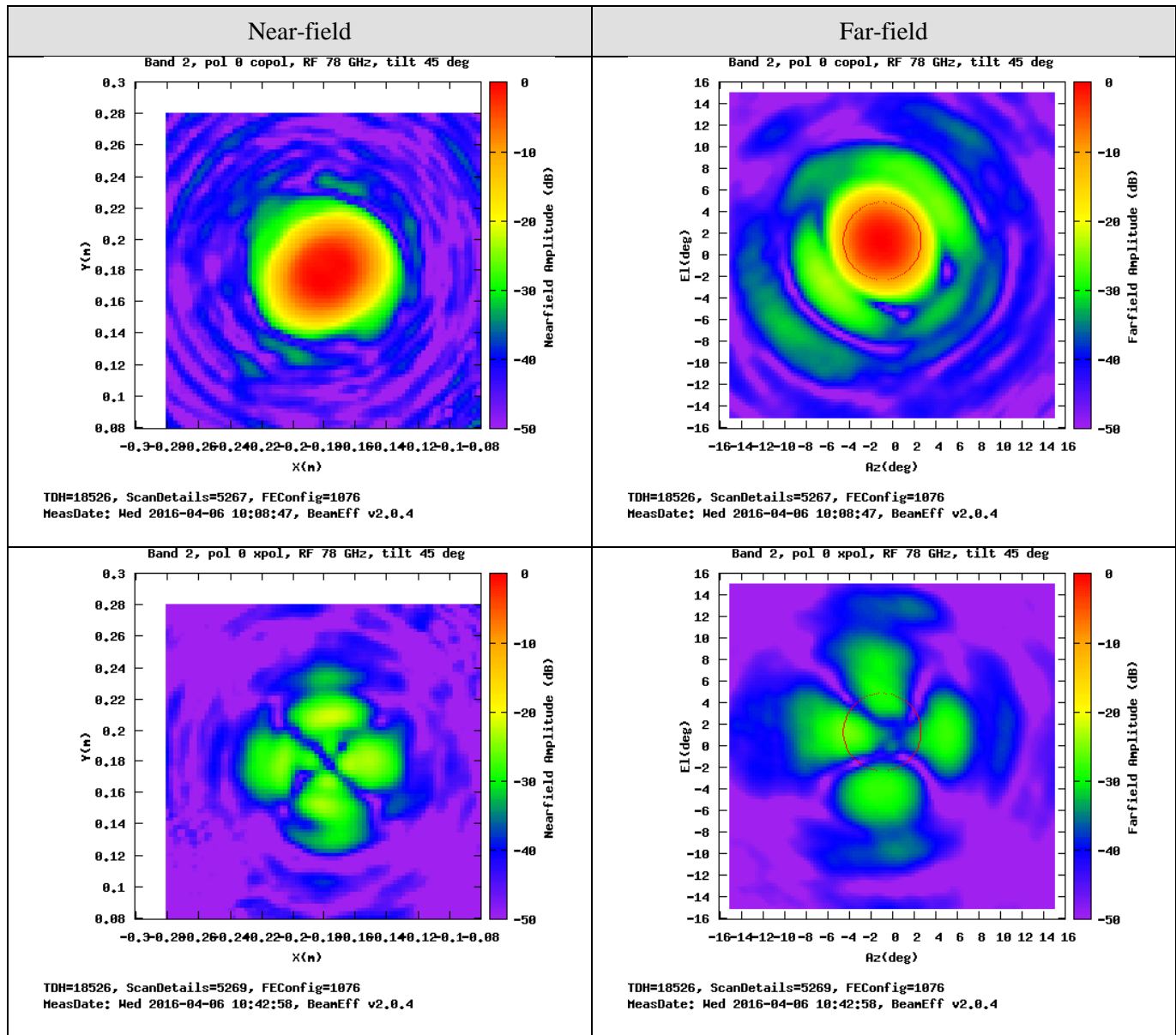


Figure 112: Pol 0 Near- and Far-field Patterns for 78 GHz: Fresnel Lens

8.8. Spurious Frequencies (FEND-40.00.00.00-00120-00/T)

As shown in [Figure 78](#) through [Figure 81](#), no spurious responses are observed in the IF output spectrum when the receiver is connected to the cold load.



Design and testing of a Prototype Band 2 Cartridge: Final Report

Date: 2017-12-27

Page: 115 of 117

8.9. Leak Rate (FEND-40.02.02.00-00470-00/R)

Band 2 and Band 6 cartridges use identical 300K plates, so the leak rate procedures for Band 6 [\[RD 51\]](#) were used and the leak rate of the 300K plate measured $< 1.06 \times 10^{-6}$ mbar×liters/sec at 20 mins.

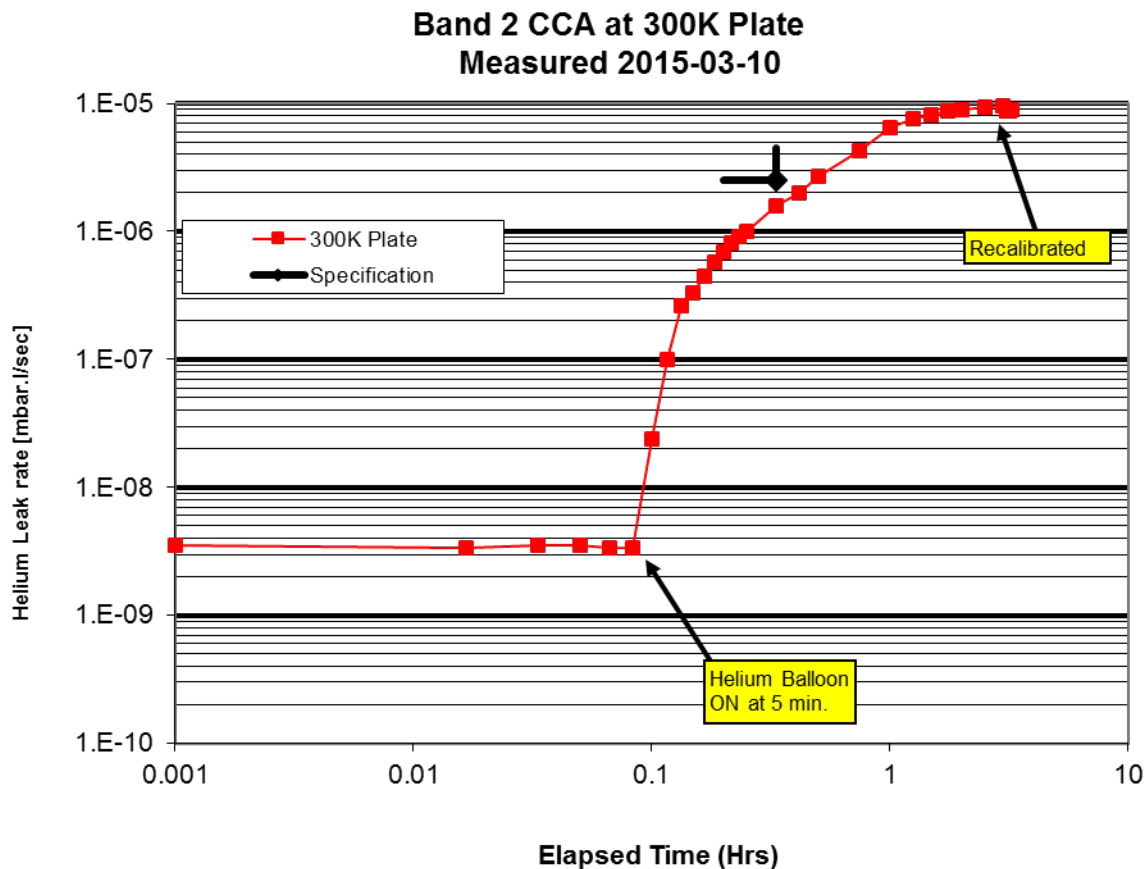


Figure 113: Measured Leak Rates of 300K Plates

8.10. Measured Mass (FEND-40.02.02.00-00310-00/T)

Cartridge mass specifications are given in [\[RD 54\]](#) and measured masses are compared to the specifications in [Table 20](#).

| Table 19: Mass Budget | |
|-------------------------------------|-------------|
| Item | Mass (kg) |
| Bare unmodified cartridge | 5.455 |
| Net additions to the bare cartridge | 2.441 |
| Total as built CCA weight | 8.000 |
| Budget allocation in FE mass budget | 10.450 |
| Mass margin | 2.45 |

9. Drawings and Parts List

9.1. Mechanical

The assembly drawing of the cold cartridge body with “find” numbers is shown in [Figure 114](#).

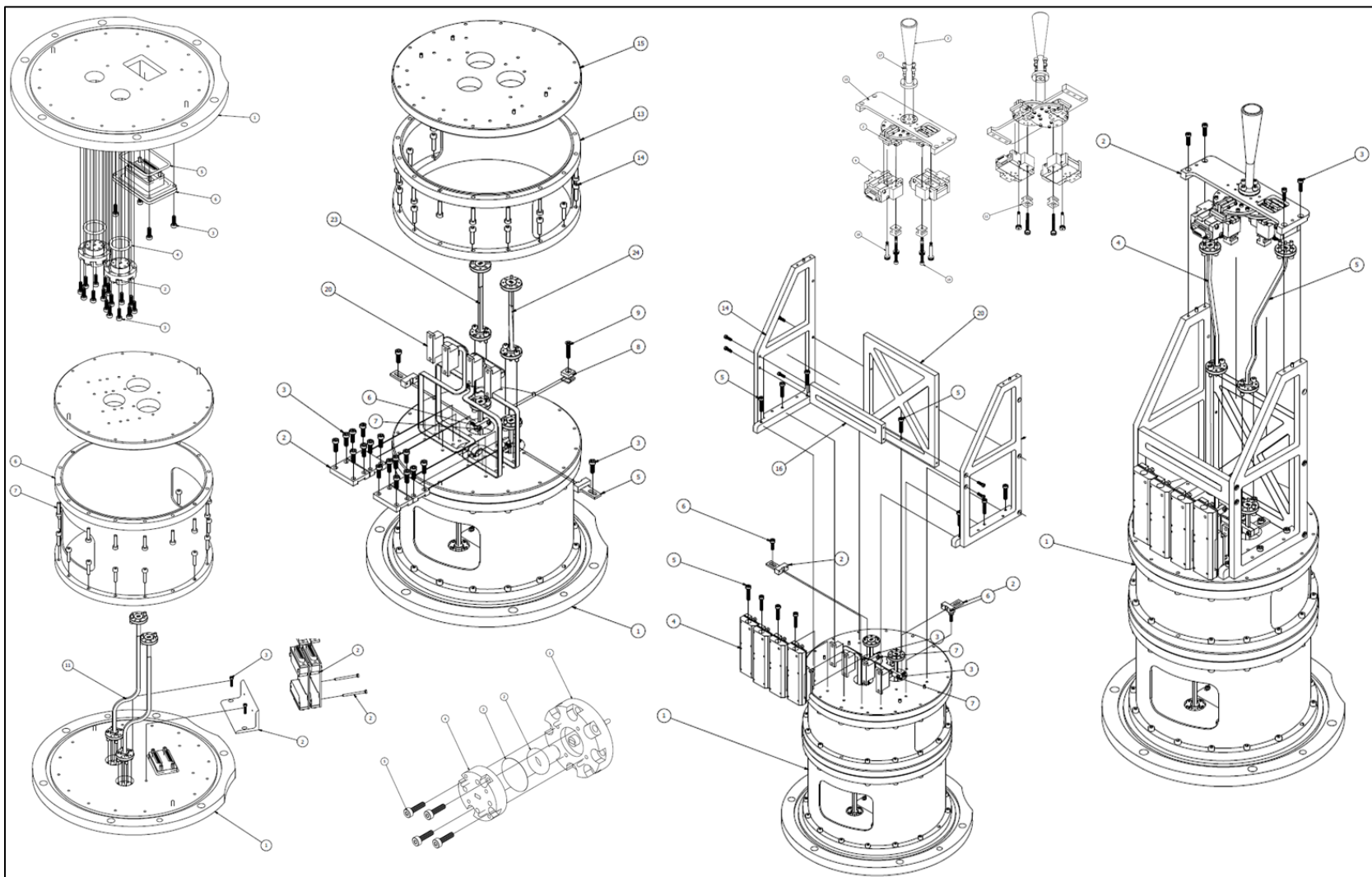


Figure 114: Assembly Drawing for Band 2 Cartridge

(Reference only, see [\[RD 38\]](#) for drawing)